

Investigation of Deformation and Failure Mechanisms in Woven and Nonwoven Fabrics under Quasi-Static Loading Conditions

by

Petch Jearanaisilawong

Sc.B., Brown University (2002)

Submitted to the Department of Mechanical Engineering
in partial fulfillment of the requirements for the degree of

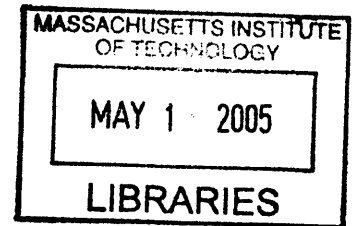
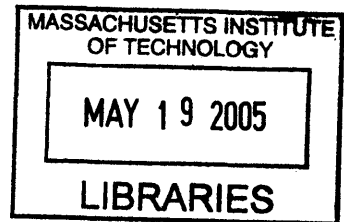
Master of Science in Mechanical Engineering

at the

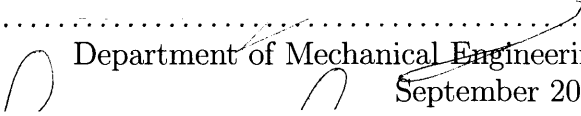
MASSACHUSETTS INSTITUTE OF TECHNOLOGY

September 2004

© Massachusetts Institute of Technology
All Rights Reserved



The author hereby grants to Massachusetts Institute of Technology permission to
reproduce and
to distribute copies of this thesis document in whole or in part.

Signature of Author
 Department of Mechanical Engineering
September 2004

Certified by
.....
Simona Socrate
Assistant Professor of Mechanical Engineering
 Thesis Supervisor

Accepted by
.....
Ain A. Sonin
Professor of Mechanical Engineering
Chairman, Department Committee on Graduate Students

BARKER

Investigation of Deformation and Failure Mechanisms in Woven and Nonwoven Fabrics under Quasi-Static Loading Conditions

by

Petch Jearanaisilawong

Submitted to the Department of Mechanical Engineering
on September 2004, in partial fulfillment of the
requirements for the degree of
Master of Science in Mechanical Engineering

Abstract

The mechanical responses of high performance ballistic woven and nonwoven fabrics under in-plane quasi-static loading conditions have been investigated. The investigations focused on the responses of fabrics at the mesostructural level as well as at the macroscopic level under uniaxial tensile and in-plane shear modes of deformation. A number of experimental methods have been developed, including techniques to test individual fibers (coupon fiber test), techniques to test fabric specimens with the aid of custom-designed fixtures, and techniques relying on image analysis to capture the deformation response of the fabric. Two continuum models have been developed for each type of fabric based on the deformation and failure mechanisms observed in the experiments. The models are able to capture essential features of the in-plane deformation of the fabrics in a computationally efficient framework.

Thesis Supervisor: Simona Socrate

Title: Assistant Professor of Mechanical Engineering

Contents

1	Introduction	8
1.1	Motivation	8
1.2	Classes of Fabrics	9
1.2.1	Woven Fabric	9
1.2.2	Nonwoven Fabric	10
1.2.3	Knitted Fabric	13
1.3	Thesis Organization	14
2	Characterization of the Mechanical Response of Woven Fabrics	15
2.1	Background	15
2.1.1	Literature Review	15
2.1.2	Continuum Model for woven fabrics	18
2.2	Woven Fabric Experiments	24
2.2.1	Microscopy	24
2.2.2	Fabric, Yarn and Fiber under Tensile Loads	25
2.2.3	Interaction of Yarns at the Crossover Points	38
2.2.4	Comparison of Model Predictions with Experimental Findings	49
3	Characterization of the Mechanical Response of Nonwoven Fabrics	53
3.1	Background	53
3.1.1	Literature Review	54
3.2	Nonwoven Fabric Experimental Investigation	55

3.2.1	Study of Nonwoven Fabric Structure	55
3.2.2	Mechanical Responses of Nonwoven Fabrics under Tensile Loads	61
3.2.3	Mechanical Responses of Nonwoven Fabrics under In-plane Shear Loads	71
3.2.4	Summary of Nonwoven Fabric Study	74
4	A Continuum Model for Needlepunched Nonwoven Fabrics	77
4.1	Background	77
4.1.1	Literature Review	77
4.2	Modeling Objectives	80
4.3	Constitutive Model Development	81
4.3.1	Constitutive Representation of the Visco-Plastic Network (Network A)	82
4.3.2	Constitutive Representation of the Elastic Network Orientation (Network B)	85
4.3.3	Determination of Model Parameters	88
4.4	Comparison of Model Predictions with Experimental Findings	89
5	Conclusions	96
5.1	Conclusions	96
5.2	Recommendations and Future Work	98
A	Uniaxial Tensile Grips for Fabric Sheets	100
B	Kinematics of Picture-frame Shear Test	103

List of Figures

- 1-1 Examples of woven fabrics 10
- 1-2 Examples of nonwoven fabrics (left - electrospun fabric, right - needlepunched fabric) 13
- 1-3 Variety of plain knitted fabrics (Hearle 1969) 14
- 2-1 Woven fabric model geometry (King et al. [42]) 20
- 2-2 Kevlar style s706 surface 25
- 2-3 Kevlar style s706 cross sections 26
- 2-4 Yarn sandwiched specimen 27
- 2-5 Single yarn test setup 28
- 2-6 Kevlar yarn tensile test results 29
- 2-7 Schematic of an unravel strip test specimen (Realf 1992) 30
- 2-8 Fabric uniaxial tensile grips (a) and Fabric unravel strip test set up (b) 31
- 2-9 Stress-strain responses of Kevlar fabric unravel strip tests on warp and weft directions 32
- 2-10 Fabric deformation and failure mechanisms during an unravel strip test 33
- 2-11 Influence of specimen width in fabric tensile tests 34
- 2-12 Fiber coupon specimen (half of fiber highlighted for clarity) 35
- 2-13 Stress-strain plots of Kevlar fiber tests from warp and weft yarns 36
- 2-14 Stress - strain plots of fabric, yarn and fiber tensile test 37
- 2-15 Schematic of out-of-plane compression sandwich test 39
- 2-16 Load and displacement plots normalized by number of crimps from various configurations of out-of-plane compression tests 40

2-17 In-plane shear response of woven fabric (adopted from Lussier 2002)	41
2-18 Picture-frame test configuration	43
2-19 Picture-frame shear test result and test evolution	44
2-20 Schematic of bias extension test (Lussier 2002)	45
2-21 Influence of aspect ratio on bias extension test (a: $AR < 1$; b: $1 < AR < 2$; c: $2 < AR$) (Wang 1998)	46
2-22 Different modes of deformation in the bias extension test (Lussier 2002)	46
2-23 Load - displacement plots of bias extension test	47
2-24 Summary of deformation mechanisms in the bias extension test	49
2-25 Predicted and observed deformation and yarn orientation for bias extension test at 17% nominal axial strain (King et al. 2004)	50
2-26 Model prediction of load-strain behavior in warp direction test compared to the experiments	51
2-27 Model prediction of load-strain behavior in weft direction test compared to the experiments (King et al. 2004)	51
2-28 Model prediction of load-strain behavior in bias extension test compared to ex- periments	52
3-1 Images of Protechtor taken from the same area (a-c: different focal plane; d: after image integration technique)	56
3-2 Images of needlepunched felt surfaces	57
3-3 Tensile test results of Protechtor fiber	59
3-4 Tensile test results of Dyneema Fiber	59
3-5 Images of fiber irregularities and two populations found in Dyneema fibers	60
3-6 Dimension of nonwoven fabric dogbone specimen (in inches)	61
3-7 Nonwoven dogbone specimen in clamped position	62
3-8 Uniaxial cyclic loading test scheme	63
3-9 Load-Extension plots of Protechtor and Dyneema Fraglight fabrics	64
3-10 Texture evolution of the Dyneema Fraglight under a tensile load	65
3-11 Needlepunched pattern on Dyneema Fraglight fabric	66
3-12 Dyneema Fraglight tensile tests from different fabric directions	67

3-13	Results of cyclic loading tests of roll direction fabric at different strain rate	68
3-14	Detailed deformation mechanisms in a cyclic loading test	69
3-15	Images corresponding to the test evolution of a cyclic loading test	70
3-16	A shear test result of Dyneema Fraglight and its deformation mechanisms	72
3-17	Cyclic loading picture-frame shear test schematic	74
3-18	Results of cyclic loading picture-frame shear test at two test speeds	75
3-19	Damage accumulation in the picture-frame shear test	76
4-1	Constitutive model with network A as a linear spring and a dashpot in series, in parallel with network B as a nonlinear spring	81
4-2	Multiplicative decomposition of deformation	83
4-3	The evolution of shear strength as a function of time	85
4-4	Fitted simulation prediction with the experimental data of the uniaxial cyclic loading test at 0.01 / second of the Dyneema Fraglight	90
4-5	Experimental result and simulation prediction of the uniaxial monotonic loading test of the Dyneema Fraglight	92
4-6	Experimental result and simulation prediction of the uniaxial cyclic loading test at 0.05 / sec of the Dyneema Fraglight	93
4-7	Experimental result and simulation prediction of the picture-frame monotonic shear test of the Dyneema Fraglight	94
4-8	Lateral contraction as observed in the experiment and as predicted by the sim- ulation	95
A-1	Drawings of fabric uniaxial tensile grip (A)	101
A-2	Drawings of fabric uniaxial tensile grip (B)	102
A-3	Drawings of fabric uniaxial tensile grip (C)	102
B-1	Deformation imposed by the picture-frame shear test	103
B-2	Shear frame kinematics	104
B-3	Plot of the applied stretch (λ_1) and the shear angle (θ)	105
B-4	Plots of the stretch in the loading direction, the stretch in the lateral direction, and the multiplication of the two stretches	106

Chapter 1

Introduction

1.1 Motivation

Fabrics are widely used in traditional applications such as apparels and protective clothing. With recent advancement of related technologies, fabrics have also become an integral part in many non-traditional applications. One example is the composite technology, where fabrics are used as a structural basis for textile composites. In addition, the development of high strength, light weight polymer fibers offers the opportunity to utilize fabrics in inflatable structures, fragment barriers, and ballistic armors. The emergence of micro- and nanotechnologies allows shape-memory materials or electrical components to be embedded in fabric structures to create "smart" apparel that can be actively controlled and/or designed to automatically respond to changes in environment. Microfluidic technologies can be used to regulate the temperature or transport fluids within fabric structures as a means to transmit electric signals or to serve as actuators for other embedded devices.

This widening range of fabric applications demands a better understanding of mechanical behavior of fabrics. For example, in an investigation of the effects of fabric deformation on the functionality of embedded electronic devices, the effects of macroscopic loading at the fabric mesostructure level should be addressed. Fabrics might be combined with other materials in multi-component structures, so the nature of their contributions to the mechanical behavior of a hierarchical ensemble needs to be understood as well.

Early studies on the mechanics of fabrics focused primarily on applications for the apparel and protective clothing industries. Attention was given to the development of fabric characterization techniques and fabric models that were capable of predicting the behaviors of textile materials. However, the introduction of novel technologies, especially in composite applications, requires new approaches for studying fabrics as components of more complex structures.

This thesis presents a systematic approach to characterizing the mechanical behavior of fabrics from the microstructural level to their macroscopic response. A continuum model is developed to predict the mechanical behavior of nonwoven fabrics in planar deformation. The proposed model is capable of capturing the essential features of the material behavior including texture evolution and damage accumulation with a sufficient degree of accuracy. The model can be combined with other continuum models to aid in the design of multi-component structures.

1.2 Classes of Fabrics

As further detailed in the following sections, fabrics are categorized into three major classes based on their structures and manufacturing processes: woven fabrics, nonwoven fabrics, and knitted fabrics.

1.2.1 Woven Fabric

Woven fabrics are formed by weaving two families of yarns together with a repeating pattern. A yarn can be a solid structure, or a twisted or untwisted bundle of fibers. The yarns along the length of the fabric are called "warp yarns" and the yarns that are perpendicular to the warp yarns are called "weft" or "fill" yarns. The warp yarns are usually the straighter, stiffer, and stronger of the two families. Woven fabrics are held together by weaving the warp and the fill yarns over and under each other. The weaving patterns determine the types of woven fabrics. A plain-weave fabric has only one cross over point of warp and weft yarns in the repeating pattern. A basket weave has a specific number of warp yarns cross over and under the same number of fill yarns. A twill weave is interlaced such that the cross over points of warp and weft yarns form parallel diagonal lines or ribs on the fabric surface. A satin weave is characterized by long floats of yarn on the face of the fabric. The yarns of satin weave are formed such that there is no

visible pattern of interlacing, and usually yield a fabric with smooth and shiny surfaces. **Figure 1-1** shows examples of woven fabrics. The mechanical properties of woven fabrics depend on a number of factors including fiber material, yarn geometry, and weave pattern. The mechanical behavior of woven fabrics will be further discussed in Chapter 2.

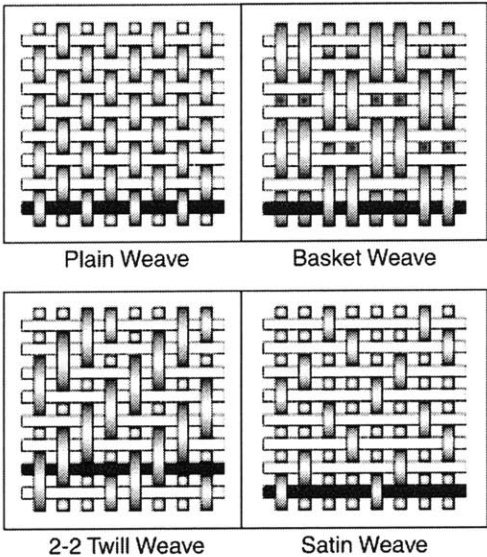


Figure 1-1: Examples of woven fabrics

1.2.2 Nonwoven Fabric

Nonwoven fabrics are sheet structures created by forming or interlocking a web of fibers through mechanical, thermal or chemical processes. A nonwoven fabric can be categorized by its web forming process and bonding technique. Current technologies in web forming include carded forming, air laying, wet laying, spunbonding, melt spinning, and electrospinning. Commercially available techniques for the bonding process are resin bonding, thermal bonding, solvent bonding, needlepunching, spunlacing and stitchbonding. A brief description of each process is presented in the following sections.

Web Forming Processes

- The carded forming process uses rotating cylinders covered with wires or needles with teeth that comb fibers into a parallel array along the machine direction. The fabrics created by this technique are anisotropic with higher strength along the machine direction. The position of the wire combs can be rearranged such that more fibers are directed perpendicular to the machine direction, resulting in an increase of the fabric strength in such direction.
- The air laying process is carried out by first suspending fibers in the air, and then blowing them across a screen that collects them as a batt. This technique is mostly limited to short staple fibers and produces a fabric with completely random fiber orientations.
- The wet laying process is similar to the air laying, except that the fibers are suspended uniformly in water instead of in air. The fiber-water mixture flows across a screen where the fibers are collected as a web. The web is squeezed and dried in an oven to remove the water content. This process produces a fabric with isotropic properties due to randomly laid fibers. This process also allows the uses of chemical binders to improve the fabric strength.
- The spunbonding process is an integrated process that produces a web of fibers directly from a polymer resin. The process begins with melted thermoplastic extruding through a linear or circular spinneret. The extruded polymer filaments are rapidly cooled and drawn by air and/or mechanical drafting rollers to form filaments of the desired diameter. The filaments are then laid down onto a conveyor belt to form a web which is later bonded to form a spunbonded fabric.
- The melt spinning process is performed by extruding a thermoplastic through a linear die containing 20-40 orifices per inch of die width. The extruded filaments are blown through high velocity air across a screen to form a melt blown web. Since the filaments are still in a semi-molten stage when depositing on the screen, the web structure is produced through fiber solidifications and fiber entanglements. No additional bonding technique is required.
- The electrospinning process is implemented by using an electric field to draw a positively

charged polymer solution from an orifice to a collector, thereby creating a jet of polymer solution. As the jet emerges at the base of the nozzle, it is stretched and split into many fibers in the spraying region. The fibers are collected on a grounded metal screen. This technique can produce fibers with diameters ranging from nanometers to micrometers. Because of their small diameters, electrospun fibers have a large surface-to-volume ratio and are ideally suited for filtration applications. In addition, the electrospun fabrics can be used as a structural reinforcement in composite materials.

Web Bonding Processes

- The resin bonding technique uses an adhesive resin, called binder, to bond the web structure. The binder can be applied by dipping the web into the resin solution and removing the excess, or by foaming, spraying, or printing the adhesive on the web.
- The thermal bonding technique uses heat to melt part of the fiber web, or the bonding material blended in the web during the web forming process to create bonds. Two common methods for this technique are through-air heating and calendaring. In the through-air heating method, hot air is blown directly onto the web to fuse the fibers. Calendaring requires the web to be compressed through a set of heated cylinders with embossed bond pattern. This method usually produces high strength, low loft fabrics.
- The solvent bonding technique is used when the filaments are partly soluble in appropriate solvents. The solvent is applied onto the web surface to dissolve some of the fibers and therefore create bonding regions. Removing the solvent causes resolidification of the fiber surface and bonding at fiber crossover points.
- The needlepunching technique uses barb wires to punch through a nonwoven mat. The process begins as the web of carded, air laid or spunbonded mat is rolled onto the punching area. The plate that supports the mat in the punching zone is called "bed plate", and the plate with needles and wires is called "stripper plate". For each cycle of punching, the fabric tufts in the punching area are hooked and entangled. The entanglement pattern and the properties of the finished product depend on the needle design, the arrangement of needles, and the punching frequency.

- The spunlacing or hydroentangling process uses fine, high velocity jets of fibers to penetrate through the fiber web and cause the fibers to entangle and wrap around each other. Binders, though not needed, are sometimes applied to the finished product to improve the fabric strength.
- The stitchbonding process uses continuous filaments or yarns to sew onto the web and create stitch patterns on the web surface.

Figure (1-2) shows some examples of nonwoven fabrics from different bonding techniques. The mechanical behavior of nonwoven fabrics will be discussed in details in Chapter 3.

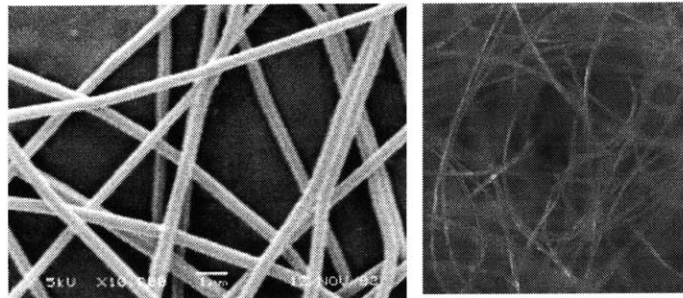


Figure 1-2: Examples of nonwoven fabrics (left - electrospun fabric, right - needlepunched fabric)

1.2.3 Knitted Fabric

Knitted fabrics are formed by intertwining yarns or threads in a series of connected loops, creating a clear repeating pattern without clearly defined yarn families. Knitted fabrics are further categorized by the pattern of loop connections and loop positions. Some examples are weft knitting, warp knitting, three-dimensional multiaxial knitting, etc. **Figure 1-3** illustrates samples of knitted fabrics. Since this study does not focus on knitted fabrics, their mechanical behavior will not be further discussed.

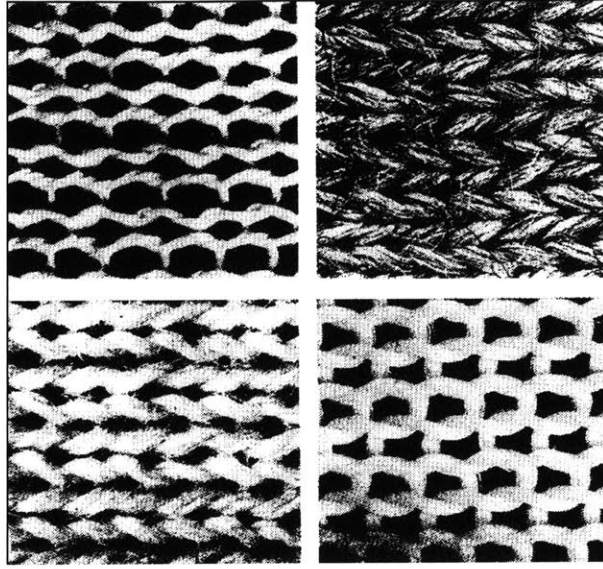


Figure 1-3: Variety of plain knitted fabrics (Hearle 1969)

1.3 Thesis Organization

This thesis is structured as follows. Chapter 2 focuses on the experimental characterization of woven fabrics. The in-plane properties and deformation mechanisms of a commercially available ballistic woven fabric, Kevlar[®] style 706, are thoroughly examined and discussed. The responses of this fabric are further explained through an investigation of the fabric mesostructure. Chapter 3 presents the results of a study on the behavior of nonwoven fabrics. Two types of high performance needlepunched fabrics are tested under quasi static loading conditions. An attempt is made to explain the observed macroscopic responses and properties through a study of the fabric mesostructure. Chapter 4 discusses an approach to create a continuum constitutive model to predict macroscopic in-plane behavior of nonwoven fabrics. The model is then tested for a range of material properties to ensure that essential features of the material behavior are captured. The model predictions are compared to the experimental results to validate the model. Chapter 5 summarizes the result of this study and discusses directions of future work.

Chapter 2

Characterization of the Mechanical Response of Woven Fabrics

2.1 Background

2.1.1 Literature Review

As the mechanical behavior of woven fabrics has been the subject of extensive studies for many years, a number of researchers have contributed to the techniques, approaches and methods for conducting experiments on fabrics under various modes of deformations. A number of woven fabric models have also been developed. When combined with model development, experimental investigations not only provide an insight into the fabric response, but also serve as a means to determine the model parameters, as well as model validation. The experimental approaches followed in these studies are varied depending on the research objectives.

For researchers interested in the behavior of woven fabrics at the microstructural level, namely at the level of the constituent fibers and yarns, experiments are usually conducted to obtain the fiber axial tensile behaviors as in the case of Allen et al. [2], who conducted an investigation on the tensile deformation and failure mechanisms of Kevlar[®] fibers, and Wang and Xia [85],[86] who studied the effects of strain rate and temperature on the axial tensile properties of Kevlar[®] fibers. The behavior of fibers in other modes of deformation such as in bending and in compression has been also investigated as in the works by Fahey [22] and

Kawabata et al. [36].

A number of researchers conducted experiments at the yarn level and related the experimental results to the behavior of the fabrics. These researchers include Rao et al. [70] who studied the influence of yarn twist on the tensile properties of fabrics, Pan et al. [59] who conducted yarn pullout tests to investigate the yarn interaction at the crossover point, and Rebouillat [73] who studied friction in the constituent yarns and compared it to the tribological properties of the fabric.

Other researchers conducted mechanical characterizations of yarns to determine properties and parameters needed in microstructurally based fabric models. The researchers who employed this approach include Realff [71],[72] who conducted yarn axial tension, yarn-on-yarn friction, yarn bending, yarn consolidating and yarn flattening tests, Shockey et al. [77]-[81] who performed yarn tension and yarn pullout tests, and Anandjiwala and Leaf [3],[4] who investigated the yarn behavior in tension, compression and bending.

The need to perform experimental investigations at the fabric level is often driven by modeling efforts. For researchers whose models are based on continuum formulations, the experiments focus on macroscopic responses that can be directly used to derive model parameters. This approach is mostly followed for fabric-reinforced composites. Typically, the most relevant model parameters are the in-plane fabric properties such as tensile and shear stiffnesses. Xue et al. [90] determined the parameters for their continuum model of woven reinforced composites by investigating the behaviors of these materials in uniaxial and biaxial tensions as well as in in-plane shear. Boisse and his colleagues [11],[12] conducted tests on a plain weave fabric composite using a biaxial tensile tester to obtain the parameters for their 4-node finite element model of plain weave fabric composites. Ng et al. [57] performed uniaxial tensile tests and rail shear tests to obtain the macroscopic properties for their model of a 2/2 twill weave fabric composite.

For researchers who formulate models based on features of the fabric mesostructure, experiments not only provide the model parameters, but also serve as model validation. Kawabata et al. [33]-[35] proposed analytical models for the biaxial, uniaxial and shear deformation behavior of woven fabrics based on pin-joined truss geometry. They developed the KESF system (Kawabata Evaluation System for Fabric) that comprises a set of mechanical testing methods required to obtain the sixteen parameters for their analytical model. Warren [87] performed

uniaxial tension experiments on the fabric strips along the yarn family direction to validate his analytical model based on elastic beam theory with couple yarn extension and bending effects. Realf [71],[72] and Shockey [77]-[81] performed uniaxial tension tests on fabric strips to validate their models.

While some researchers focus on the formulation of fabric models that can be used in multiple modes of deformation, other research groups only consider the fabric responses under certain modes of deformation. A number of researchers consider the fabric deformation under uniaxial tensile loads. Among these are Leaf and Kandil [46] who formulated a closed form solution to predict the initial load extension behavior of plain weave fabrics, Seo et al. [75] who considered the mechanisms of in-situ tensile failure at the microstructural level during uniaxial loading by performing the tests under a scanning electron microscope, and Shim et al. [76] who investigated the mechanical properties of Twaron[®] fabric under high-speed tensile tests using a split Hopkinson bar.

Fabric response under shear loads has been investigated by a number of researchers. These include Kothari and Tandon [43] who investigated the shear behavior and shear hysteresis of finished wool and wool blend woven fabrics using a simple shear tester, Baker [7] who also used the simple-shear technique to evaluate the response of kevlar-epoxy fabric panels, Wang et al. [84] who performed both simple shear tests and bias extension tests to study the draping properties of plastic-reinforced fabric. Mohammed et al. [56] reviewed the three techniques commonly used to categorize the shear properties: simple shear, bias extension and picture-frame shear. They concluded that the data obtained from the simple shear and the bias extension tests are not suitable for analysis of the fabric shear response due to the presence of both tensile and shear stresses in the specimens and that the picture-frame shear test is preferred. They also conducted an investigation on the shear deformation of woven fabric with various types of weave structure using the picture-frame shear test. Other researchers, including Lussier [54], Lebrun et al. [47], Peng et al. [62], and McGuinness [55], conducted shear experiments on woven composites using the bias extension test and the picture-frame shear test. Each provided discussions and comparisons on the two types of tests. They also introduced models for the fabric shear behavior using a number of different approaches.

A number of research groups concentrate their studies on the development of new techniques

to measure the mechanical properties of fabrics. Pan et al. [58] proposed a set of techniques that can measure the fabric behavior under various modes of deformation such as in-plane tensile and shear deformation, and out-of-plane compression, as well as fabric surface friction, by using only one unidirectional mechanical testing machine. Basset et al. [8] reviewed a number of experimental approaches used for measuring the fabric mechanical properties for in-plane shear and biaxial tension. They also proposed a new test configuration that can measure the tensile and shear properties of fabrics simultaneously and independently.

The experimental investigation of the mechanical response of woven fabrics reported in this work is a companion study to the modeling effort of King [41], which was aimed at the development of a continuum model for the in-plane mechanical response of woven fabrics [42]. The experimental approach selected to characterize the fabric behavior was thus influenced by the modeling choices, as a number of experiments were aimed at determining specific model parameters. In order to present the experimental results in this logical framework, it is then necessary to review the essential features of the continuum model for woven fabrics as outlined in the following section.

2.1.2 Continuum Model for woven fabrics

The continuum model proposed by King et al. [41],[42] is designed to accurately capture the in-plane macroscopic response of the fabric by homogenizing the behavior of the underlying mesostructure and approximating the fabric as an anisotropic continuum. The model accounts for the primary mechanisms of deformation in woven fabrics including:

- *yarn stretching* - a mechanism where the length of a yarn increases under tensile loading;
- *yarn bending* - a mechanism by which a woven yarn changes its crimp angle as the fabric is stretched;
- *crimp interchange* - a mechanism by which the fabric elongates without yarn stretching in one yarn family direction as those yarns straighten out and become less crimped (i.e. longer wavelength and smaller wave amplitude) while the fabric contracts in the other yarn family direction as the yarns of the other family become more crimped;

- *locking* - a mechanism by which the fabric resists deformations as the interwoven yarns jam against each other;
- *resistance to relative yarn rotation* - which is the dominant mechanism for the response of fabric to in-plane shear.

In this model, a number of limiting assumptions are adopted to simplify the model. First, the model is intended for quasi-static analysis of fabrics in planar deformation and subjected only to in-plane loads. No failure mechanism such as yarn breakage, unraveling of the weave and yarn pullout is included. Under the "no failure" assumption, yarn slippage at the crossover points is negligible, and consequently, the crossover points are constrained to deform in an affine manner with the fabric continuum and the vectors describing the yarn family orientations and wavelengths are material lines. All of these limiting assumptions remain accurate until yarn slip begins to dominate the fabric response at the onset of failure.

The fabric configuration, yarn loads, and macroscopic stresses can be determined from the state of macroscopic deformation through the following five steps:

- 1) Identify the repetitive geometry that represents the fabric and define a unit cell.
 - 2) Associate constitutive relations with the interactions and deformations of the yarns within the unit cell.
 - 3) Establish a method for determining the geometric configuration of the fabric mesostructure from the macroscopic deformation gradient.
 - 4) Calculate loads carried by the yarns that result in a deformed fabric configuration.
 - 5) Transform these mesostructural loads into continuum stresses at the macroscopic scale.
- Details on the procedure to accomplish these tasks can be found in [41] and [42].

To demonstrate the application of this approach, a continuum model was developed for the behavior of a plain weave ballistic fabric, Kevlar[®] S706, manufactured by DuPont. In the following sections we review the geometric and constitutive properties that are necessary to fully characterize the continuum model for the mechanical response of the fabric.

Geometry

The model adopts a geometry similar to the model proposed by Kawabata [33] as shown in **Figure 2-1**.

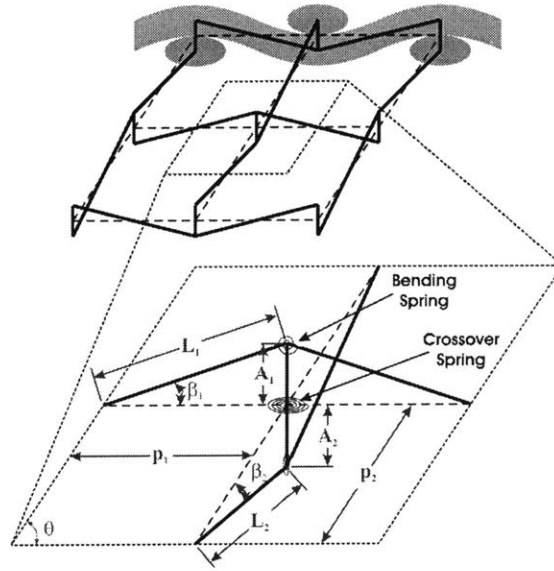


Figure 2-1: Woven fabric model geometry (King et al. [42])

The yarns are represented as a network of trusses connected by pin-joints at their crossover points. These trusses do not lie in the plane of the fabric but are interwoven to capture crimp interchange. They have axial compliance to allow for yarn stretch but are infinitely stiff in bending. The effects of yarn bending are modeled as being concentrated at the pin joints, where relative rotations of the two contiguous segments of the yarn are resisted by rotational "bending springs". Interactions between yarns at the crossover points are captured by "crossover springs" connecting the pin joints. The crossover springs have two modes of deformation. They are capable of extending and contracting to simulate the effects of cross-sectional deformation, allowing the yarns to change their crimp amplitude while remaining in contact. The spring elements also offer resistance to twist, modeling the effects of elastic and dissipative resistance to relative rotation of the two yarn families at the crossover points—the mechanisms for in-plane fabric shear.

Using this geometrical representation along with the assumption that the cross sections of the yarns are elliptical, the geometric parameters required for the model consist of

- the angles ${}^0\theta_i$ giving the initial orientations of the yarn families
- the minor (through-thickness) radii r_i and major (in-plane) radii R_i of the yarns

- the initial quarter wavelengths of the yarn families 0p_i
- one of the initial half yarn lengths between crossovers 0L_1 (the length for the other yarn family 0L_2 can be calculated from geometric constraints); this parameter determines the initial crimp in both directions
- the relaxed crimp angles ${}^0\beta_i$, which reflect the amount of "crimp set" in the yarns.

The initial quarter wavelengths and the initial yarn family orientations can be measured directly from a woven fabric sample. The yarn major and minor radii, the yarn lengths between crossovers and the relaxed crimp angles can be measured from images of the fabric cross section. A detailed discussion of the approaches to determine these geometric properties are given in Section 2.2.1.

Constitutive Relations

There are eight constitutive relations required to describe all modes of energy storage and dissipation in the model. The first two describe the linear elastic behavior of the two yarn families. the model uses linear elastic relations to describe yarn extension from an initial length 0L_i to a deformed length L_i :

$$T_i = k_i (L_i - {}^0L_i), \quad (2.1)$$

where T_i is the tensile force in the yarn of the i^{th} -family and k_i is the stiffness of the yarn segments in the unit cell (which may differ between the two yarn families).

The third and the fourth relations describe the yarn bending resistance, which is critical to the analysis of the fabric response in the low stress regime. For the selected geometry, bending is modeled as concentrated at the pin joints corresponding to the crossover points. Bending resistance is imparted through rotational springs at these points and is assumed to be linear elastic, with the bending moment M_{bi} exerted on the yarns at the crossover points proportional to the change in the crimp angle β_i :

$$M_{bi} = k_{bi} (\beta_i - {}^0\beta_i). \quad (2.2)$$

If necessary, the "initial" crimp angle ${}^0\beta_i$ can be adjusted to account for different amounts of permanent set in the yarns.

The fifth relation describes the interactions between yarns at the crossover points. In the proposed model, the effects of cross sectional deformations at the crossover points are captured by a nonlinear "interference spring". This spring simulates soft contact conditions, with negligible stiffness in tension and an initially compliant compressive response that becomes increasingly stiff as the interference increases. An exponential relation with two material parameters K_I and a has been chosen to capture this behavior:

$$F_I = K_I (e^{aI} - 1). \quad (2.3)$$

Here I is the interference between the cross sections of the crossing yarns and is defined as the sum of the initial crimp amplitudes (one half of the fabric thickness) minus the sum of the current crimp amplitudes.

The sixth relation describes the locking response of the fabric. A power law relation is used to describe the compressive force F_L that develops in the locking trusses when their length has been shortened by an amount I_L :

$$F_L = \begin{cases} 0 & I_L \leq 0 \\ K_d (I_L)^c & 0 < I_L \end{cases}, \quad (2.4)$$

with $I_L = d - d$, where d is the length of the locking truss and d , the length of the truss when locking first starts to occur, depends on the initial geometry of the yarns and weave.

The seventh and the eighth relations describe the elastic and the dissipative responses as yarns of the two families rotate relative to each other at the crossover points to accommodate in-plane fabric shear. Elastic rotation can only accommodate very small shear angles. Experiments indicate that the shear response over a very small initial purely elastic region is approximately linear:

$$M = K_s \gamma_e. \quad (2.5)$$

The dissipative rotation initiates at very small shear angles. A rate-dependent power law is chosen to represent the dissipative component of the yarn rotation, with $\dot{\gamma}_0$ giving the reference dissipative rotation rate at a reference moment M_0 , and an exponent b capturing the rate

sensitivity of the dissipative shear behavior:

$$\dot{\gamma}_f = \dot{\gamma}_0 \left(\frac{M}{M_0} \right)^b \quad (2.6)$$

Based on these constitutive relations, the following fifteen parameters define the response of the fabric unit cell:

- the axial stiffnesses k_i of the yarn segments of length L_i
- the bending stiffnesses of the yarns k_{bi}
- the mass densities of the yarns (for inertial stabilization) ρ_i (See [41], [42] for details)
- the two parameters describing exponential interference at the crossover points, K_I and a
- the two parameters describing the power law locking relation, K_d and c
- the elastic stiffness associated with relative yarn rotation K_s
- the two parameters describing rate-dependent dissipative yarn rotation, b and $\frac{\dot{\gamma}_0}{M_0^b}$.

Among these parameters, the yarn mass densities are the only properties obtained directly from the published data on Kevlar[®]. The remaining constitutive parameters were determined from experimental investigations. The yarn axial and bending stiffnesses were determined from tension tests performed on single yarns. The parameters describing exponential interference at the yarn crossover points were determined from out-of-plane compression tests on sheets of fabric. The locking parameters and the yarn rotation parameters were determined from fabric in-plane shear tests. These experimental investigations are discussed in details in the following sections.

In addition to the tests used to determine the constitutive properties for the models, a number of experiments were performed to gain an insight into the fabric deformation mechanisms and to serve as model validations. Such experiments include the uniaxial loading of fabric strips along the direction of a yarn family, as well as at 45 degree to the direction of yarn families. Tensile tests on the Kevlar[®] fibers were also performed to obtain properties to be compared to the behaviors of Kevlar[®] yarns and fabrics.

Properties	Value	Unit
Fabric properties		
Fabric weight	180	g/m^2
Type of warp yarn	Kevlar KM-2, 600 denier	-
Type of weft yarn	Kevlar KM-2, 600 denier	-
Warp yarn count	34	yarns/inch
Weft yarn count	34	yarns/inch
Fabric Thickness	0.23	mm
Kevlar KM-2 Single Yarn Properties		
Tenacity	3400	MPa
Elongation at Break	3.6	%
Young's Modulus	81	GPa

Table 2.1: Published properties of Kevlar fabric style 706

2.2 Woven Fabric Experiments

2.2.1 Microscopy

A method for measuring the geometric properties of the ballistic grade plain weave Kevlar[®] fabric style 706 is presented in this section. This particular fabric is constructed by interlacing two families of untwisted continuous Kevlar[®] fiber-bundle yarns as shown in **Figure 2-2**. **Table 2.1** provides the published properties of Kevlar[®] S706 as provided by the manufacturer.

The initial quarter wavelengths and the initial yarn family orientations can be directly measured from surface images as illustrated in **Figure 2-2**. To measure the other geometric properties, images of the fabric cross section created by embedding fabric in epoxy, sectioning the sample, polishing the surface and photographing the section using an optical microscope were obtained, as illustrated in **Figure 2-3**. The cross section images suggest that the yarns have approximately oval cross sections and that the weft yarn family has greater initial crimp than the warp yarn. **Figure 2-3** also provides the other geometric properties in the model such as the yarn radii, the yarn half wavelengths and the relaxed crimp angles. However, due to variations in the position and orientation of the sectioning plane, these values are not entirely consistent with the wavelengths and yarn lengths measured from **Figure 2-2**. Hence, an indirect method of estimating the yarn radii and yarn wavelengths has been used instead.

To obtain the yarn minor (through-thickness) radii, the total thickness of the fabric is measured and apportioned between the two yarn families. The major (in-plane) radii are

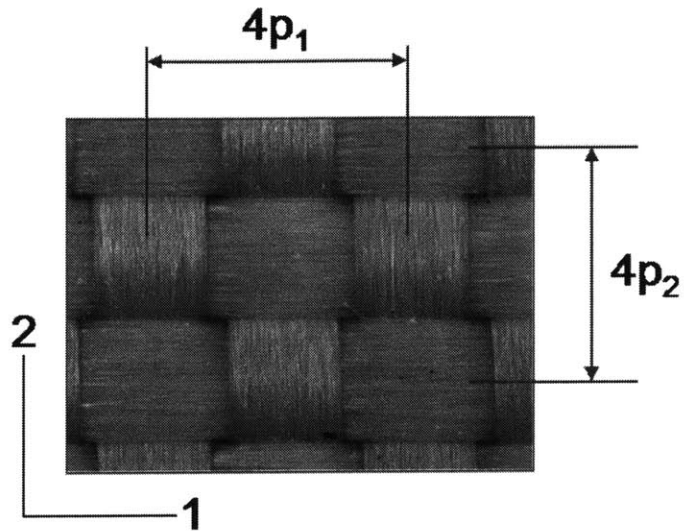


Figure 2-2: Kevlar style s706 surface

approximated from the measurement of yarn width on the fabric surface. The relaxed crimp angles are approximated to be equal to the initial crimp angle calculated from the geometric constraint of elliptical yarn cross section. The measured geometric properties of Kevlar[®] fabric style 706 are presented in **Table 2.3**.

2.2.2 Fabric, Yarn and Fiber under Tensile Loads

This section describes a method to measure the yarn tensile and bending stiffnesses by performing tests on single yarns. A study on the tensile behaviors of fabric and fibers is also presented for comparison to the yarn behavior under similar loading conditions. The results from the fabric study also serve as validation data to assess the adequacy of the model.

Yarn Tensile Test

As described in the previous section, Kevlar[®] yarns are obtained by bundling untwisted continuous Kevlar[®] fibers and are naturally smooth. The yarns tend to slip out of traditional smooth tensile grips or could be frayed from the uneven pressure distribution imposed by grips with grooved surfaces. As a solution to this problem, a new technique for testing Kevlar[®] yarns is

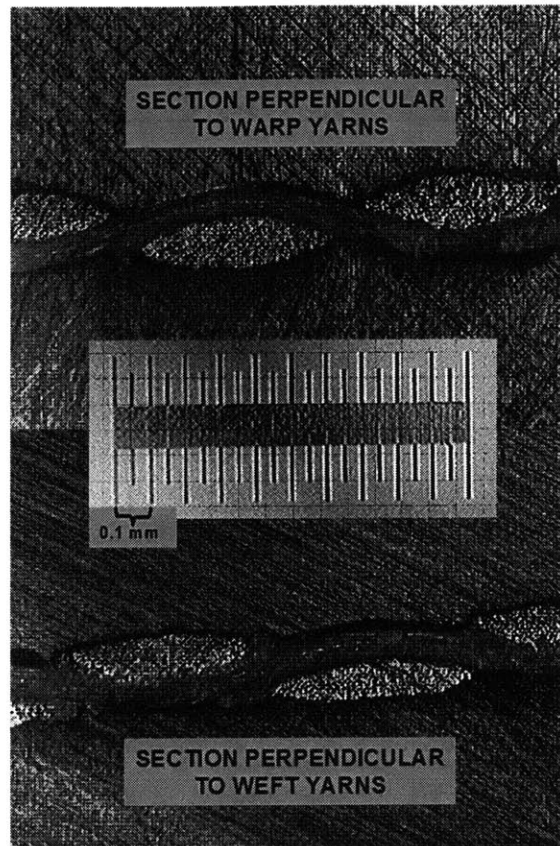


Figure 2-3: Kevlar style s706 cross sections

proposed.

Both ends of each yarn are first coated with a drop of 5-minute epoxy upon removal from the fabric to prevent the yarns from fraying. After measuring and marking the desired gauge length, the yarns are sandwiched and glued between two plates of material with rough surfaces such as emery boards. The initial gauge length of the specimen is taken as the yarn length between the two plates. During the test, the plates are gripped in the tensile jaws and help distribute a uniform pressure on the gripped region of the yarns. **Figure 2-4** shows a sandwiched yarn specimen. **Figure 2-5** shows a tensile test on Kevlar[®] yarn. With this techniques, slippage of the yarn and premature yarn failure at the grips were eliminated

A number of 3-inch single yarn specimens from both warp and weft directions were tested on a Zwick tensile tester model BTC-FR010TH.A50 at a strain rate of 0.01 s^{-1} . Strain is

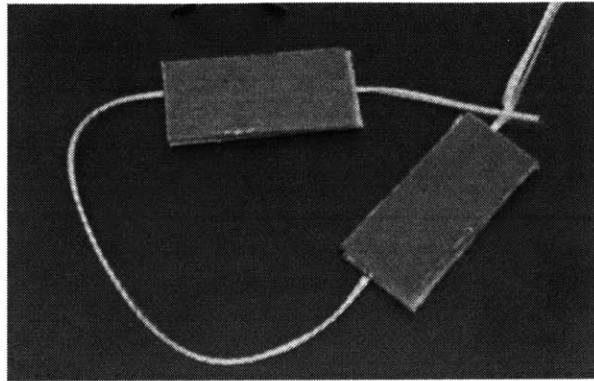


Figure 2-4: Yarn sandwiched specimen

measured from a contact-point extensometer attached on the inner edges of the plates as close to the initial yarn length as possible (see **Figure 2-5**). This precaution ensures that the effects of yarn stretch inside the plates and those of machine compliance are eliminated. Prior to each test, a preload of 0.5 N is applied to the specimen to obtain a consistent initial condition by eliminating the effects of yarn slack. A careful alignment of the specimen in the grips is also critical since yarn twist causes a non-uniform stress distribution in the yarn during the test.

Typical yarn responses under tensile loading are shown in **Figure 2-6**. The stress-strain response shows an initially compliant regime as the yarn uncrimps and straightens, followed by a linear elastic response up to failure. The warp yarns have a shorter compliant response due to lower initial crimp, and a larger average breaking stress, probably due to more moderate damage during the weaving process.

The axial stretching stiffness of the yarns is calculated from the slope of the linear portion of these curves and is reported in **Table 2.3**. The bending stiffness is calculated by manipulating the load-extension data in the uncrimping (low load) regime to obtain the moment acting at the crimp peaks as a function of the crimp angle. The measured bending stiffnesses reported in **Table 2.3** were relatively close (within 25%) to values estimated from the radii and moduli of the yarns.

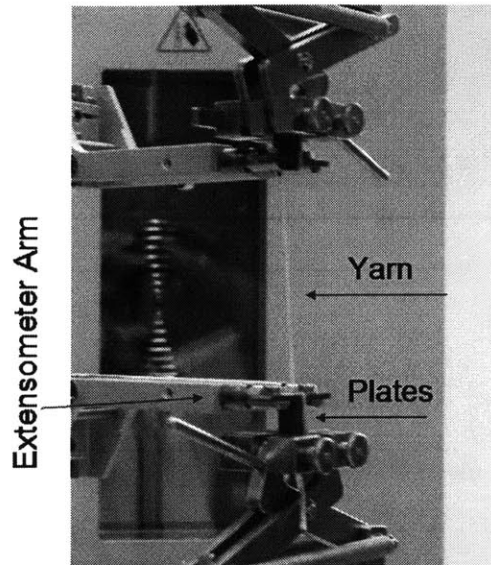


Figure 2-5: Single yarn test setup

Fabric Tensile Test

The characterization of fabric behavior under uniaxial loading along the direction of a yarn family is normally performed by one of two standard test methods. The first method is called "unravel strip test" and is performed by stretching a strip specimen of fabric with a large length-to-width ratio along the lengthwise direction. A unique characteristic of this test lies in a special step taken during the specimen preparation. To create a strip of specimen, the fabric is first cut into rectangular strips. Then, a number of yarns along the fabric length are removed from both sides of the fabric width, thereby producing a sample without yarn crossovers along the edges. This step is necessary to ensure that the effects of edge defects are minimized and that the loaded yarns will not slip out of the cross yarns during the test. The other standard method to evaluate the tensile response of a fabric is called "grab test". In contrast to the unravel strip test, a specimen for the grab test consists of a fabric strip with a small length to width ratio. The specimen width is usually larger than the width of the jaw grips, allowing the sample to be 'grabbed' in a central region while leaving the edges outside the jaws. As a result, the effect of damaged edges is eliminated.

In this study, the unravel strip test is selected over the grab test as a means to study the

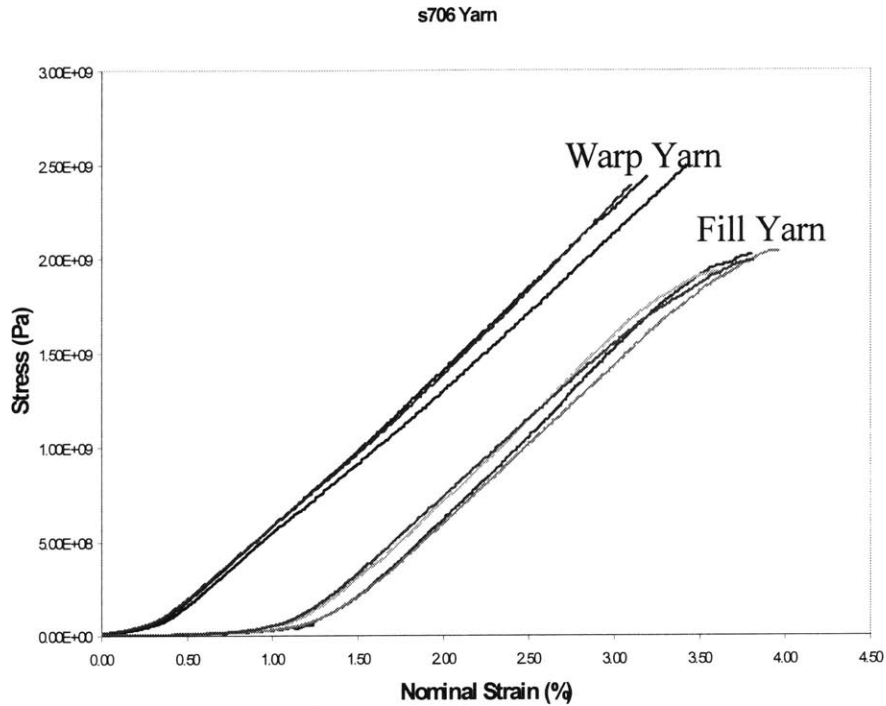


Figure 2-6: Kevlar yarn tensile test results

fabric behavior under tensile loading because the fabric properties obtained from the unravel strip test can be more directly related to the yarn properties.

Fabric Unravel Strip Test

Experimental Procedure A schematic of the unravel strip test specimen is shown in **Figure 2-7**. The Kevlar[®] fabric is cut into strips with a length of 14 inches and four sets of width - 1.5, 1, 0.75 and 0.5 inches. In each set, yarns were removed from both sides of the strip such that the samples are left with 34, 20, 10 and 5 longitudinal yarns, respectively.

Tests are conducted along both warp and weft directions on a Zwick tensile tester model BTC-FR010TH.A50 at a nominal strain rate of 0.01 s^{-1} . An optical extensometer from Correlated Solutions is used to record the real-time test progression and to analyze the local deformations on the specimen surface. A contact point extensometer is also used to obtain macroscopic strain measures. For each of the sample sets, tests were performed until at least five consistent

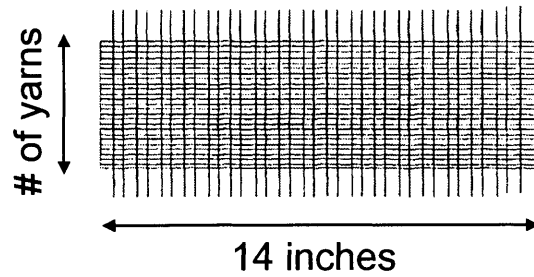


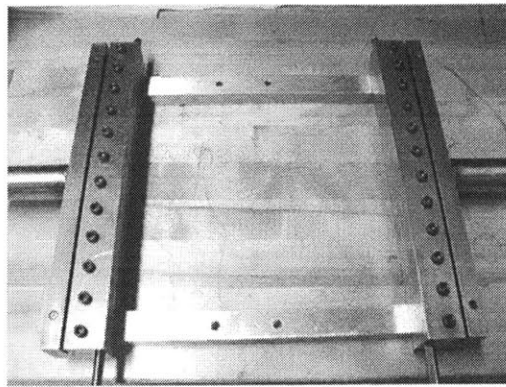
Figure 2-7: Schematic of an unravel strip test specimen (Realff 1992)

results were obtained.

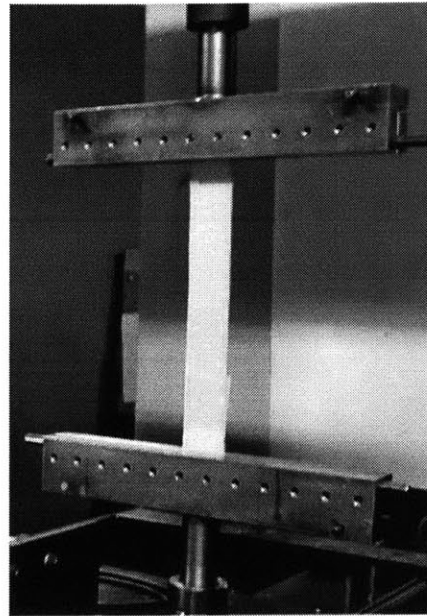
Due to the smooth surface of this particular fabric, standard approaches for gripping specimens in typical pincer or jaw grips resulted in sample slipping. Another drawback in using the standard tensile grips is the stress concentration induced around the jaw edges that causes the fabric to fail prematurely at the grips. In this study, a new set of custom made grips was fabricated to perform the fabric tensile strip tests, see **Figure 2-8**. The design details for these grips are given in Appendix A. By wrapping the sample around a small bar which fits in a groove between the jaws inserts, the fabric strip is prevented from slipping out of the jaws. The clamping edges define the fabric initial gauge length. The initial gauge length of the unravel strip specimens was 10 inches.

Results and Discussions Typical stress-strain responses of the unravel strip tensile test along warp and weft directions are shown in **Figure 2-9**. The deformation progression of the test is monitored by a video camera, and can be described as follows.

In the low-load region of the response, the crimp in the loading direction decreases while the crimp in the cross direction increases. This behavior termed "crimp interchange" continues until the yarns in the loading directions are fully straightened, or in some cases, until cross yarns wrap around loaded yarns and thereby prevent them from extending. This yarn wrapping behavior is called "jamming" or "locking" and usually occurs in dense weave fabrics. As the strain is increased, the yarns in the loading direction are extended and become compacted. The load-extension relationship in this region depends on the mechanical properties of constituent



(a)



(b)

Figure 2-8: Fabric uniaxial tensile grips (a) and Fabric unravel strip test set up (b)

yarns. In this case, the Kevlar[®] fabric exhibits a linear response.

At some level of applied deformation, yarns in the loading direction will reach their maximum elongation and fail, resulting in a decrease in the fabric load-carrying capacity, and eventually, failure of the fabric strip. The onset of fabric failure, with the first yarn breakages, typically occurs at the edges of the strip. As strain increases, the failed yarns slip away from the failure site and the load is partially redistributed onto neighboring yarns, causing them to fail as well. This load transferring mechanism continues until the fabric fails catastrophically as observed by a dramatic drop in load. A wavy pattern can be observed on the fabric surface, suggesting that yarns are slipping and pulling out of the fabric. **Figure 2-10** summarizes the discussed behaviors.

As indicated in **Figure 2-9**, the load-per-unit-width data can be expressed in terms of a nominal average stress, as the quarter wavelength of the fabric and the yarn net cross sectional area are known - the slope of the stress-strain curve in the linear region can then be considered a measure of the "Young's Modulus" for the fabric along the yarn family parallel to the loading

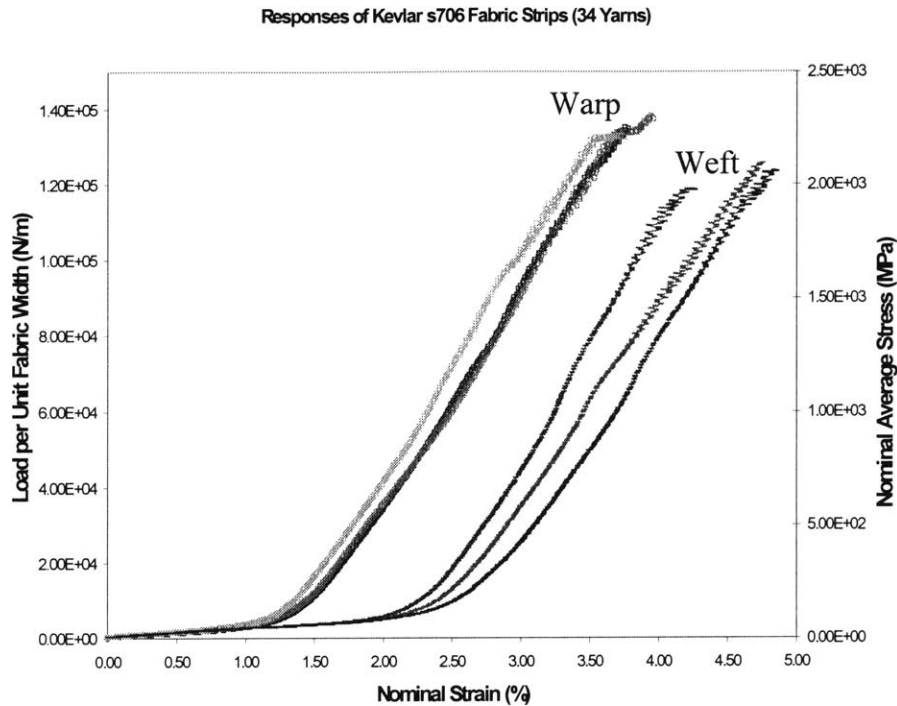


Figure 2-9: Stress-strain responses of Kevlar fabric unravel strip tests on warp and weft directions

axis.

The effects of specimen width on this normalized fabric parameter were investigated. **Figure 2-11** shows the results of such investigation plotted in term of the averaged "Young's Moduli" as a function of number of yarns in the specimen width. This plot suggests that, for the considered range of configuration, this property can be considered independent of the specimen width-to-length ratio.

Fiber Tensile Test

With a diameter of approximately 12 microns, single Kevlar[®] fibers are fragile and are not suitable for regular tensile testing techniques. Pulling fibers out of the yarn or gripping fibers on regular jaws can potentially damage the fibers by causing them to kink or fail. A novel approach of testing fiber on a regular tensile tester is therefore proposed as follows. First a

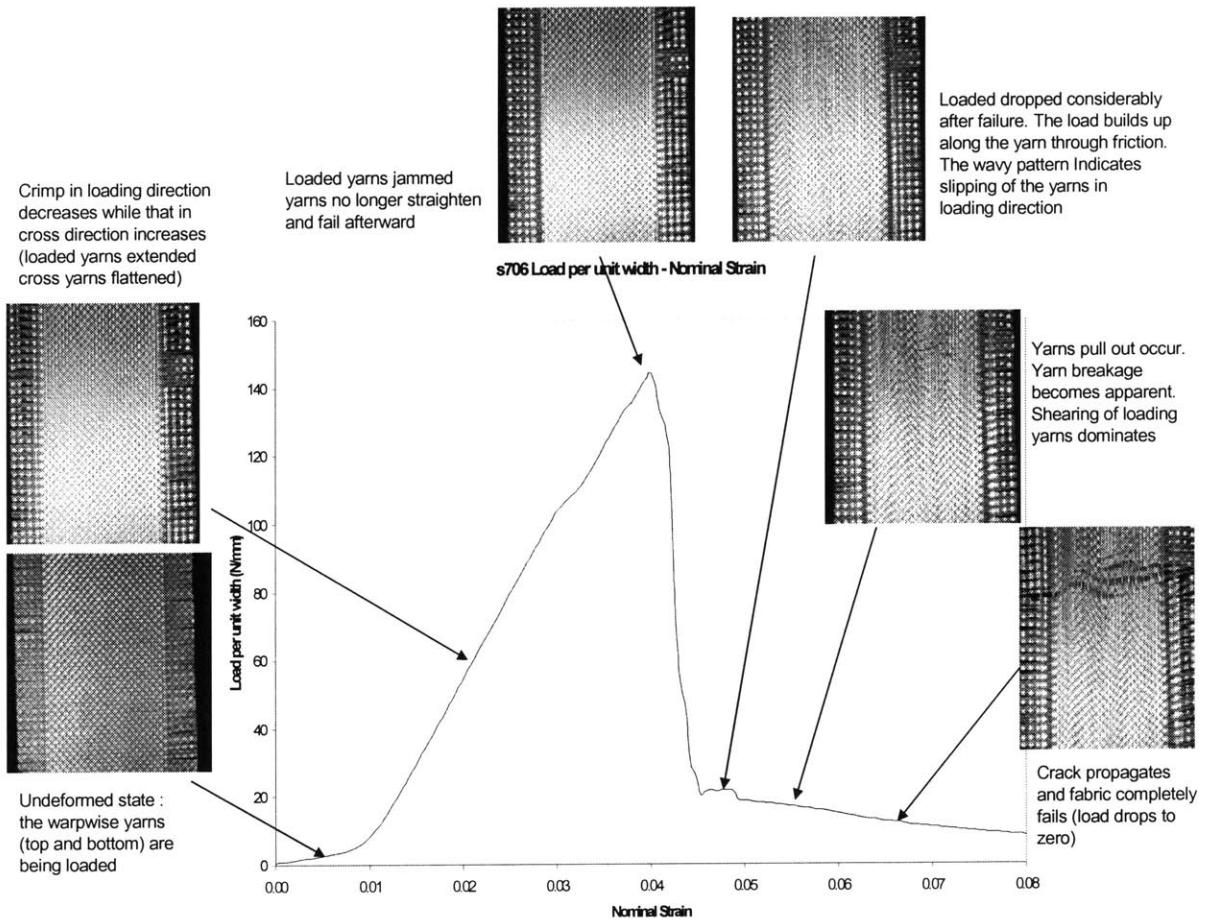


Figure 2-10: Fabric deformation and failure mechanisms during an unravel strip test

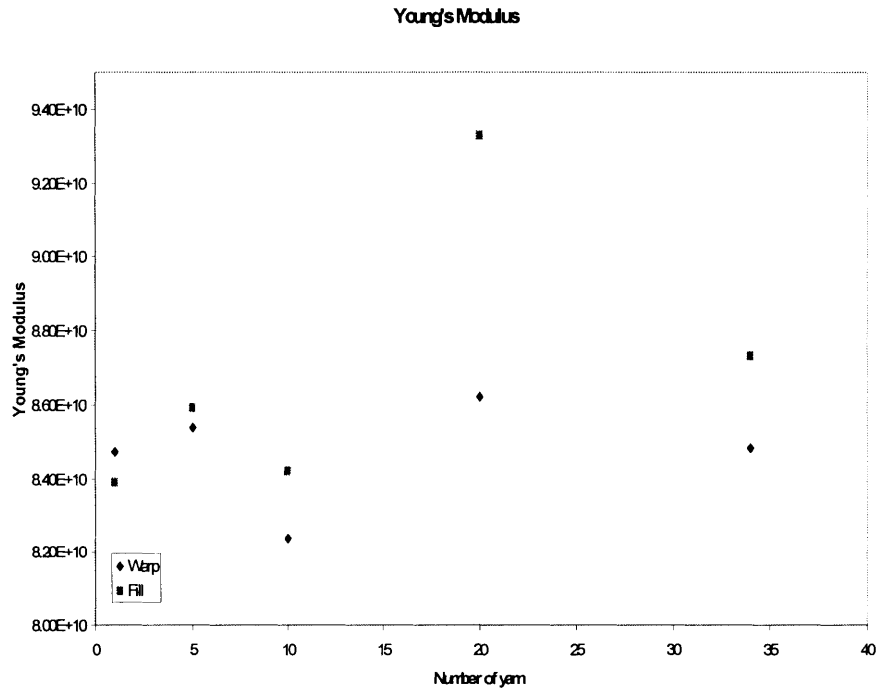


Figure 2-11: Influence of specimen width in fabric tensile tests

yarn is cut into a desired length and single fibers are pulled out of the yarn under an optical microscope. To ensure consistency between the fibers, each of them is carefully checked for irregularities such as kinks or surface damage. Each of the "good fiber" strands is then placed on a paper coupon cut into 40 by 20 mm with a center slot of 20 by 10 mm. Tape is used to loosely hold the single fiber onto the coupon. The regions of the fiber along the edges of the slot are marked and glued to the coupon using 5-min epoxy, creating a coupon specimen with approximately 20 mm initial gauge length. The marking on the fiber serves as a means to check for fiber slipping during the test. **Figure 2-12** shows a coupon specimen of Kevlar[®] fiber.

The coupon specimens can be gripped directly on any jaw inserts of regular tensile testing machine. In this study, the Kevlar[®] fibers were tested using the same Zwick machine used in the yarn and fabric tests but a load cell with a smaller force resolution (one micronewton) was used. After gripping the coupon in the testing machine, the coupon lateral legs are cut prior to each test so that the fiber carries the entire applied load. A preload of approximately one

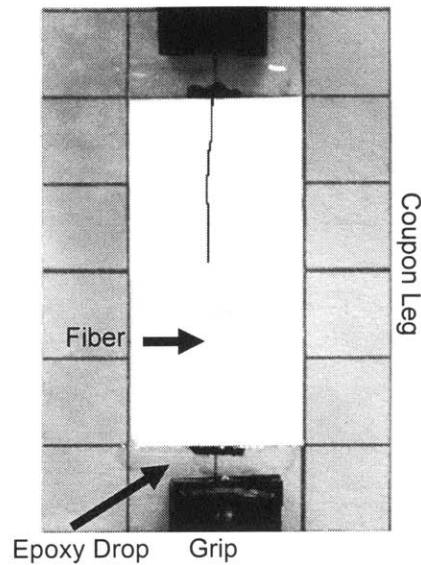


Figure 2-12: Fiber coupon specimen (half of fiber highlighted for clarity)

millinewton was applied to the fiber before each test to eliminate kinks and slacks on the fibers. Ten tests were performed for the fibers taken from warp and weft yarns at a nominal strain rate of 0.01 s^{-1} .

Figure 2-13 shows typical plots of stress-strain data from fiber tests. The graph indicates that Kevlar[®] fibers exhibit a linearly elastic behavior up to failure, which is consistent with the results from yarn and fabric strip tests.

Comparison between Fabric, Yarn and Fiber Behaviors from Tensile Tests

Figure 2-14 shows the stress-strain plots for tensile tests on Kevlar[®] fabric style 706, its constituent yarns and fibers along both warp and weft directions. **Table 2.2** summarizes the values of averaged Young's moduli, ultimate tensile stresses, and elongations at break calculated from this figure. The modulus of Kevlar[®] fabric style 706 obtained from the strip tests are within 10% of the manufacturer's value listed in **Table 2.1**. The Young's moduli of fibers, yarns and fabric strips are consistent, thus validating the three different testing protocols developed for the fabric and its components.

According to **Table 2.2**, the ultimate tensile strength decreases as the length scale and

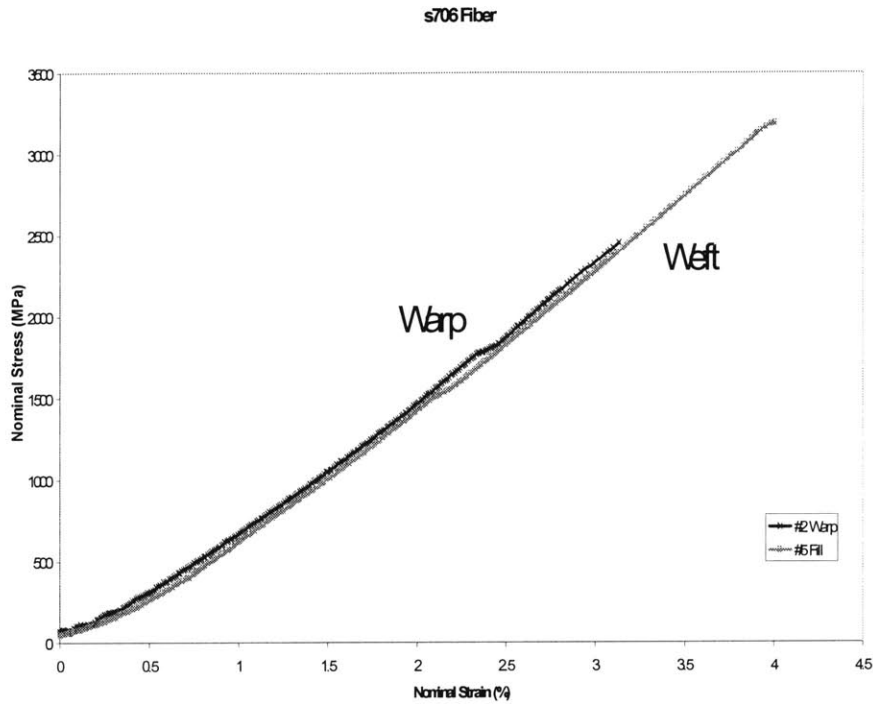


Figure 2-13: Stress-strain plots of Kevlar fiber tests from warp and weft yarns

complexity of the structure increases. The decrease in ultimate tensile strength is a result of uneven load distribution and defects in the larger structures. For example, some fibers in a yarn bundle could have defects that cause them to fail earlier than perfect fibers. The load initially experienced by the failed fibers then has to be redistributed among the remaining fibers, causing them to fail as well. A similar argument could be applied for the lower ultimate tensile strength observed in the fabric, although for this case, numerical simulations of the fabric strip test ([41], [42]) indicate that effects of fabric constraints at the grips and the resulting uneven

S706	Fiber		Yarn		Fabric	
	Warp	Weft	Warp	Weft	Warp	Weft
Young's Modulus (GPa)	82	85	85	84	85	87
Ultimate Tensile Strength (MPa)	2950	3200	2330	2960	2250	2040
Elongation at Break (%)	3.4	3.8	3.2	3.8	3.8	4.6

Table 2.2: Comparison of the tensile test results from fabric, yarn and fiber of Kevlar S706

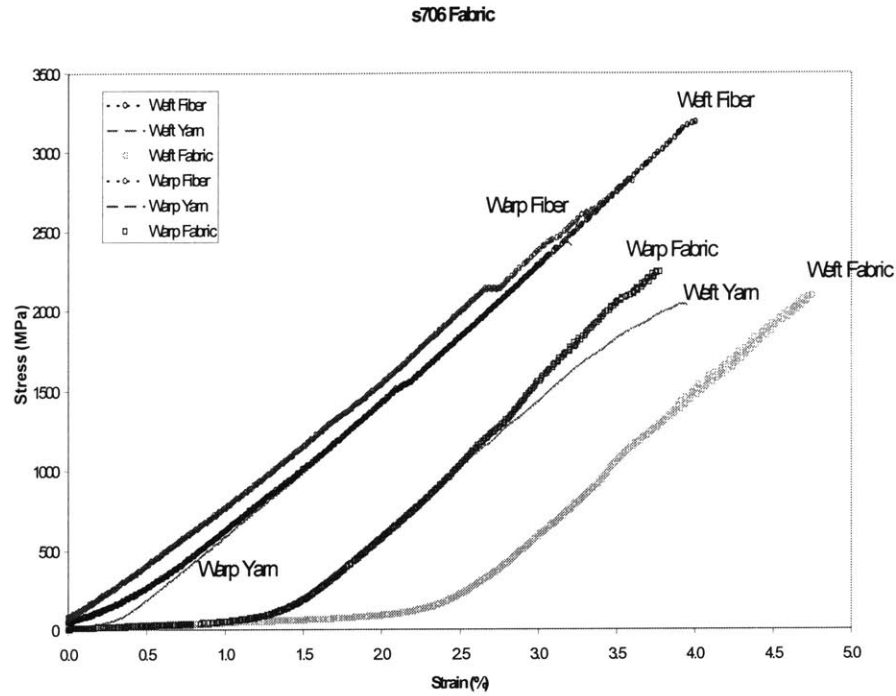


Figure 2-14: Stress - strain plots of fabric, yarn and fiber tensile test

stress distribution are the cause of the premature strip failure.

A comparison of elongation at break for the three structures is not meaningful since each of them undergoes different deformation mechanisms. In the other words, the axial tensile response of fibers is purely dominated by fiber stretching, while that of the yarns is dominated by yarn unbending followed by yarn stretching. The fabric tensile response is the most complex, since it is initially governed by crimp interchange followed by locking and stretching of yarns parallel to the loading direction.

On the other hand, the values of the elongation at break of the two yarn families for the same structure can be directly compared since they undergo similar deformation mechanisms. A comparison of these values reveals that the structures along the weft direction have higher breaking strains than those along the warp direction. This is due to the combination of two factors: first, the weft fibers have sustained less damage from weaving process, and therefore have a slightly higher average elongation at break; and second, the weft yarns have higher initial

crimps as shown in **Figure ??**, and therefore these yarns can undergo a longer stretch.

2.2.3 Interaction of Yarns at the Crossover Points

Of the 15 constitutive parameters required by the fabric model, the six parameters involving the tensile and bending stiffnesses of the yarns are obtained from data presented in the previous section and the two mass densities of the yarns are obtained from published values. The remaining properties, which describe the crossover point interference behavior, the locking behavior and the yarn rotation behavior, relate to deformation mechanisms that are controlled by interactions between yarns of different families. These properties are determined by fitting the fabric response in simple, homogeneous modes of deformation. These tests are targeted to identify the specific physical properties relating to the interaction of the yarn.

Out-of-plane Compression Test

The first set of tests is the out-of-plane compression test aimed toward determining the properties that govern interference at the crossover points. Since fabrics usually have small thicknesses, transverse compression tests on a single layer of fabric require high-precision testing equipment. Also, errors in such test could easily arise from fabric mishandlings such as twisting or bending. Compressing multiple layers of fabric minimizes these problems, and provides a larger displacement signal. Multiple layers of fabric are sandwiched between plates of aluminum and stacked. A schematic of this "sandwich compression test" is shown in **Figure 2-15**. By assuming that the deformation of the aluminum could be neglected and that all fabric layers are identical, the test configuration can be represented by a series of spring, with each spring corresponding to the out-of-plane stiffness of a fabric layer. The stiffness of a fabric layer could be further normalized by the number of yarn crossover points on the fabric surface to obtain an estimate for the transverse stiffness for each yarn crossover point.

Experimental Procedure Fabrics are cut along the yarns into square specimens with sizes of 20 by 20 mm and 10 by 10 mm. Yarns along the cut edge are removed and the number of yarns on each direction is manually counted to ensure consistency among the specimens. Tests are performed by compressing a stack of aluminum plates and fabric sheets, as depicted in

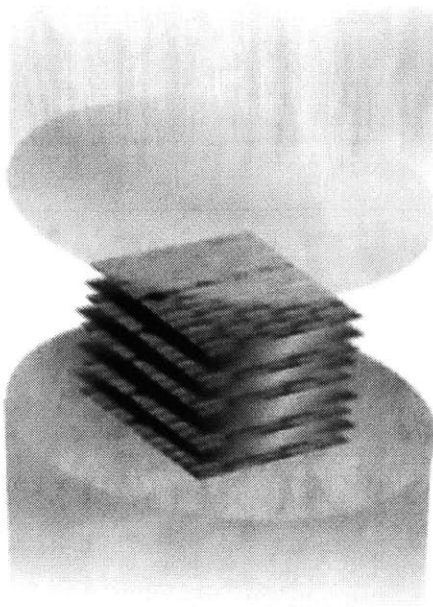


Figure 2-15: Schematic of out-of-plane compression sandwich test

Figure 2-15, to a pre-specified distance, using a 2" cylindrical aluminum compression platen on a Texture Analyzer model TA-XT Plus. Stacks of 2, 3, and 4 layers of fabric-aluminum pairs are tested for both sizes of fabric specimens at a displacement rate of 0.4 millimeters per minute.

Results and Discussions Test results are plotted in term of normalized load and transverse displacement per crossover point in **Figure 2-16**. The graph shows a consistent set of data for all testing configurations.

An exponential fit to these data provides the trends in yarn intersection properties that directly relate to interference stiffness at the crossover points as well as locking. Since the interference stiffness at the yarn crossover points is only one of many competing deformation modes present in this test configuration, the material parameters directly obtained from a fit of these data are excessively compliant to represent interference stiffness and need to be appropriately scaled. The scaling factor was obtained by fitting the constitutive fabric model to the low-load portion of the tensile test on fabric strips, as crimp interchange dominates the

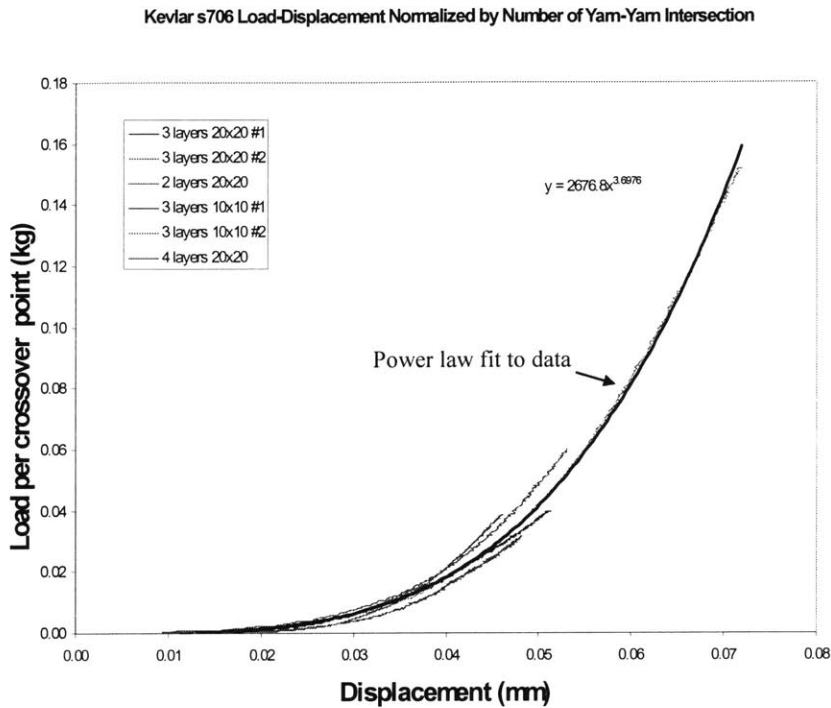


Figure 2-16: Load and displacement plots normalized by number of crimps from various configurations of out-of-plane compression tests

fabric response in the region. The values selected for the scaled interference properties are given in **Table 2.3**.

In-plane shear test

The shear response of woven fabric is different from the shear response in metals and other homogeneous material sheets due to the fabric unique interlacing structure. In particular, the in-plane shear response of fabric is dominated by the relative rotation of the two yarn families. This behavior, termed intraply shear, is responsible for many distinct features observed during shear deformation of woven fabrics. **Figure 2-17** shows the typical response of a woven fabric under a shear load accompanied by a description of mechanisms corresponding to each stage of deformation.

In the initial stage, the yarns are orthogonal to one another. As the load increases, the yarns

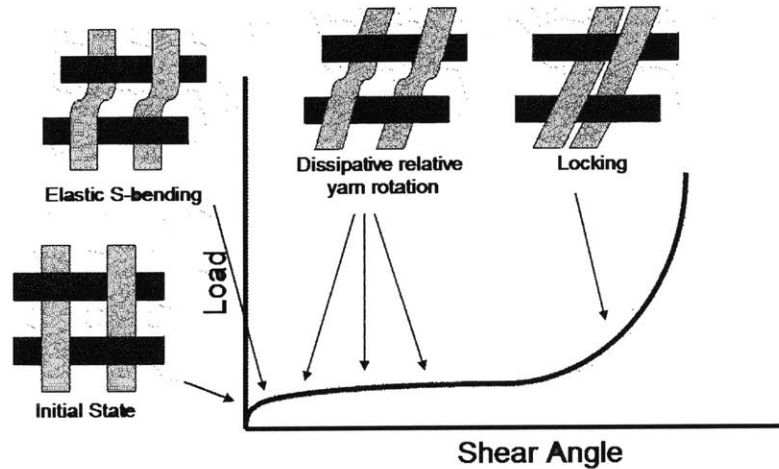


Figure 2-17: In-plane shear response of woven fabric (adopted from Lussier 2002)

initially accommodate very small macroscopic shear angles through elastic s-bending. The onset of dissipative relative yarn rotation occurs when the movement transmitted at yarn crossover points exceeds the static frictional resistance to relative yarn rotation. Further deformation results in yarns touching and compacting upon one another. As yarns are compressed, shearing stiffness in the fabric increases. The yarn-on-yarn compression continues up to the point where the yarns cannot be compacted further and the in-plane movements of the yarns are prohibited. The level of the deformation corresponding to this condition is commonly referred to as fabric's locking angle. Further increase in load causes the fabric to wrinkle out of plane, with a further increase in stiffness.

Two types of in-plane tests where shear is the predominant mode of deformation are investigated in this study. Picture-frame shear tests were performed by clamping all four edges of a square sheet of fabric on a rhomboidal fixture with hinged corners, fixing one corner of the fixture, and displacing the opposite corner along the diagonal direction. The imposed frame deformation causes the yarns to rotate. Results from the picture-frame shear test provide a means to measure parameters related to the elastic stiffness of yarn rotation through s-bending, the rate-dependent dissipative yarn rotation properties, and the locking parameters

The other type of in-plane shear test conducted in this study is the bias extension test, which is performed by pulling a strip of fabric at 45 degrees to the yarn directions, thereby

imposing a shear deformation on the central portion of the specimen. The portions of the specimen where the yarns are constrained by the fixtures experience more complex modes of deformation involving yarn tension. The complex modes of deformation imposed by this test configuration make this test unsuitable for fitting model parameters. Hence, the results of the bias extension tests are primarily used as validation for the fabric model. Detailed descriptions of these tests are presented in the following sections.

Picture-frame shear test The picture-frame or trellis frame shear test uses a specially designed fixture that imposes a deformation on a square sheet of fabric which preserves yarn lengths, thus preventing the yarns from being stretched. This apparatus is essentially a square, four-bar linkage with hinged corners as shown in **Figure 2-18**. Initially, the fabric is clamped such that the two yarn families are oriented parallel to the two perpendicular sides of the square frame. A test is performed by fixing one corner of the square and displacing the opposite corner along the diagonal direction. As the test progresses, the fabric assumes a rhomboidal shape that continuously evolves with the applied displacement. To compare test results from different specimen dimensions and fixtures, the data can be further normalized by the total deformable area of the fabric as suggested by Lussier [54] and Peng et al. [62].

There is one major drawback associated with this testing technique. It has been found [26],[54] that fabric irregularities such as wrinkles or yarns misalignments (i.e. if the two yarn families are not exactly perpendicular to each other) significantly affect the test results. A number of approaches have been proposed to eliminate the effect of the fabric irregularities. Harrison et al. [26] proposed the method of pre-tensioning the specimen prior to the test. Though this approach can eliminate wrinkle and yarns misalignment, the level of load used in the pre-tension process is still subjective and affects test results. Lussier [54] proposed another alternative technique, termed "mechanical conditioning", which consists of repeating the same shear test a few times before recording the data. The method is proven to be quite effective in obtaining consistent test results, but the interpretation of the results obtained from this approach is still questionable due to effects of inelastic deformation in the cyclic conditioning that precedes the test.

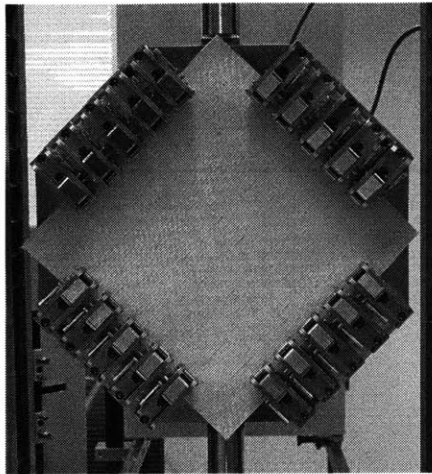
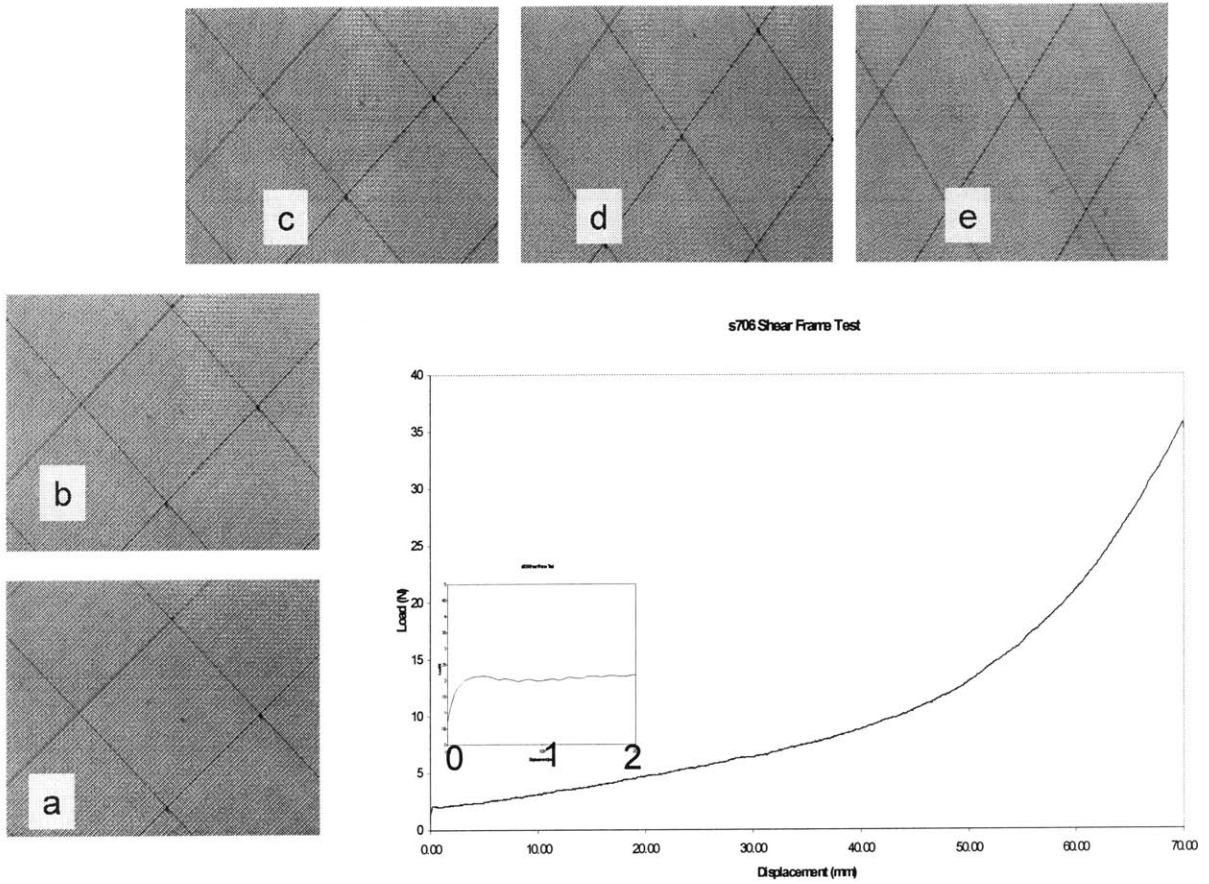


Figure 2-18: Picture-frame test configuration

Experimental Procedure The picture-frame shear fixture was fabricated by Deben Co., UK as shown in **Figure 2-18**. The specimen for this fixture is a square sheet of fabric with dimensions of 290 by 290 mm. The specimen is clamped onto the fixture through a set of toggle clamps called QuickRelease[®] grips manufactured by Deben. In the clamped position, the specimen is left with an area of 250 by 250 mm of deformable material. Lines are drawn on the specimen parallel to the yarn directions at a constant interval to help visualize the evolution of the angle between the two yarn families. An optical extensometer system is used to observe the yarn movements and to correlate the recorded progression with the experimental data. Tests are performed at a displacement rate of 30 mm per minute along the specimen diagonal, which corresponds to an initial yarn rotation rate of approximately 3×10^{-3} radian per second on the Zwick mechanical tester.

Results and Discussions **Figure 2-19** shows a load-displacement plot for a picture-frame shear test with images corresponding to subsequent stages of deformation. The initial portion of the graph depicts a linear response corresponding to the elastic macroscopic rotation through yarn S-bending. Following this regime is a region where the yarns undergo dissipative relative rotation at the yarn crossover points. The last portion of the curve is dominated by shear locking effects. Fabric wrinkles can be observed on the specimen at loads higher than 15N.



a = 0mm; b = 10mm; c = 20mm; d = 50mm; e = 70 mm

Figure 2-19: Picture-frame shear test result and test evolution

Model parameters related to locking, as well as the elastic and dissipative components of the yarn rotation response are determined by fitting the results of a shear frame numerical simulation to the experimental data. These parameters are reported in **Table 2.3**.

Bias Extension Test The bias extension test is performed in this study primarily to test the prediction capability of the proposed fabric model. The descriptions of experimental procedure, common problems, and typical responses of this testing technique are given as follows.

The bias extension test is similar to the uniaxial test of fabric strips, except that the fabric specimen is prepared with yarns oriented at a ± 45 degree with respect to the clamps. The test is performed by applying a displacement at the top clamp, causing the yarns that are not

constrained by the grips to rotate. The rotation of the yarns induces a moment on the yarn crossover points. **Figure 2-20** shows the schematic of a bias extension test.

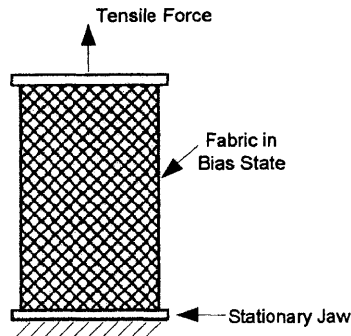


Figure 2-20: Schematic of bias extension test (Lussier 2002)

Two major problems associated with the bias extension test are the sensitivity of results to specimen length to width ratio and the non-uniform shear deformation experienced by the specimens. Wang et al. [84] suggested that to obtain a pure shear deformation region in the bias extension test, the length to width ratio of the specimen must be at least two or greater. If the aspect ratio is less than or equal to one, there will be an excessive constraint from the clamp ends that prohibits yarn rotation. If the aspect ratio is greater than one but less than two, only a small region at the center of the specimen will undergo a pure shear deformation while the remaining region experiences a combination of tension and shear. If the specimen aspect ratio is greater than two, the center region of the specimen will no longer be constrained by the clamps. The yarns in this region are free to rotate, and a pure shear deformation can be observed. **Figure 2-21** illustrates the effect of the specimen aspect ratio to the modes of deformation in the bias extension test.

There are three distinct zones representing different modes of deformation in the bias extension specimen as shown in **Figure 2-22**. Zone 1 is represented by a triangular area at the grips at which the yarn movements are fully constrained, resulting in no noticeable deformation. Zone 2 is composed of four triangular regions adjacent to Zone 1. The deformation governing these regions is a combination of shear, yarn extension and yarn slip. Zone 3 is the middle region of the specimen where the yarns can freely rotate and a pure shear deformation can be

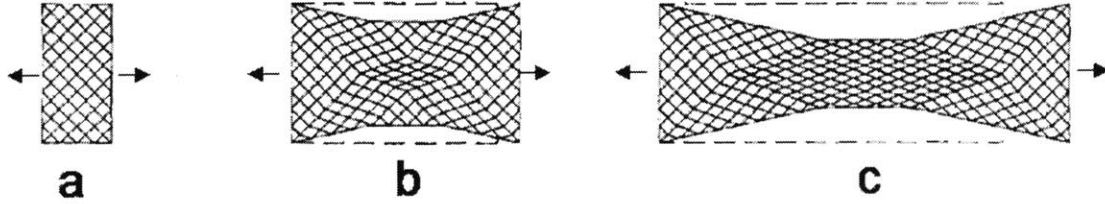


Figure 2-21: Influence of aspect ratio on bias extension test (a: $AR < 1$; b: $1 < AR < 2$; c: $2 < AR$) (Wang 1998)

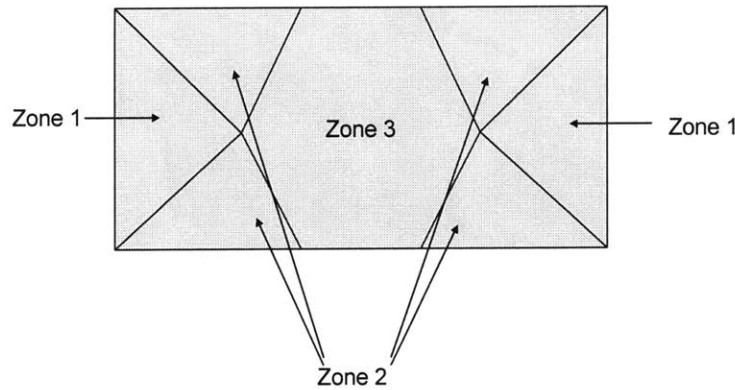


Figure 2-22: Different modes of deformation in the bias extension test (Lussier 2002)

observed.

Experimental Procedure The experimental setup for the bias extension test is similar to the set up for the uniaxial unravel strip test. The specimen dimensions, however, are slightly different ($1\frac{3}{8}$ in (35 mm) wide by 3.75 in (95 mm) long). Nine tests were performed at a nominal axial strain rate of 1 mm/sec until the fabric fails following the onset of yarns slipping. An optical extensometer was used to record the test progression and to correlate the recorded images with the load and extension data.

Results and Discussions Figure 2-23 shows the load-extension plots for all tests. The extremely low initial resistance to shear deformation combined with the sensitivity to initial bias angle at failure causes substantial variations in test results, both in terms of the initial rise

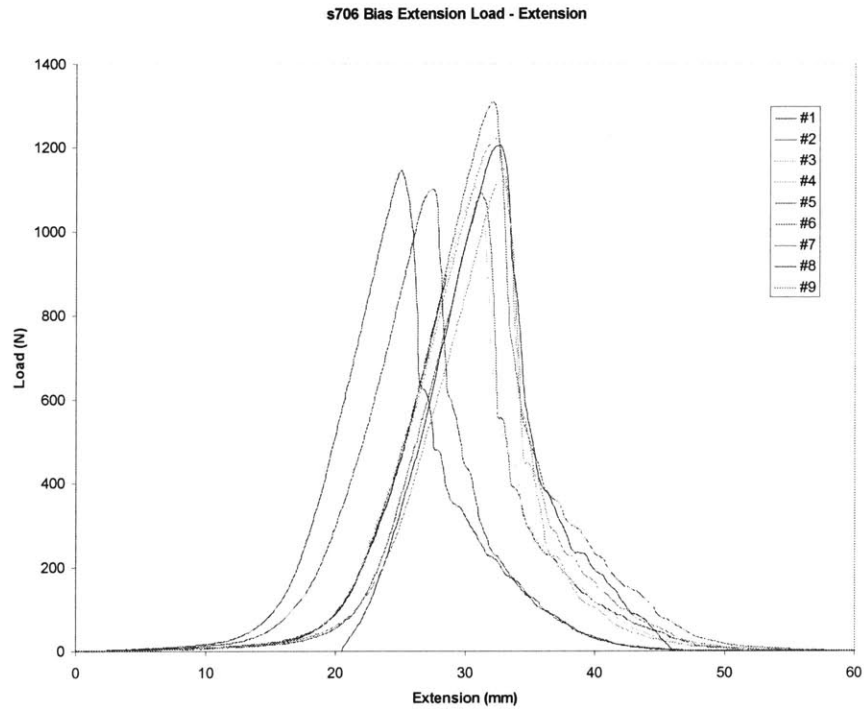


Figure 2-23: Load - displacement plots of bias extension test

in stiffness as well as of the maximum load at break. The initial portion of the graph, where the stiffness is extremely low, corresponds to the regime of free rotation for the yarns in Zone 3. The stiffness begins to rise at the shear-locking angle. After this point, a wrinkle occurs in the pure shear region (Zone 3) and the yarns around the zone boundaries begin to slip. Failure occurs when the yarns at the boundaries are completely pulled out of the fabric. **Figure 2-24** summarizes the discussed mechanisms.

The bias extension test is not suitable for determining the model parameters due to the coupling effect of shear and tensile deformations presented in the macroscopic response of this test. The test results are instead used as a qualitative comparison to the model prediction as will be discussed in the following section.

Property	Symbol	Value	Unit
Geometric Properties			
Fabric Thickness	-	0.3	mm
Warp Through-thickness Radius	r_1	0.075	mm
Weft Through-thickness Radius	r_2	0.075	mm
Warp In-plane Radius	R_1	0.4	mm
Weft In-plane Radius	R_2	0.4	mm
Initial Warp Quarter Wavelength	0p_1	0.374	mm
Initial Weft Quarter Wavelength	0p_2	0.374	mm
Initial Warp Amplitude	0A_1	0.060	mm
Initial Weft Amplitude	0A_2	0.090	mm
Initial Warp Half Yarn Length Between Crossovers	0L_1	0.378	mm
Initial Weft Half Yarn Length Between Crossovers	0L_2	0.384	mm
Warp Relaxed Crimp Angle	${}^0\beta_1$	1.412	radians
Weft Relaxed Crimp Angle	${}^0\beta_2$	1.334	radians
Constitutive Properties			
Warp Yarn Stiffness Per Half Yarn Length	k_1	3764	N/m
Weft Yarn Stiffness Per Half Yarn Length	k_2	3948	N/m
Warp Yarn Bending Stiffness	k_{b1}	0.00124	Nm/radian
Weft Yarn Bending Stiffness	k_{b2}	0.00073	Nm/radian
Warp Yarn Mass Density	ρ_1	1441	kg/m ³
Weft Yarn Mass Density	ρ_2	1441	kg/m ³
Interference Relation Coefficient	K_I	0.00309	N
Interference Relation Exponent	a	1×10^6	1/m
Locking Stiffness	K_d	1.36×10^{13}	N/m
Locking Exponent	c	3.7	-
Elastic Rotational Stiffness	K_s	0.0131	Nm/radian
Reference Dissipative Rotation Rate	$(d\gamma/dt)_0$	0.00284	radians/s
Reference Dissipative Rotation Moment	M_0	3.2×10^{-6}	Nm
Dissipative Rotation Rate Sensitivity	b	4.0	-

Table 2.3: Parameters for King's woven fabric model (King 2004)

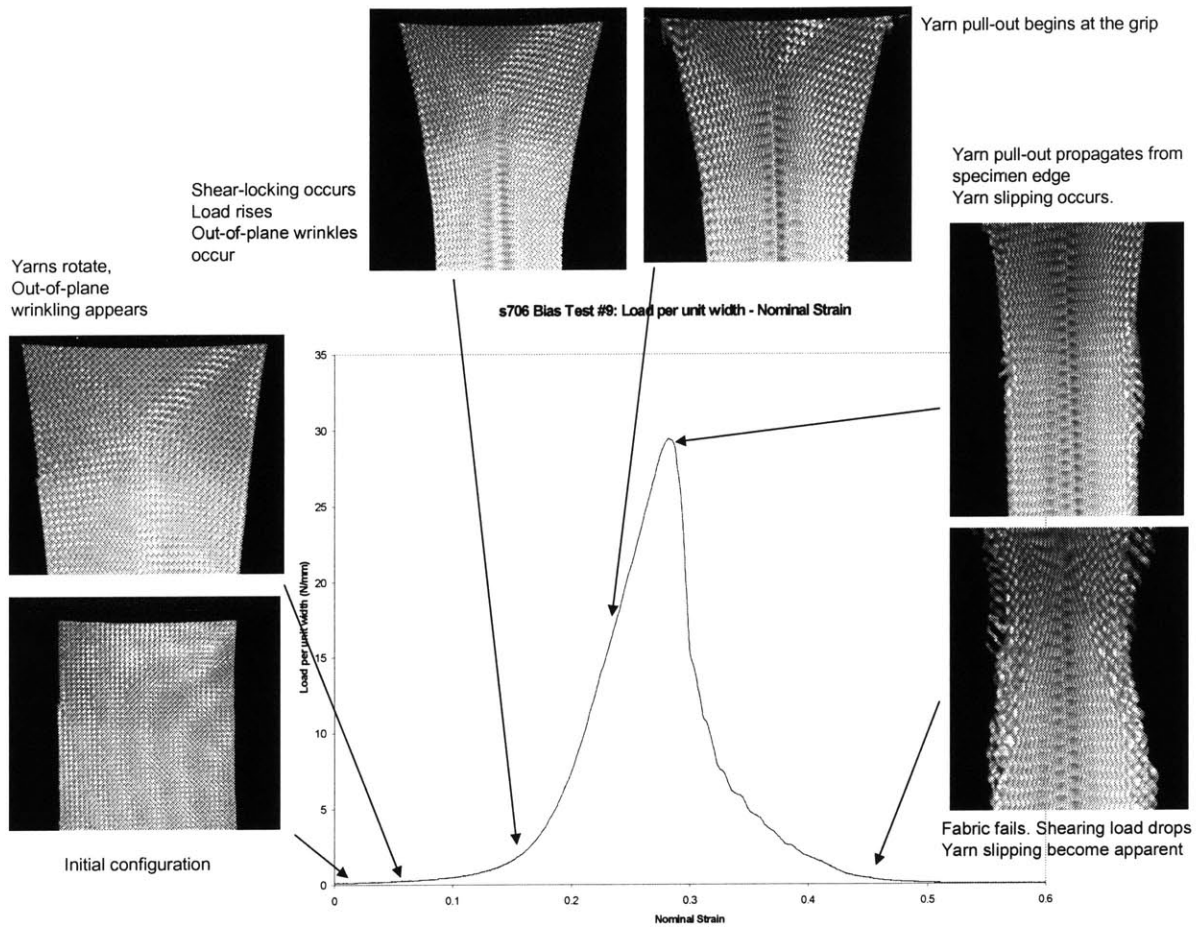


Figure 2-24: Summary of deformation mechanisms in the bias extension test

2.2.4 Comparison of Model Predictions with Experimental Findings

Three sets of simulation corresponding to the unravel strip tests of two yarn family directions, and the bias extension tests of Kevlar[®] fabric are created in ABAQUS/Standard using the model parameters in **Table 2.3**. The predictive capabilities of the constitutive model are assessed by comparing the predictions of these simulations to the experimental results in three areas: the macroscopic deformation, the macroscopic load-extension response, and the mesostructural response of fabric subjected to macroscopic loading.

In term of the prediction of macroscopic deformation, the model can accurately predict the level of contractions in the uniaxial strip tests due to crimp interchange. Specifically, the

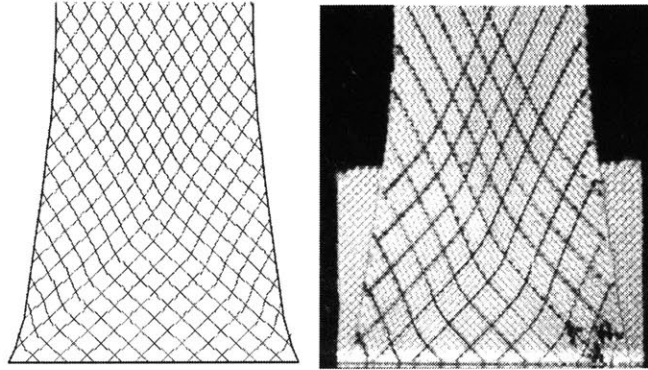


Figure 2-25: Predicted and observed deformation and yarn orientation for bias extension test at 17% nominal axial strain (King et al. 2004)

model predicts that, for the warp direction, the region of uniform contraction in fabric strip at 4% nominal axial strain will have undergone a 4.5% transverse contraction compared to a 4.0% average contraction observed in the experiment. For the weft direction tests, the model predicts a 5.8% contraction at 4% nominal axial strain, compared to a 5.9% average contraction observed in the experiments. The model can also accurately predict the macroscopic deformation in the bias extension test as shown in **Figure 2-25**, which illustrates the predicted and observed deformed shapes and yarn orientations for the bias extension test near the lower grip.

The model is also capable of predicting the macroscopic load-extension response of the fabric. **Figure 2-26** and **2-27** show the experimental load-extension curves for the warp and weft direction tests, along with the corresponding model predictions. The model accurately predicts the correct mechanical response using only the properties determined independently from the previously described tests; no curve fitting is performed.

Figure 2-28 shows the model prediction of the load-extension curve in the bias extension test. This figure illustrates that the model is capable of capturing the macroscopic response of the bias-extension test up to when the experimental observation indicates the beginning of fabric failure by means of yarn slipping (refer to **Figure 2-24**). The model response is too stiff after this point compared to the experiments because the wrinkling and unraveling of the fabric weave result in a more compliant response and because the current model is only capable of capturing failure-free in-plane deformation.

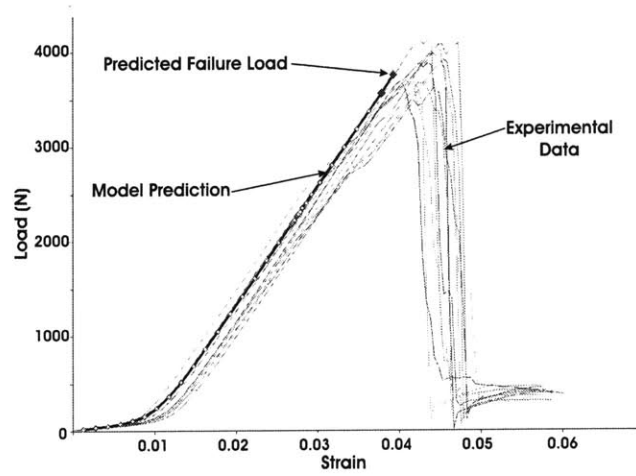


Figure 2-26: Model prediction of load-strain behavior in warp direction test compared to the experiments

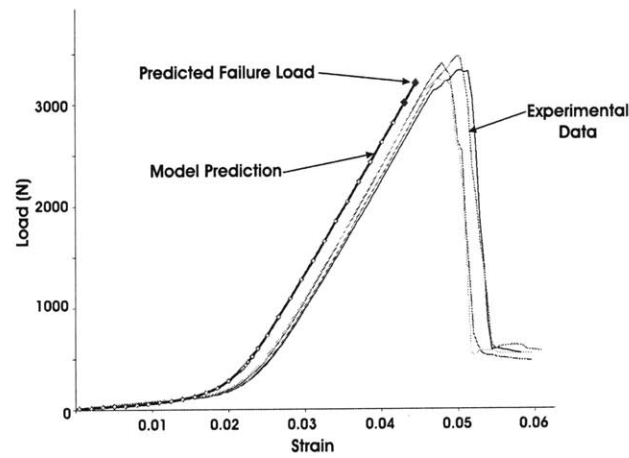


Figure 2-27: Model prediction of load-strain behavior in weft direction test compared to the experiments (King et al. 2004)

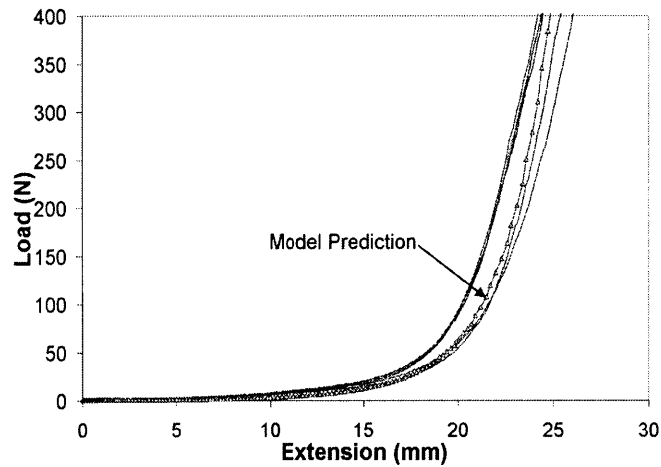


Figure 2-28: Model prediction of load-strain behavior in bias extension test compared to experiments

The model is also capable of predicting the mesostructural response of the fabric subjected to macroscopic loading, particularly in regards to the onset of failure. In **Figure 2-26** and **2-27**, the data points that lie at the end of the model curves mark the conditions at which the model predicts the onset of failure. The model predictions agree very well with the experimentally observed macroscopic fabric failure loads.

Chapter 3

Characterization of the Mechanical Response of Nonwoven Fabrics

3.1 Background

Nonwoven fabrics are sheet structures created by forming or interlocking a web of fibers through mechanical, thermal or chemical processes. In general, the mechanical response of nonwoven fabrics exhibit two major characteristics. First, the response of nonwoven fabrics is inhomogeneous, as areas where the fibers are bonded or entangled are stiffer than areas where the fibers are free to move. Second, the response of the fabric varies significantly when the fabric is loaded along different directions. This behavior, termed "fabric anisotropy", is particularly evident when comparing the fabric responses for in-plane loading and for out-of-plane loading. The responses for different in-plane loading directions can also vary depending on the existence of preferential orientation in the arrangement of the fibers.

This study focuses on the mechanical response of high performance ballistic nonwoven fabrics. Many of the commercially available ballistic nonwoven fabrics are provided in the form of needlepunched nonwoven felts. To limit the scope of the study, two ballistic nonwoven fabrics are selected as representative materials. The first selected fabric is a needledpunched web of aramid fibers called "ProTechtor[®]", manufactured by National Nonwovens. The second fabric is called "Dyneema Fraglight[®]", a web of high density polyethylene (HDPE) fibers manufactured by DSM. These needlepunched fabrics are created by entanglements of a single fiber

material, hence, their mechanical responses are governed by the properties of the web layout, which usually are expressed in terms of statistical distributions of the geometrical features such as fiber entanglement, fiber curl and fiber orientation, and the mechanical properties of constituent fibers.

In this study, the investigations of the two needlepunched fabrics are carried out in a two-step approach. First, the fabric microstructures are characterized in terms of the morphological properties and the mechanical properties of individual constituent fibers using image analysis technique and mechanical characterization technique, respectively. Then, the fabric macroscopic responses under in-plane modes of deformation are investigated. Attention is given to the evolution of the fabric microstructure with respect to the level of macroscopic loadings, the damage accumulation in the fabric structure due to fiber slip and fiber entanglement, and the effect of rate of deformation on the macroscopic response of the fabrics. Knowledge obtained from these characterizations is crucial for the development of a constitutive model for nonwoven fabrics discussed in Chapter 4.

3.1.1 Literature Review

Literature on the characterization of nonwoven fabrics can be classified into two major areas. The first area focuses on the investigation of fabric geometric properties by means of microscopy and image analysis techniques. One of the pioneering research in this area is the work by Ericson and Baxter [21] in 1973. They introduced a means to measure the weight uniformity by studying the statistical distribution of fabric weight for a given fixed sampling area. They also introduced a technique, called Randometer, to measure the fiber orientation and the fiber separation by illuminating the fabric surface using a collimated light source, measuring the intensity of reflected and transmitted light, and using the principle of light-scattering to relate the light intensity to the fiber orientation distribution.

The researchers in the following years took advantage of the development of computers by formulating image analysis algorithms that automatically evaluated the geometric properties of nonwoven fabrics from fabric images. These researchers include : Kang and Lee [32], who developed an image analysis algorithm to determine the structural parameters including fiber orientation, fiber length, and needlepunching density, of needlepunched nonwoven composites;

Pourdeyhimi et al. [64]-[69], who proposed a set of algorithms that measure and simulate fiber orientation and fiber diameter distribution of needlepunched nonwoven fabrics; Xu et al. [88],[89], who introduced a novel method to measure the structural characteristics of fiber segments such as fiber crimp, length, thickness and orientation by image analysis techniques; Chhabra [17], who described a method to characterize the web mass uniformity; Gong et al. [24],[25], who introduced new pattern recognition algorithms that can be used to analyze fiber orientation and pore size distribution in nonwoven fabrics.

The other area of research focuses on the investigation of macroscopic response of nonwoven fabrics under in-plane modes of deformation. Researchers that focused on the behavior of nonwoven fabrics under uniaxial loading include: Patel and Kothari [60],[61], who investigated the relationship between the tensile properties of heat-bonded and needlepunched nonwoven fabrics and their constituent fibers, along with the effects of rate of deformation and specimen dimension to the fabric tensile response; Bias-singh et al. [10], who studied the lateral contraction during uniaxial tensile deformation of spunbonded nonwovens; Kim et al. [37]-[40], who combined the image analysis technique developed by Pourdeyhimi et al. [64]-[69] with a mechanical testing device to investigate the deformation evolution of a point-bonded nonwoven fabric during tensile loads; Chocron et al. [18], who investigated the tensile properties of Dyneema Fraglight[®] and their dependences on rate of deformation, direction of load and temperature.

3.2 Nonwoven Fabric Experimental Investigation

3.2.1 Study of Nonwoven Fabric Structure

The structure of nonwoven fabrics is typically analyzed by means of image analysis. Fabric images are usually obtained by photographing the fabric surface under a reflective light source optical microscope. However, these 2D images cannot provide a complete set of information on the features of the 3D network structure of nonwoven materials. In other words, the images obtained from this method only portray the characteristic of fabrics on the focal plane of the microscope while leaving the fabric features in other focal planes indistinguishable. Examples of such images are shown in **Figure 3-1** (a-c). In order to create an image which contains the

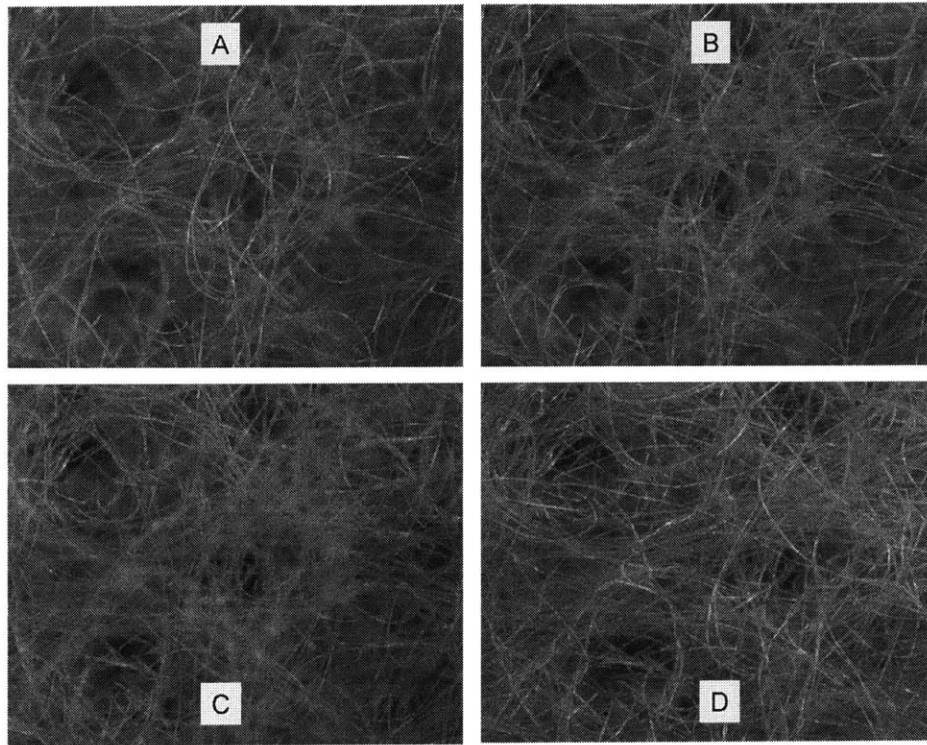


Figure 3-1: Images of Protechtor taken from the same area (a-c: different focal plane; d: after image integration technique)

information of the fabric network structure, an image processing technique must be used to integrate the images along the different focal planes and construct a new image that combines the focused features of each image. This image processing technique is carried out as follows.

First, a set of images is obtained by photographing the same fabric area along different focal planes at an equidistant interval. Then, the images are combined into a stack of images using ImageJ, an open-source image processing software developed by Wayne Rasband of the National Institute of Health. By using the extended depth of focus plug-in developed by the biomedical imaging group at Ecole Polytechnique Federale De Lausanne, the stack of images is converted into a single image containing the focused fibers from all images. **Figure 3-1** (d) shows the output image after combining the image (a) to (c).

By using this technique, two processed images representing ProTecthor[®] and Dyneema Fraglight[®] fabrics are produced as illustrated in **Figure 3-2**. Since these two images are

taken at the lowest magnification (10x) under the same microscope, these images show that the ProTechtor[®] fabric has a higher fiber density but a smaller fiber size than the Dyneema Fraglight[®] fabric. The needlepunch pattern can be clearly distinguished on the ProTechtor[®] image, but is less clear in the case of the Fraglight[®]. The fibers of these two fabrics tend to align along the cross direction rather than the roll direction, indicating that both fabrics are anisotropic and are probably stiffer along the cross direction. Fabric anisotropy will be further investigated in section 3.2.3.

An observation on the constituent fibers of the two fabrics suggests that the ProTechtor[®] fabric consists of a network of fibers with diameter of approximately 10 microns entangled mostly around the needlepunch areas. The Fraglight[®]'s fibers, however, are more randomly laid probably because the microscope magnification in **Figure 3-2** is too high to detect the needlepunch pattern. The individual fibers of the Fraglight[®] are transparent while those of the ProTechtor[®] are opaque. Further investigation on the mechanical properties of individual fibers of both fabrics will be covered in the section 3.2.2.

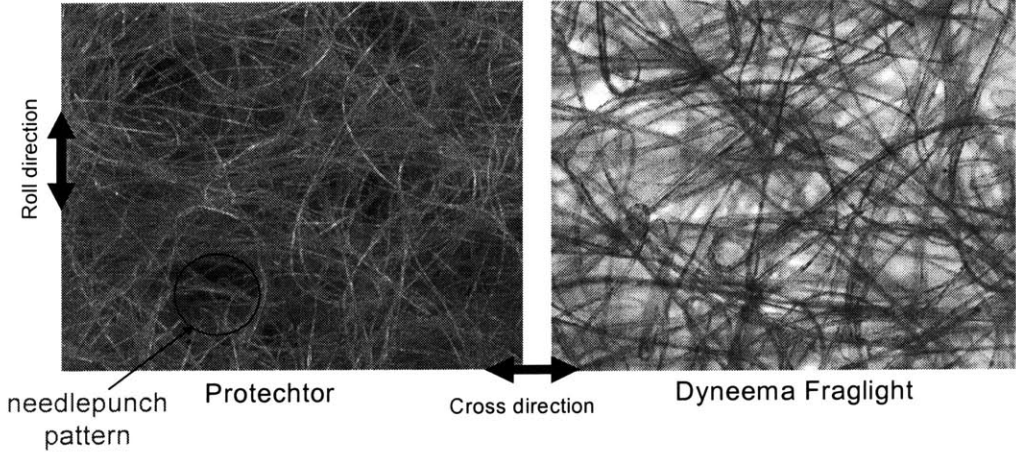


Figure 3-2: Images of needlepunched felt surfaces

Table 3.1 shows the geometric properties provided by the fabric manufacturers.

Properties	Unit	ProTechtor [®] CBS001	Dyneema Fraglight [®]
Roll Width	cm	152.4	160
Areal Density	g/m ²	~117	190-220
Thickness	mm	1.45-1.85	N/A

Table 3.1: Properties of ProTechtor and Dyneema Fraglight provided by the manufacturers

Tensile Response of Individual Fibers

The mechanical response of constituent fibers is investigated as a means to gain a better understanding of the macroscopic response of the fabrics under tensile loading, particularly in the large strain regime. To test the fibers of a needlepunched nonwoven fabric, a bundle of fibers is pulled out of the fabric using tweezers, and the damaged fibers displaying defects such as kinks or frays are removed. An individual fiber is isolated from the bundle, attached to a paper coupon, and tested in a manner similar to the procedure described to test single fibers of woven fabric (section 2.2.2). This technique gives consistent results for the ProTechtor[®] fibers as shown in **Figure 3-3**. However, this technique does not work well for the Dyneema Fraglight[®] fibers because the fibers tend to slip out of the epoxy. As a solution to this problem, the fiber is looped around a small, thin rod, such as staple or paper clip, and bonded to the rod by a drop of 5-minute epoxy. The assembly of fibers and rod is then glued to the paper coupon. This specimen preparation technique provides larger bonded area of the fiber to the coupon, and successfully eliminates the fiber slip problem. The test results for the Dyneema Fraglight[®] fibers shown in **Figure 3-4**, suggest the presence of two families of fibers with different stiffnesses.

A study of individual Dyneema[®] fibers under a microscope reveals that the fibers contain many defects including bulges, kinks, splits and fray. Observations of a number of fiber images suggest that there are two main populations of fibers: one population is a cylindrical shape fiber with a diameter of 20 microns, the fibers in the second population are composed of two joined 10 microns fibers as illustrated in **Figure 3-4**. This observation provides an interpretation for the two stiffness levels observed in the load-strain plots of tensile tests (**Figure 3-4**).

By using the measured dimensions of the ProTechtor[®] fiber and of the two populations of the Dyneema Fraglight[®], the average tensile properties of the individual fibers are calculated as shown in **Table 3.2**. Since the Dyneema[®] fibers are varied in sizes and shapes, a statistical distribution must be used to characterize the mechanical properties of such fiber.

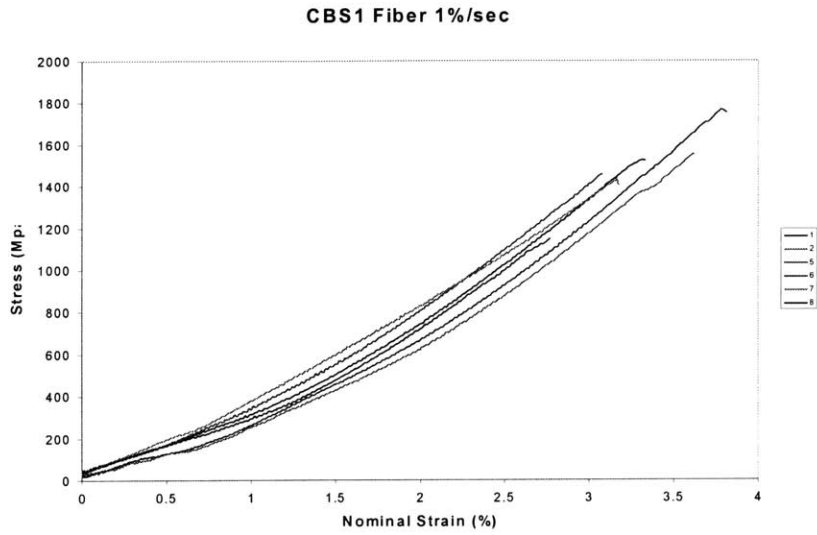


Figure 3-3: Tensile test results of Protektor fiber

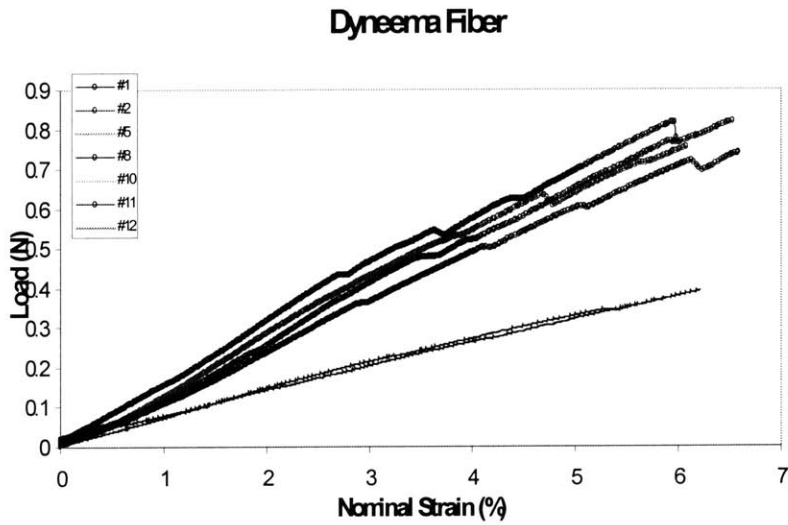


Figure 3-4: Tensile test results of Dyneema Fiber

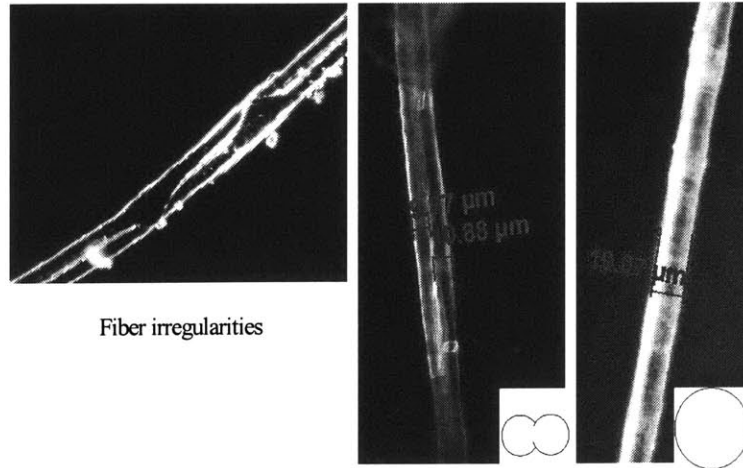


Figure 3-5: Images of fiber irregularities and two populations found in Dyneema fibers

Properties	Unit	ProTecthor Fiber	Dyneema Fiber
Diameter	μm	12	10-20
Young's Modulus	GPa	42	32
Strength	MPa	1500	2000
Elongation at Break	%	3.25	6.0

Table 3.2: Mechanical properties of ProTecthor and Dyneema fibers measured from the experiments

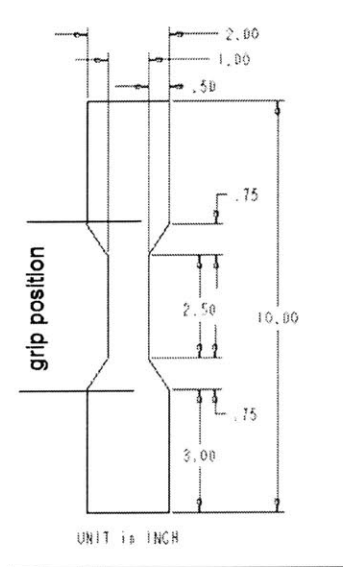


Figure 3-6: Dimension of nonwoven fabric dogbone specimen (in inches)

3.2.2 Mechanical Responses of Nonwoven Fabrics under Tensile Loads

A number of standard techniques have been established in the literature to test nonwoven fabrics under tensile loads. Examples of these are a grab test of narrow-width specimen (ASTM D1682-64), and a grab test of wide-width specimen (ASTM D4595-86). According to the ASTM D5034-95, the standard grab test is only applicable when the total fabric deformation is less than 11% nominal strain. However, the Dyneema Fraglight[®] has been reported by Chocron [18] to undergo uniaxial deformation more than 100% strain before failure, and therefore, the standard tensile testing methods are at least not suitable for characterizing the large strain response of this fabric. In this study, a new technique that allows the measurement of fabric deformation at large strains is proposed as described below.

First, the fabric is cut into dogbone-shape strips as illustrated in **Figure 3-6**. This specimen shape ensures that the central region of the specimen is subjected to a uniform uniaxial stress state for all levels of deformation. The specimens are gripped in a fabric fixture similar to the tensile test fixture used for the woven fabric experiments. In its initial unloaded, gripped configuration, the specimen has a total length of 4 inches; $2\frac{1}{2}$ inches of this length is in the constant narrow width region. The displacement is measured by a contact extensometer with

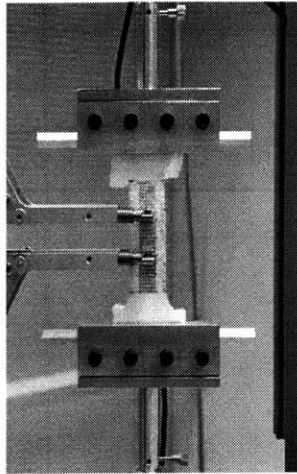


Figure 3-7: Nonwoven dogbone specimen in clamped position

an initial gauge length of one inch positioned in the central region of the specimen. **Figure 3-7** illustrates the nonwoven fabric dogbone specimens in the gripped position.

The ProTector[®] and the Dyneema Fraglight[®] fabrics were tested under two types of uniaxial tensile loading conditions: monotonic loading and cyclic loading. The uniaxial tensile tests with monotonic loading provide a means to measure the fabric tensile properties as well as to identify the deformation mechanisms of the fabric under tensile loads. The tests are performed at a nominal strain rate of 0.01 s^{-1} until failure.

The cyclic loading tests are conducted to investigate the effects of the inelastic deformations such as fiber disentanglement and fiber-on-fiber friction on the macroscopic response of fabrics. The cyclic loading test is a displacement controlled test consisted of a series of loading-unloading sequence, each following the pattern described below;

- 1) Load - the specimen is pulled up to a pre-specified strain,
- 2) 1st Hold - the specimen is held at the pre-specified strain for a short interval
- 3) Unload - the strain on the specimen is decreased to reach a condition of zero load
- 4) 2nd Hold - the specimen is held at this lower strain for a short interval

The cycle continues with the higher values of pre-specified loading strains until the specimen fails. **Figure 3-8** shows the schematic of the nominal strain history for the uniaxial tensile cyclic loading test. To closely approximate a true strain rate response of the fabrics, the test speed is

varied between the cycles, and is calculated so as to obtain the same constant nominal strain rate with respect to the specimen length at the beginning of the loading step. For example, if the desired true strain rate is 0.01 s^{-1} and the specimen length at the beginning of the third cycle is 5 mm, the test speed of that particular cycle is 0.05 mm s^{-1} .

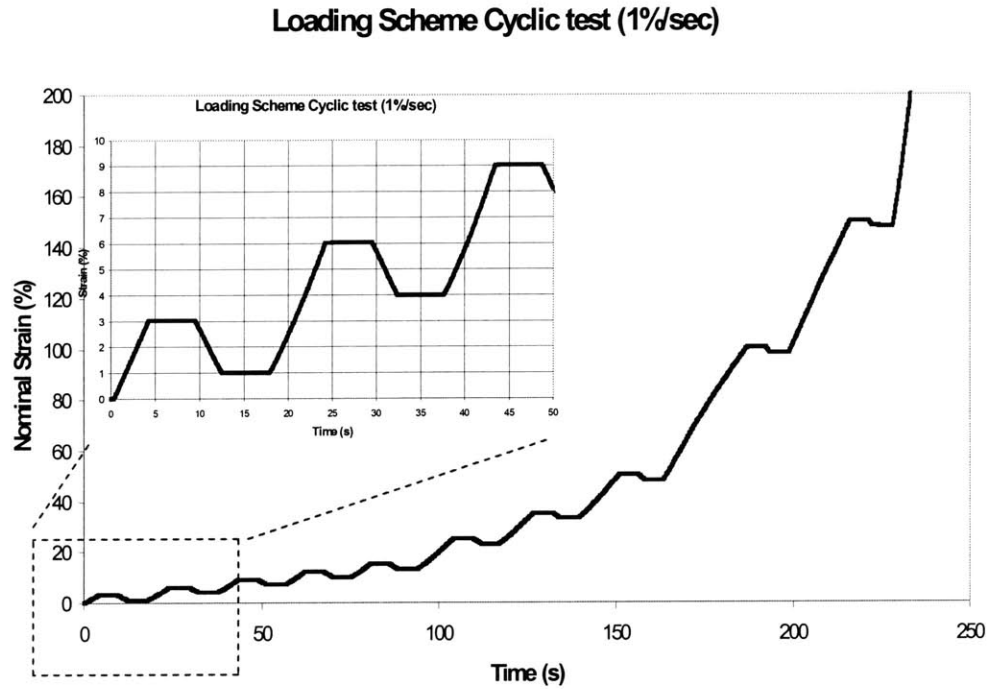


Figure 3-8: Uniaxial cyclic loading test scheme

For both types of fabrics, a number of tests were conducted along the manufacturing roll direction as well as in the perpendicular direction. In addition, tests were performed along the needlepunch and perpendicular to the needlepunch directions on the Dyneema Fraglight[®] fabric to investigate the effect of needlepunch pattern on the tensile properties. All of the tests were conducted on the Zwick machine using a test set up similar to the one adopted in the woven fabric tensile experiments (section 2.2.2). A contact extensometer was used to measure the displacement on the constant-width region of the dogbone specimen, and an optical extensometer is used to record the deformation progression during the test.

Uniaxial Test with Monotonic Loading

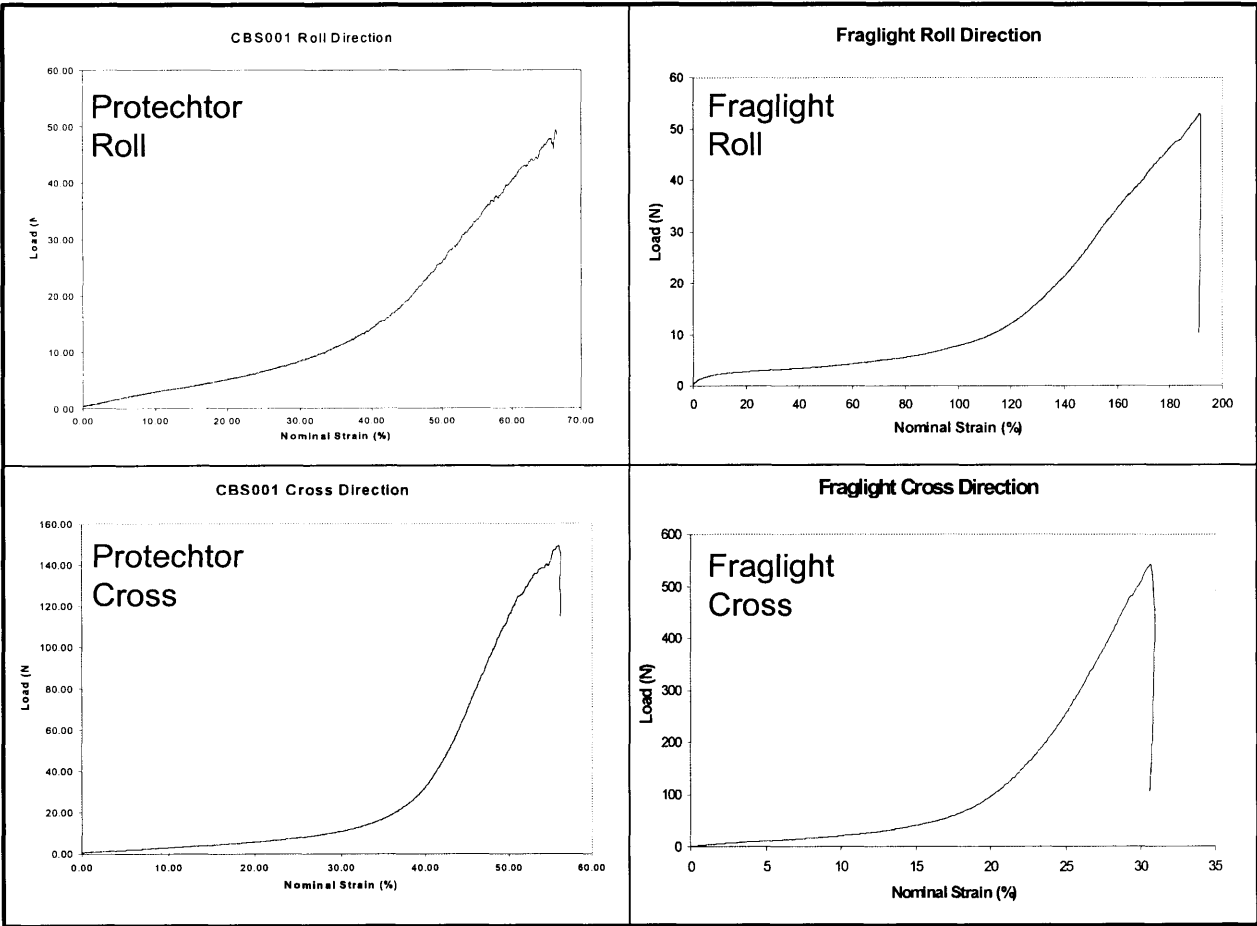


Figure 3-9: Load-Extension plots of Protechtor and Dyneema Fraglight fabrics

Typical results of the monotonic tensile tests, plotted in terms of applied load and nominal strain for the ProTechtor[®] and the Dyneema Fraglight[®] fabrics along the roll and the cross directions are shown in **Figure 3-9**. Similarity in the behaviors of both fabrics along the two directions implies that the fabrics undergo similar deformation mechanisms, as described below.

In the initial compliance region of the load-strain plot, macroscopic deformation is primarily accommodated by rotation of constituent fibers. As strain increases, the fibers attempt to realign themselves with the loading direction by means of rotating, slipping and wrapping around each other, which results in a contraction of the specimen along the lateral direction.

Some researchers [6],[28],[30] describe this behavior as a Poisson's-like effect for the nonwoven structure. The fibers realignment continues until the fibers are uncurled and densely compacted and further fiber re-orientations are prevented by the neighboring fibers. At this point, further deformation can only be accommodated by fiber stretching, resulting in an increase in stiffness. As the strain increases, the fibers disentangle by breakage or reptation out of the entanglement sites, causing the stiffness to decrease. The sample eventually fails by a combination of fiber disentanglement and fiber failure. **Figure 3-10** shows a representative load-strain plot along with the images corresponding to the discussed behavior.

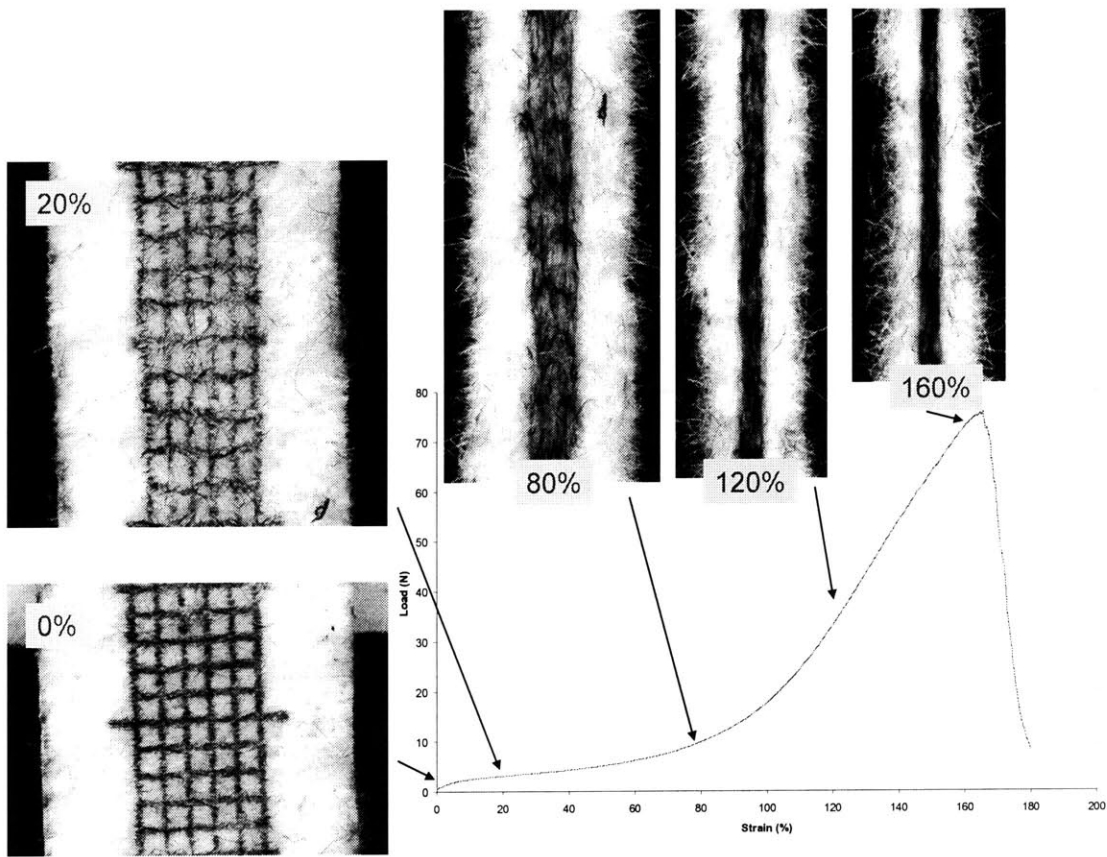


Figure 3-10: Texture evolution of the Dyneema Fraglight under a tensile load

Fabric Anisotropy As shown in **Figure 3-2**, the fibers tend to be preferentially aligned along the cross direction. This fiber network arrangement results in a stronger and stiffer response

along the fabric cross direction as illustrated in **Figure 3-9**. This observation, however, does not necessarily implies that the cross direction is the maximum principal stress direction, especially in the Dyneema Fraglight[®] where needlepunch pattern is well-defined at the angle of 63 degrees to the machine direction (**Figure 3-11**). To investigate the effect of the needlepunch pattern, a number of tests were conducted along the needlepunch direction and perpendicular to the needlepunch direction under the same condition as in the monotonic loading experiments along the cross and the roll directions. The results of these tests are plotted in **Figure 3-12**. According to this figure, the fabric along the cross direction exhibits the stiffest response with the shortest elongation at break, and further deviation from the cross direction results in a decrease in stiffness and an increase in elongation at break.

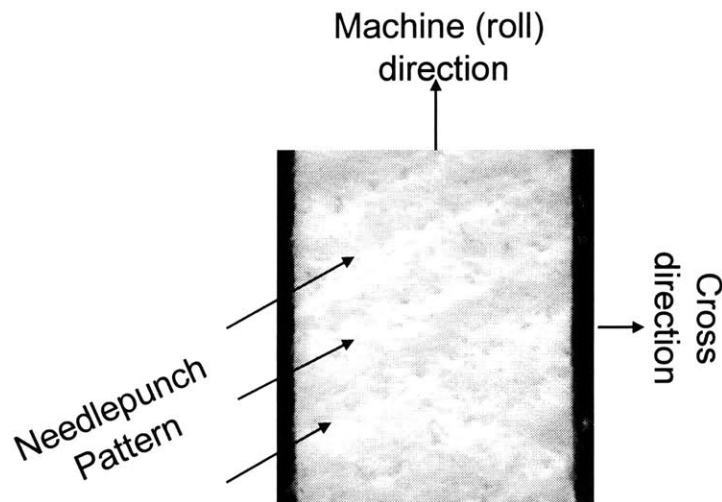


Figure 3-11: Needle punched pattern on Dyneema Fraglight fabric

The different responses among the results from different directions can be explained by the fabric microstructure. The low strain region of the load-strain graphs corresponds to the fiber rotation and the fiber realignment with the loading direction. Since more fibers are originally aligned along the cross direction as shown in **Figure 3-2**, the rotation contribution along the cross direction is small compared to the other directions, and hence, the elongation at break of the fabric in this direction is the shortest. The non-uniform fiber alignment also causes the fabric to exhibit a higher stiffness and a greater failure load in the cross direction.

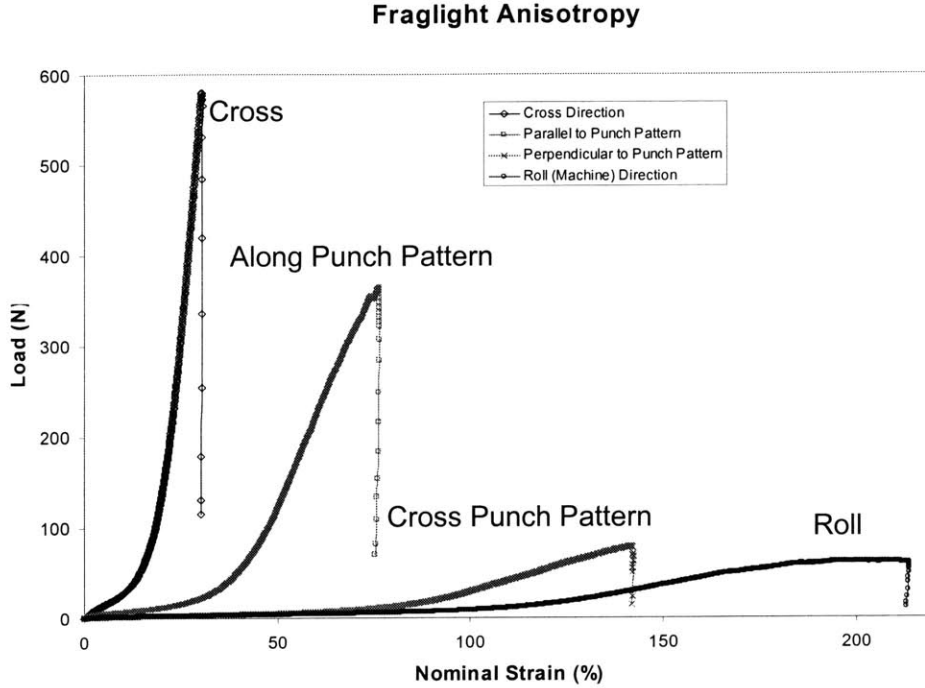


Figure 3-12: Dyneema Fraglight tensile tests from different fabric directions

Cyclic Loading Tests

For the cyclic loading tests, we used the same test configuration adopted for the monotonic uniaxial tensile test, but with a complex loading scheme to gain further insight into stress relaxation, damage accumulation due to fiber slips and fiber disentanglements, and texture evolution due to fiber reorientation. The loading scheme consists of a series of cycles of loading, holding, and unloading of the fabric at a speed that represents a constant nominal strain rate with respect to the specimen length at the beginning of each loading step. A series of tests were performed for the Dyneema Fraglight[®] along the machine and the cross directions at nominal strain rates of 0.001, 0.003, 0.01 and 0.05 s⁻¹. A number of tests were also performed along the needlepunch pattern and perpendicular to the needlepunch pattern on the Dyneema Fraglight[®] fabric.

Typical results of these tests are shown in **Figure 3-13** for the roll direction of Dyneema Fraglight[®]. The tests at the highest speed (i.e., 0.05 s⁻¹) are performed for fewer cycles than

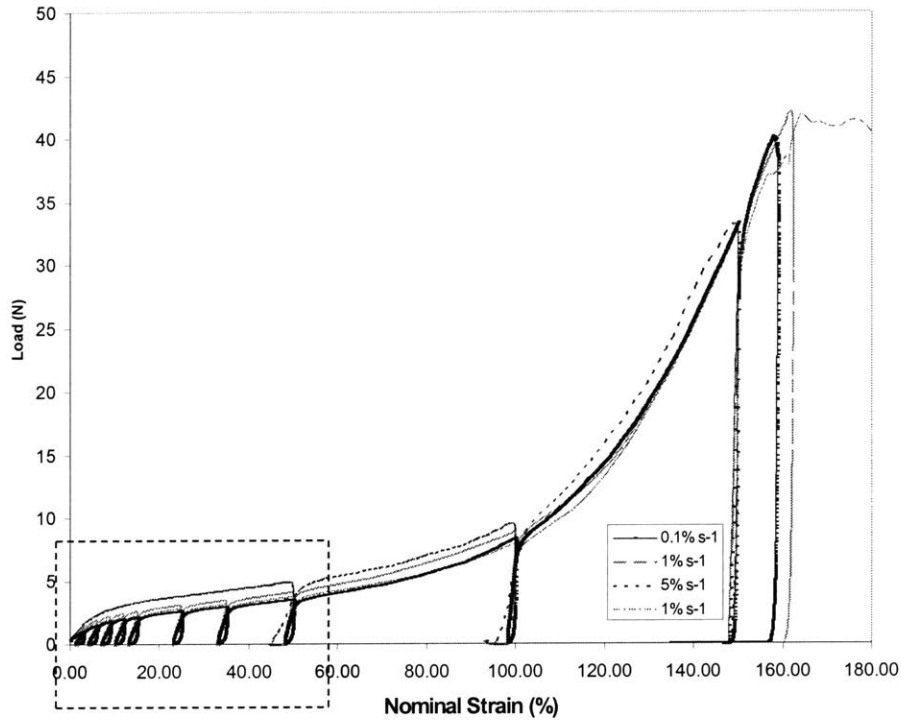


Figure 3-13: Results of cyclic loading tests of roll direction fabric at different strain rate

those at lower speeds because of limitations due to inertia stabilization of machine crosshead movement at high speed. Despite the different rates of deformation and cycle steps, the overall behavior of the four graphs are quite similar to those in uniaxial tension tests, but with a larger elongation at break and a lower failure load due to the damage accumulated in each loading cycle. This figure also implies that the influence of the rate of deformation is very weak for this range of strain rates as the plots at different speeds display almost identical load-strain curve.

Figure 3-14 and 3-15 illustrate the detailed deformation mechanisms with corresponding stages of the loading cycle and their images. In the loading step, the fabric first undergoes an elastic extension accommodated primarily by elastic rotations in the fiber network (image C). Once a sufficient stress level is reached, fiber stretching and fiber slip become the dominant deformation mechanism, with a marked decrease in stiffness. Once the fabric deformation

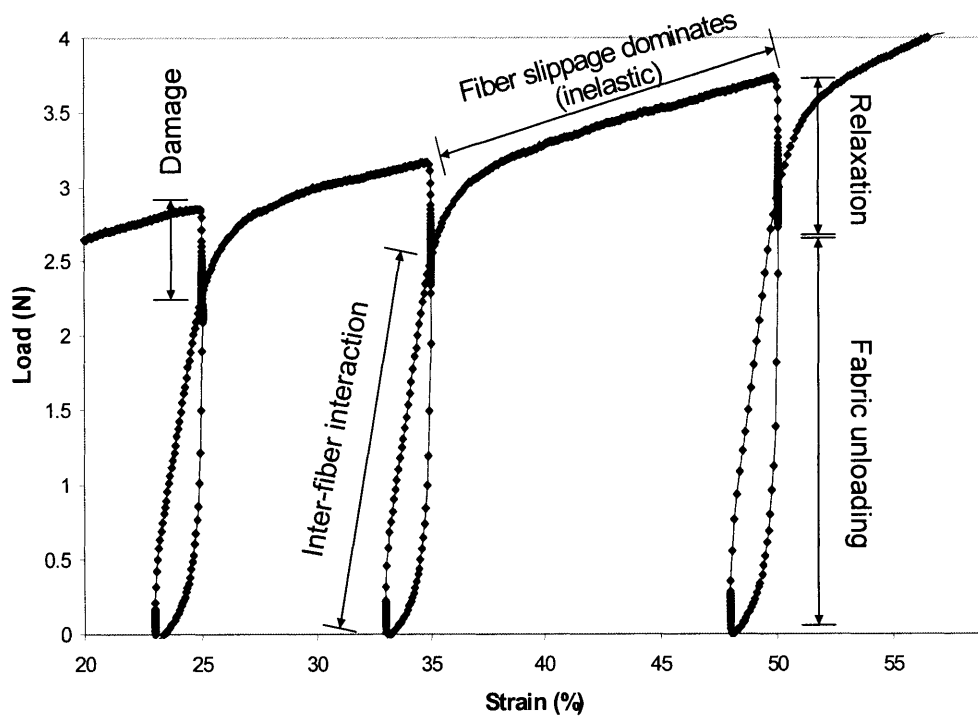


Figure 3-14: Detailed deformation mechanisms in a cyclic loading test

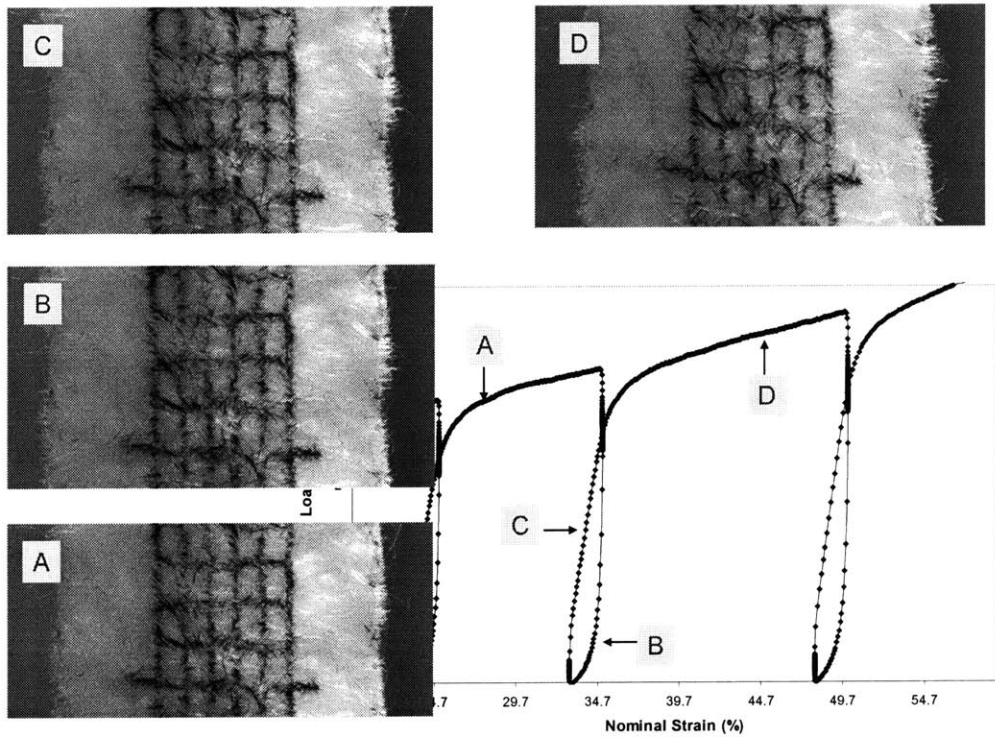


Figure 3-15: Images corresponding to the test evolution of a cyclic loading test

reaches the target strain, the fabric is held for a short period over which the stress relaxes by means of fibers slip and rearrangement. When the fabric is unloaded, the elastic component of deformation is recovered. As indicated by the graph, the magnitude of the load in the reloading step is usually lower than that in the loading step at the same strain, mainly due to the inelastic deformations (damage) from fiber slip and fiber disentanglement in the fabric.

3.2.3 Mechanical Responses of Nonwoven Fabrics under In-plane Shear Loads

The mechanical response of nonwoven fabrics under an in-plane shear load is usually overlooked by most researchers, mainly because the in-plane shear resistance of nonwoven fabrics is very small compared to the tensile resistance, and the shear deformation is dominated by the out-of-plane wrinkling once the rotation of constituent fibers is prohibited. Nevertheless, the investigation of the in-plane shear response of nonwoven fabrics provides an in-depth understanding of the deformation mechanisms in this particular mode of deformation. This knowledge is also critical in the development of a constitutive model for nonwoven fabrics. In this study, the in-plane shear response of the Dyneema Fraglight[®] is investigated by performing the picture-frame shear tests previously described in the woven fabric experiments. The kinematics of this test is described in Appendix B.

Picture-frame Shear Test

The in-plane shear response of Dyneema Fraglight[®] is investigated by performing the picture-frame shear test under two types of loading conditions: monotonic loading and cyclic loading. The monotonic loading experiments provide the overall response of the fabric under a shear load, while the cyclic loading experiments allow an investigation of the hysteresis properties of the fabric. To investigate the effect of the rate of deformation, the tests are run at two sets of speed; 30 mm per minute and 300 mm per minute for both types of loading conditions. A video capturing technique is applied during the test to observe the test evolution and the damage progression in the fabric sample.

Monotonic Loading Figure 3-16 shows a typical result from a monotonic shear loading test along with the images of deforming sample corresponding to the test evolution. Since the

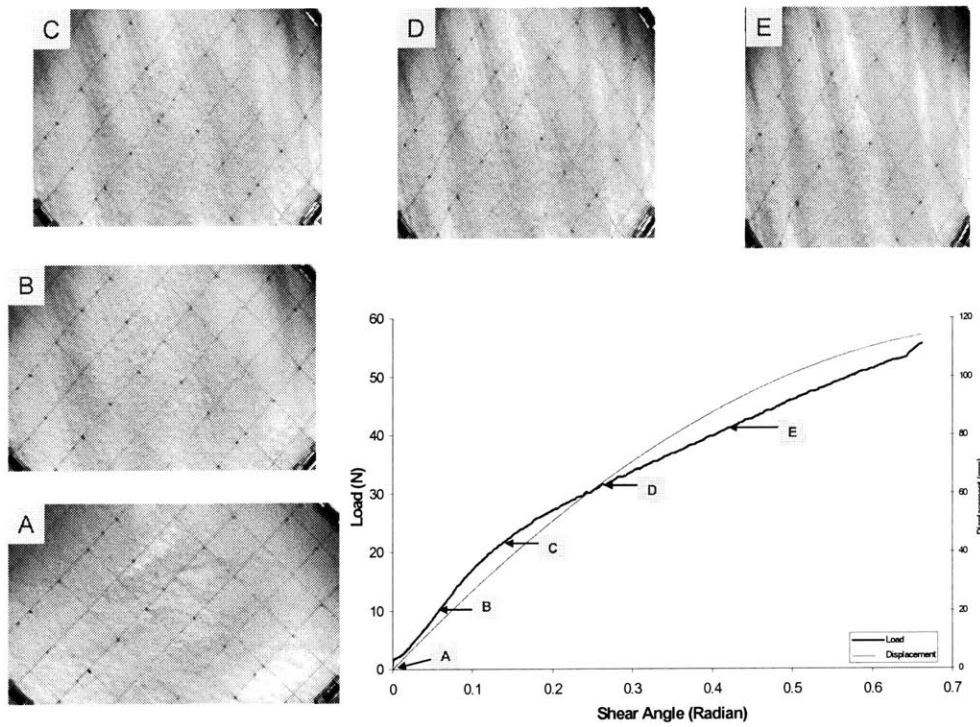


Figure 3-16: A shear test result of Dyneema Fraglight and its deformation mechanisms

picture-frame shear tests impose a combination of two modes of deformation: tensile mode along the loading direction and compressive mode along the lateral direction, the deformation mechanisms governing in this type of test reflects two types of deformation mechanisms. The fabric along the tensile dominated region is deformed in a similar manner to the fabric tensile test. The fabric along the compressive-dominated region buckles out of plane since the fabric has no resistance to the compressive loads. At the higher shear angle (point C to E), the fabric buckling dominates, resulting in a decrease in load as shear angle increases.

Cyclic Loading A series of cyclic loading tests have been performed to study the effect of the damage accumulated due to the inelastic deformations in the Dyneema Fraglight[®] fabric. The tests consist of a series of loading and reverse-loading sequences, all of them at a constant crosshead displacement speed. In each cycle, the specimen is loaded to a predetermined level of axial displacement (elongation), reverse-loaded to the same displacement in the opposite direction (contraction), and brought back to the original configuration. The cycles are repeated three times before the fabric is loaded to a higher displacement. **Figure 3-17** shows the schematic plot of shear angle-time of this test. According to the kinematics of this test (Appendix B), two identical displacements in the loading step and in the reverse loading step provide two different values of shear angles, as shown in **Figure 3-17**, and hence, the results of the loading-reverse loading test are expected to be unsymmetric.

Figure 3-18 shows typical results of this test performed at two rates of deformation: 30 mm per minute and 300 mm per minute. The load and unload parts of the graphs are unsymmetric, however, both parts resemble the response of the fabric under monotonic loading. The damage accumulated in the fabric due to the inelastic deformation is illustrated by the decrease in the curve stiffness as the number of cycle increases. The rate of decreasing stiffness at the same shear angle also decreases (See **Figure 3-19**), suggesting that there exists limiting damage for the fabric at each deformation level.

Figure 3-18 also implies an effect of strain rate on the shear behavior. The data suggests that this particular fabric exhibits a limited dependence on shear strain rate.

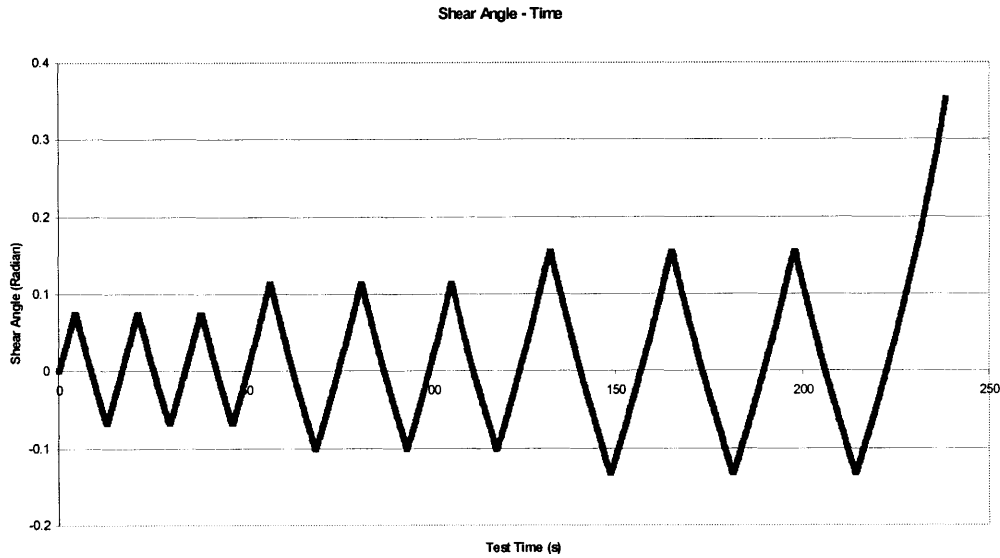


Figure 3-17: Cyclic loading picture-frame shear test schematic

3.2.4 Summary of Nonwoven Fabric Study

This chapter reviewed our investigation of the geometric properties and the in-plane responses of the ProTector[®] and the Dyneema Fraglight[®] fabrics. The examination of the fabric structures suggests that both fabrics are webs of staple fibers entangled around needlepunch patterns. The ProTector[®] has a denser fiber network and a smaller fiber size than the Dyneema Fraglight[®]. Despite the randomly laid fiber arrangement observed in the images of both fabric surfaces, the uniaxial tensile testing of the two fabrics reveals that both fabrics exhibit anisotropic responses with the cross machine direction stronger and stiffer than the machine (roll) direction, and show a weak dependence of the material response on the rate of deformation. The results of the cyclic loading tests suggest that the tensile deformation of the fabric is a combination of the elastic deformation from fiber rotation, and the inelastic deformation from relative fiber slip as well as fiber disentanglement. The inelastic deformation can be associated with the decrease in load after each cycle, and the accumulated damage can be measured accordingly.

The results of the in-plane shear tests suggest that the fabrics have low in-plane shear stiffnesses compared to the tensile stiffnesses. At the structural level, the in-plane shear response

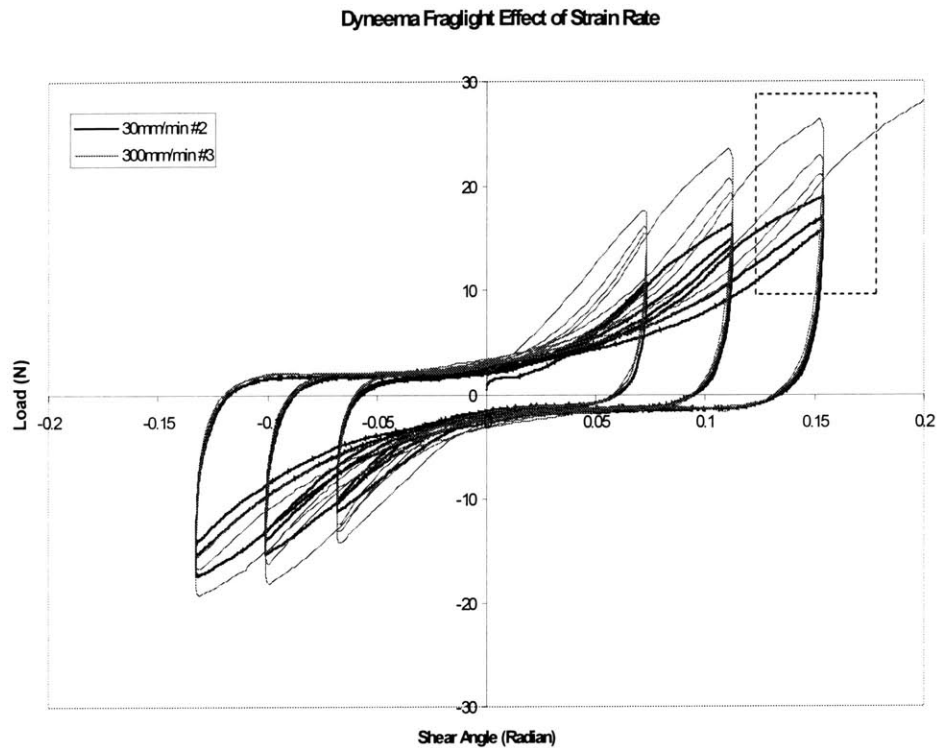


Figure 3-18: Results of cyclic loading picture-frame shear test at two test speeds

is a combination of the fabric undergoing in-plane tension and compression along two orthogonal directions. The results of the in-plane cyclic shear tests provide a means to measure the damage accumulation and the texture evolution of the fabrics.

With knowledge of the fabric macroscopic responses, the fabric deformation and failure mechanisms as well as the fabric properties obtained from the in-plane tests, a fabric model can be developed based on continuum description of the material. The formulation and development of the model will be discussed in the following chapter.

Dyneema Fraglight Effect of Strain Rate

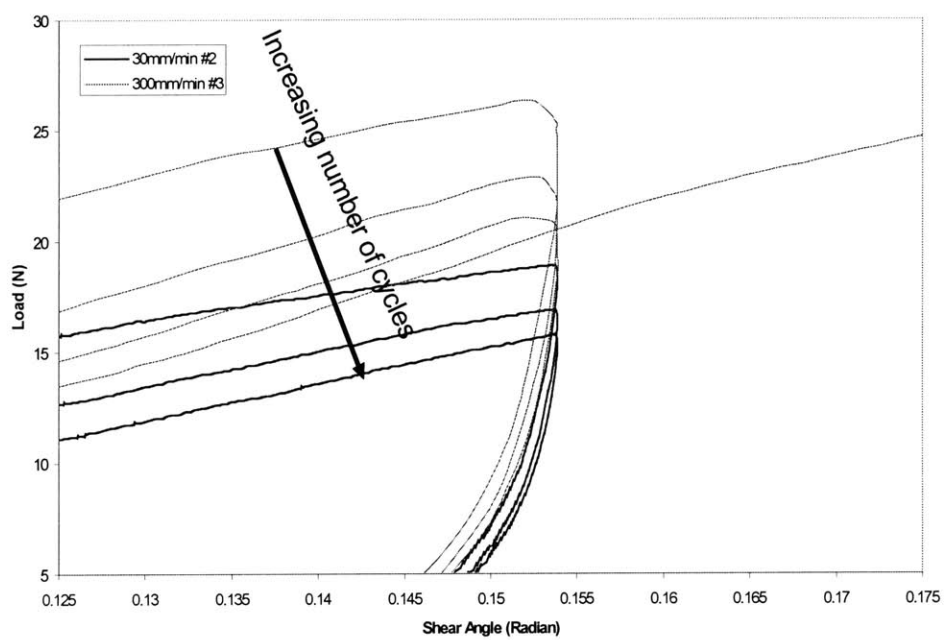


Figure 3-19: Damage accumulation in the picture-frame shear test

Chapter 4

A Continuum Model for Needlepunched Nonwoven Fabrics

4.1 Background

4.1.1 Literature Review

As nonwoven fabrics have been used in a wide range of applications, there exist a number of fabric models in the literature. Many of these models were developed specifically to predict the responses of nonwoven fabrics under certain modes of deformations, while a few of them served as a design tool for composite structure involving nonwoven fabric network-like reinforcements. Regardless of the development purpose of these models, they can be divided into two main categories based on their idealization approaches for nonwoven materials.

The first approach considers the bulk responses of nonwoven fabrics by idealizing them as either a homogeneous continuum or a combination of many homogeneous continua. This idealization forgoes the analysis of interactions of fabric microstructures to gain an ability to predict the macroscopic response of the fabrics at a low computational cost. The continuum models also enjoy a benefit of being able to interface with other continuum material models to create complex models for hierarchical structures. Examples of the continuum models proposed in the literature include the linear elastic orthotropic continuum models employed by Backer and Petterson [6] to model the response of a staple fiber, wet-laid, area-bonded nonwoven fabric

under a tensile load, and by Chocron [18] to simulate the tensile response of the Dyneema Fraglight[®] fabric. Hearle et al. [30] introduced a continuum model based on the energy minimization and the assumption of affine deformation of fiber bonded points to simulate the tensile properties of point-bond fabrics.

As the previously described continuum models rely on a homogenization of fiber webs, this models are unable to capture the effects of fabric heterogeneities, such as irregular patterns of bonded areas, and local deformation of fabric at the microstructural level. To address these limitations, a number of researchers have idealized nonwoven fabric as a composite consisting of many continuum components, each representing a part of the fabric structure. Researchers who used this method include Lee and Argon [48]-[51], who modeled the bending response of nonwoven fabrics by idealizing them as a composite structures consisting of two types of continuum materials: a stiffer linear elastic through-thickness disk representing the junction point (i.e. bonds) and a softer surrounding matrix representing the unconstrained fibers. This model is capable of predicting the bending responses of spunbonded and print-bonded fabrics with different bonding technologies. Other examples of this composite approach are the models proposed by Bias-Singh et al. [9], and by Liao and Adanur [1],[52],[53]. Bias-Singh's composite model consists of a number of layers of fibers such that all fibers in one layer are oriented in the same direction, the layers of different fiber orientations are bonded at the contacting interface, and the response of the continuum is calculated according to the theory of laminate composites. This model is able to capture the nonuniformity in the strain field and the necking in the tensile deformation of spunbonded nonwoven fabrics. Liao and Adanur introduced a similar approach of idealizing the fabrics as a composite of unidirectional fiber layers, but instead of having the layers bonded continuously along the layer surfaces as in the laminate composite theory, they are joined at the nodal points of the finite element mesh. This idealization allows for fiber re-orientation and fiber failure during the deformation process, and was able to capture the behavior of spunbonded nonwoven fabric under uniaxial tensile deformation.

The second approach considers nonwoven fabrics as a complex fiber-network structure, and the macroscopic response of the fabric is calculated from the interactions between the components of the structure, particularly at the fiber and bond levels. This approach enjoys the benefit of capturing the physics of fabric deformation mechanisms at the expense of a very high

computational cost. This microstructurally-based approach enjoys a few advantages over the continuum approach, including the ability to model fabric response at the structural level as well as the fabric nonuniformity. However, since this method requires an idealization of every fabric component (fibers and bonds), its computational cost is very intensive. The researchers who utilize the network approach include Britton et al. [14]-[16], who simulated individual fibers and bonds as a fabric sheet under a tensile load, and Grindstaff et al. [23], whose model was generated by connecting the point-bonded patterns with a number of fibers adjusted to produce the same areal density as the fabric being modeled. Jirsak et al. [31] proposed a net-like model consisting of bonding sites arranged in a two-dimensional triangular net. This model emphasizes the effect of the bond strength on the mechanical response of the fibers, but neglects the interactions between the fibers.

Another example of the micromechanical modeling approach is the fiber web model proposed by Petterson [63]. This model considers a representative area element that contains enough fibers and bonds to represent the behavior of the entire fabric. The model tracks the orientation and the stretch of individual fibers assuming that the fiber bonds are rigid, and relates these micromechanics to the macroscopic response of the entire fabric particularly under uniaxial tensile loads. The fiber web model was later modified by Hearle et al. [28],[29] to incorporate the effect of fiber curls, and again by Kothari and Patel [44] to include the creep response of individual fibers by formulating an empirical fiber stress-stretch response as a function of time.

In another micromechanics approach, Termonia [82],[83] introduced a discrete lattice model as a means to predict the deformation behavior of heat-bonded sheets. In this model, the fabric is represented as an array of fiber strands on two dimensional x-y lattice layers. The lattice layers are bonded by connecting the nearest-neighbor fiber sites along the transverse axis. The fiber bonds are allowed to break and consolidate during the deformation. This model is able to predict the tensile behavior as well as the bending behavior of point-bonded nonwoven fabrics at a high level of accuracy, however, its usage is limited by the high computational expense required to formulate a small area of fabric as an array of discrete lattices.

4.2 Modeling Objectives

Some of the existing fabric models are suitable for predicting specific behaviors or fabric characteristics, while others are limited to certain classes of materials and loading conditions. With the advancement of new technologies, there is a need to develop a more general fabric model to facilitate the growth of these technologies. Fabric model should meet the following requirements:

1) The model should accurately simulate the mechanical response of nonwoven fabrics for all types of loading conditions. The model should be able to predict the macroscopic response of the fabrics (i.e., stress and strain or load and displacement responses) as well as to capture the important features of the deformation mechanisms at the structural level, such as the fiber re-orientation, and the interactions between fibers. This capability allows the model to serve as a mechanical analysis tool for the novel technologies.

2) The model should be able to serve as a design tool. In other words, the model should be able to predict the response of a fabric given the mechanical properties of the fabric components, namely fibers and binding materials, and the geometric properties of the fabric.

3) The model should be of practical use. Many of the proposed models, although they can effectively predict fabric response under certain modes of deformation, are not of practical use because of the high computational expense or the limitations imposed by the models. In addition, the fabric model should also be able to interface with other material models to aid in the design of multi-component structures required by the new technologies.

With such requirements, the most suitable approach to model the mechanical response of nonwoven fabrics is by means of continuum approach. The main advantage of the continuum models is their efficiency in modeling a large scale fabric application. And by homogenizing the response of the representative fiber network accounting for the elastic and inelastic deformation mechanisms based on the fabric macroscopic response, the continuum models can also capture the fabric behavior at the microstructural level. In addition, the continuum models can be easily interfaced with the continuum models of different materials to formulate models of hierarchical structures.

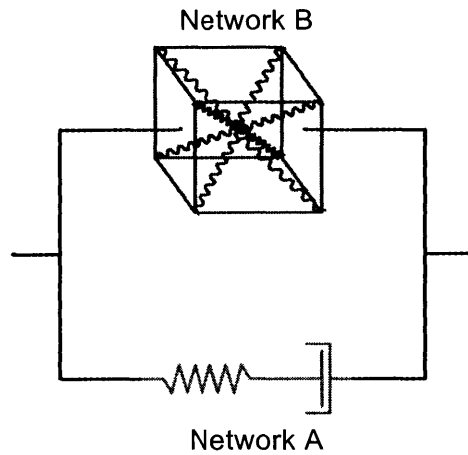


Figure 4-1: Constitutive model with network A as a linear spring and a dashpot in series, in parallel with network B as a nonlinear spring

4.3 Constitutive Model Development

The experimental data presented in the previous chapter demonstrates the complicated non-linear anisotropic elastic and inelastic behavior of nonwoven fabrics. As a preliminary attempt to capture the behaviors exhibited in these experiments, a continuum model is developed that incorporates the effects of elastic and inelastic deformation mechanisms, such as fiber rotation, fiber stretch, and inter-fiber friction, and the time-dependent nature of the material. The experimental data suggests that the material response can be decomposed into two parts: an elastic response from the fiber rotation and stretch, and an elastic response from the rate-dependent effect and the damage accumulated from fiber slipping and unraveling. The material can then be idealized by the rheological model with two networks acting in parallel shown in **Figure 4-1**.

Network A contains two elements: a spring and a dashpot, which represent the initial elastic resistance to the relative fiber slip and rotation, and the inelastic response due to fiber-on-fiber friction. The spring element in network B represents which denotes the elastic response from fiber rotation and fiber stretch observed at large deformation.

By treating the nonwoven fabric as a homogenized material, the macroscopic state of deformation is described by a total deformation gradient \mathbf{F} acting on both network A and network

B . \mathbf{F} is defined in a Cartesian coordinate system as

$$\mathbf{F}_{ij}(t) = \frac{dx_i(t)}{dX_j} \quad (4.1)$$

where $x_i(t)$ is the i -coordinate of a material point at time t in the deformed configuration and X_j is the j -coordinate of that point in the undeformed configuration, and

$$\mathbf{F} = \mathbf{F}_{(A)} = \mathbf{F}_{(B)} \quad (4.2)$$

where $\mathbf{F}_{(A)}$ denotes the total deformation gradient tensor acting on the elements in network A , and $\mathbf{F}_{(B)}$ denotes the deformation gradient tensor acting on the network orientation spring in network B .

$\mathbf{F}_{(A)}$ is further decomposed into elastic and inelastic components by a multiplicative decomposition (Lee decomposition):

$$\mathbf{F}_{(A)} = \mathbf{F}_{(A)}^e \mathbf{F}_{(A)}^p \quad (4.3)$$

where $\mathbf{F}_{(A)}^p$ is the inelastic deformation representing the relaxed configuration obtained by elastically unloading network A to a stress free state. **Figure 4-2** illustrates the multiplicative decomposition of the model.

4.3.1 Constitutive Representation of the Visco-Plastic Network (Network A)

From Equation 4.3, the elastic deformation in network A , $\mathbf{F}_{(A)}^e$, can be further decomposed by using the left polar decomposition into stretch and rotation, $\mathbf{F}_{(A)}^e = \mathbf{V}_{(A)}^e \mathbf{R}_{(A)}^e$. The velocity gradient of network A , $\mathbf{L}_{(A)}$, can be decomposed into elastic and inelastic components:

$$\mathbf{L}_{(A)} = \dot{\mathbf{F}}_{(A)} \mathbf{F}_{(A)}^{-1} = \mathbf{D}_{(A)} + \mathbf{W}_{(A)} = \mathbf{L}_{(A)}^e + \mathbf{F}_{(A)}^e \mathbf{L}_{(A)}^p \mathbf{F}_{(A)}^{e-1} \quad (4.4)$$

where $\mathbf{D}_{(A)}$ is the rate of deformation and $\mathbf{W}_{(A)}$ is the spin. The velocity gradient of the relaxed configuration, $\mathbf{L}_{(A)}^p = \dot{\mathbf{F}}_{(A)}^p \mathbf{F}_{(A)}^{p-1}$ is represented as

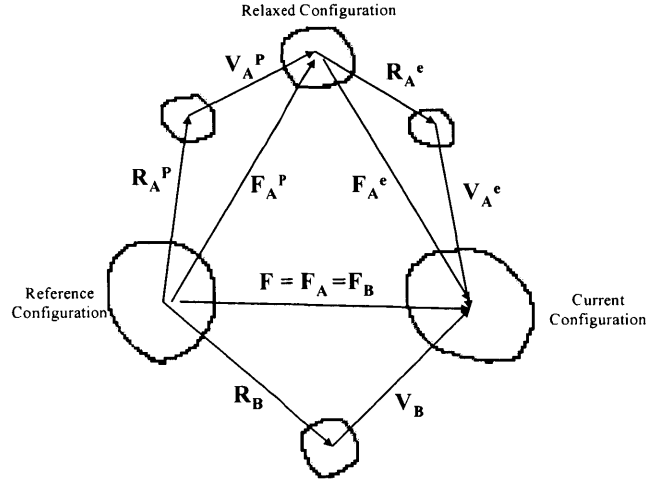


Figure 4-2: Multiplicative decomposition of deformation

$$\mathbf{L}_{(A)}^P = \mathbf{D}_{(A)}^P + \mathbf{W}_{(A)}^P \quad (4.5)$$

where $\mathbf{D}_{(A)}^P$ is the rate of shape change in the relaxed configuration and $\mathbf{W}_{(A)}^P$ is the spin. The spin in the relaxed configuration can be taken as zero with no loss in generality (as shown by Boyce [13]): $\mathbf{W}_{(A)}^P = 0$.

$\mathbf{D}_{(A)}^P$ is constitutively prescribed:

$$\mathbf{D}_{(A)}^P = \dot{\gamma}^P \mathbf{N}_{(A)} \quad (4.6)$$

where $\mathbf{N}_{(A)}$ is the direction of the driving stress in the relaxed configuration and $\dot{\gamma}^P$ is the inelastic shear strain rate, which is described by a power law relation

$$\dot{\gamma}^P = \dot{\gamma}_0 \left(\frac{\tau_{(A)}}{S} \right)^m \quad (4.7)$$

where $\dot{\gamma}_0$ and m control the rate at which the network responds to the driving stress, S is the resistance to the shear stress (to be defined later), and $\tau_{(A)}$ is the equivalent shear stress calculated from the deviatoric components, $\mathbf{T}_{(A)}^{* \prime}$, of the driving stress state on the relaxed

configuration of network A , $\mathbf{T}_{(A)}^*$:

$$\tau_{(A)} = \left[\frac{1}{2} \text{trace} \left(\mathbf{T}_{(A)}^{*'} \cdot \mathbf{T}_{(A)}^{*'} \right) \right]^{\frac{1}{2}} \quad (4.8)$$

$$\mathbf{T}_{(A)}^{*'} = \mathbf{T}_{(A)}^* - \frac{1}{3} \text{trace} \left(\mathbf{T}_{(A)}^* \right) \mathbf{I} \quad (4.9)$$

where $\mathbf{T}_{(A)}^*$ is equal to the stress in the loaded configuration in network A , $\mathbf{T}_{(A)}$, or $\mathbf{T}_{(A)}^* = \mathbf{T}_{(A)}$.

The direction of the driving stress $\mathbf{N}_{(A)}$ is obtained by normalizing the deviatoric stress with its equivalent shear stress

$$\mathbf{N}_{(A)} = \frac{1}{\sqrt{2}\tau_{(A)}} \mathbf{T}_{(A)}^{*'} \quad (4.10)$$

The shear resistance, S , physically representing the initial barrier to fiber rotation (i.e., fiber-on-fiber friction), evolves with inelastic strain from an initial value, S_0 , to a hardened steady state, S_{ss} , representing the increasing effect of inter-fiber friction due to the stiffer response of fiber network rotation as observed in the fabric uniaxial tensile experiments (**Figure 3-14**).

$$\dot{S} = h_{ss} \left(1 - \frac{S}{S_{ss}} \right) \dot{\gamma}^P \quad (4.11)$$

However, for larger times under load, disentanglement events lead to a decrease of shear resistance to a long-term value S_{damage} , as observed in the results of cyclic picture-frame loading experiments (**Figure 3-19**). Thus, S_{ss} evolves with inelastic strain from its initial value S_{ss0} to a long-term state corresponding to the damaged fabric S_{damage} :

$$\dot{S}_{ss} = h_{damage} \left(1 - \frac{S_{ss}}{S_{damage}} \right) \dot{\gamma}^P \quad (4.12)$$

with $h_{damage} \ll h_{ss}$. **Figure 4-3** summarizes the evolution of the inter-fiber frictional strength, S , as a function of time, that tries to capture the behavior observed in the experiments.

The initial resistance to the fiber network rotation is modeled by a linear elastic isotropic spring in network A , and is constitutively characterized by the fourth order tensor operator of elastic constants, ψ^e

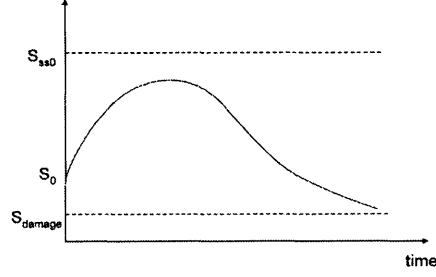


Figure 4-3: The evolution of shear strength as a function of time

$$\mathbf{T}_{(A)} = \frac{1}{\det \mathbf{F}_{(A)}^e} \psi^e \left[\ln \mathbf{V}_{(A)}^e \right] \quad (4.13)$$

where $\ln \mathbf{V}_{(A)}^e$ is the Hencky strain.

4.3.2 Constitutive Representation of the Elastic Network Orientation (Network B)

By using the left polar decomposition, the deformation gradient in network B , $\mathbf{F}_{(B)}$, can be decomposed into stretch and rotation contributions:

$$\mathbf{F}_{(B)} = \mathbf{V}_{(B)} \mathbf{R}_{(B)} \quad (4.14)$$

where $\mathbf{V}_{(B)}$ is the left stretch tensor and $\mathbf{R}_{(B)}$ is the rotation tensor.

The left Cauchy-Green tensor of network B , $\mathbf{b}_{(B)}$ is defined by

$$\mathbf{b}_{(B)} = \mathbf{F}_{(B)} \mathbf{F}_{(B)}^T = \mathbf{V}_{(B)}^2 \quad (4.15)$$

The left Cauchy-Green tensor is symmetric and positive definite, and therefore can be decomposed using a spectral decomposition into the following form:

$$\mathbf{b}_{(B)} = \sum_{i=1}^3 \lambda_i^{(B)2} \hat{n}_i^{(B)} \otimes \hat{n}_i^{(B)} \quad (4.16)$$

where $\lambda_i^{(B)}$ is the principal stretch of network B in its i^{th} principal direction, $\hat{n}_i^{(B)}$.

The experimental data indicate that an individual fiber between two junction (bond) points exhibits a highly compliant response in the initial regime of deformation corresponding to fiber uncurling, followed by a very stiff response corresponding to the fiber stretching. This fiber behavior is modeled by an exponential load-stretch response:

$$f(\lambda_f) = \alpha \exp[\beta(\lambda_f - 1)] \quad (4.17)$$

where $f(\lambda_f)$ is the force in the fiber, α and β are constants and λ_f is the fiber stretch. The strain energy density, w_f , needed to extend a fiber by a stretch λ_f is calculated by integrating the equation 4.17:

$$w_f = \int_1^{\lambda_f} f(\tilde{\lambda}_f) l_{f0} d\tilde{\lambda}_f \quad (4.18)$$

where l_{f0} is the original length of the fiber in the undeformed configuration. If the fiber network can be modeled by the unit cell representation of the eight-chain network model of Arruda and Boyce [5], then the chain stretch can be expressed in terms of the macroscopic principal stretches $\lambda_i^{(B)}$ as:

$$\lambda_f = \left[\frac{(\lambda_1^{(B)})^2 + \lambda_2^{(B)2} + \lambda_3^{(B)2}}{3} \right]^{\frac{1}{2}} \quad (4.19)$$

and the strain energy density, U_{cell} , is the sum of the work required to stretch the eight fibers and the energy originated from the volume change of the unit cell, U_{vol} .

$$U_{cell} = 8w_f + U_{vol} \quad (4.20)$$

$$U_{vol} = K \ln J \quad (4.21)$$

where K is a constant and J is the volumetric jacobian defined in terms of the deformation gradient or the macroscopic principal stretches, $\lambda_i^{(B)}$, as:

$$J = \det \mathbf{F}_{(B)} = \det \mathbf{F} = \lambda_1^{(B)} \lambda_2^{(B)} \lambda_3^{(B)} \quad (4.22)$$

The inclusion of the volumetric term, U_{vol} , ensures that the strain energy function is convex,

and that the reference configuration is stress-free.

Equation 4.20 can be rewritten as:

$$U_{cell} = \frac{C}{\beta} [\exp[\beta(\lambda_f - 1)] - 1] + K \ln J \quad (4.23)$$

where the constants in 4.17-4.21 have been combined into two constants, C and β .

The strain energy density can be conveniently expressed in terms of the stretch invariants I_1 , I_2 and I_3 , where:

$$\begin{aligned} I_1 &= \lambda_1^{(B)2} + \lambda_2^{(B)2} + \lambda_3^{(B)2} \\ I_2 &= \lambda_1^{(B)2} \lambda_2^{(B)2} + \lambda_1^{(B)2} \lambda_3^{(B)2} + \lambda_2^{(B)2} \lambda_3^{(B)2} \\ I_3 &= \lambda_1^{(B)2} \lambda_2^{(B)2} \lambda_3^{(B)2} = J^2 \end{aligned} \quad (4.24)$$

The Cauchy stress tensor, $\mathbf{T}_{(B)}$, acting on the network can then be obtained by differentiating the strain energy function in Equation 4.23 and can be expressed as:

$$\mathbf{T}_{(B)} = \frac{2}{J} \frac{\partial U_{cell}}{\partial I_1} \mathbf{b}_{(B)} + \frac{\partial U_{cell}}{\partial J} \mathbf{I} \quad (4.25)$$

or

$$\mathbf{T}_{(B)} = \frac{C}{3J\lambda_f} \exp[\beta(\lambda_f - 1)] \mathbf{b}_{(B)} + \frac{K}{J} \mathbf{I} \quad (4.26)$$

where \mathbf{I} is the identity matrix. Imposing the stress-free constraint for the reference configuration ($\mathbf{T}_{(B)} = 0$ when $\lambda_f = 1$ and $J = 1$), the relationship between C and K is found to be $K = -\frac{C}{3}$. By using $\tilde{C} = \frac{C}{3}$, Equation 4.26 can be expressed as:

$$\mathbf{T}_{(B)} = \frac{\tilde{C}}{J} \left[\frac{\exp[\beta(\lambda_f - 1)]}{\lambda_f} \mathbf{b}_{(B)} - \mathbf{I} \right] \quad (4.27)$$

The total stress in the system becomes

$$\mathbf{T} = \mathbf{T}_{(A)} + \mathbf{T}_{(B)} \quad (4.28)$$

4.3.3 Determination of Model Parameters

The model requires 11 constitutive parameters:

- $\dot{\gamma}_0$ and m control the sensitivity of the material to the rate of deformation
- S_0 is the initial resistance to the shear stress, physically representing the friction that resists fiber rotation
- S_{ss0} is the hardened short-term shear resistance
- S_{damage} is the long-term shear resistance which accounts for disentanglement effects
- H_{ss} and H_{damage} control the rate of evolution of the shear resistance, S , and the hardened resistance, S_{ss} , respectively
- μ and κ are the shear modulus and the bulk modulus describing the linearly elastic isotropic spring, and
- \tilde{C} and β describe the nonlinear elastic spring in network B .

Among these parameters, the power law parameters, $\dot{\gamma}_0$ and m , can be calculated directly from the experimental results of uniaxial cyclic loading tests at various speeds. The remaining parameters must be determined by fitting the simulation predictions to the experimental data. The technique used for fitting the model parameters can be outlined as follows.

The elastic spring is designed to capture the portion of the response where reversible fiber rotation is dominant. Hence, the shear modulus and the bulk modulus describing this linearly elastic isotropic spring must be selected such that model predictions match the initial linear portion of the uniaxial tensile and shear tests, as well as the unloading part of the cyclic tensile shear tests. The selections of the two constants are constrained by the isotropic elastic relations

$$\begin{aligned}\mu &= \frac{E}{2(1+\nu)} \\ \kappa &= \frac{E}{3(1-2\nu)}\end{aligned}\tag{4.29}$$

where E is Young's modulus and ν is Poisson's ratio. Young's modulus gives the slope of the stress-strain curve, while Poisson's ratio corresponds to the volumetric response of the material.

The nonlinear spring is designed to capture the large strain elastic response of the fiber network. Hence, the two parameters describing this constitutive element must be selected such that the extension and locking of the fiber network correspond to the long-term response of the fabric.

The initial resistance to the shear stress, S_0 , is determined by fitting the simulation curves with the experimental results at the onset of fiber slippage (i.e., when the load-extension curve becomes nonlinear). The remaining four parameters which describe the short-term hardened steady state and the long-term damage are obtained by fitting the simulation predictions with the load-unload portions of the cyclic uniaxial and shear tests.

4.4 Comparison of Model Predictions with Experimental Findings

The constitutive model is implemented into ABAQUS/Standard, an implicit finite element code, through a user-defined material subroutine. The current implementation of the model is limited to in-plane, quasi-static analyses only. To determine the model parameters, a simulation is created to replicate the uniaxial cyclic loading test of the Dyneema Fraglight[®] along the roll direction at a strain rate of 0.01 s^{-1} . The fitted model prediction and the experimental result are shown together in **Figure 4-4** and the model parameters obtained from this simulation are presented in **Table 4.1**.

To investigate the predictive capability of the proposed model, three sets of simulations corresponding to the Dyneema Fraglight[®] under a uniaxial monotonic loading test at a strain rate of 0.01 s^{-1} , a uniaxial cyclic loading test at 0.05 s^{-1} , and an in-plane picture-frame shear test with monotonic loads at a diagonal displacement rate of 30 mm per minute, are generated using the model parameters in **Table 4.1**. The load-extension outputs of these simulations are plotted together with their respective experimental findings in **Figures 4-5** to **4-7**.

From **Figures 4-5** to **4-7**, the model is found to accurately capture the uniaxial monotonic loading data at 0.01 s^{-1} (recall that the models are fit to the uniaxial cyclic loading data at

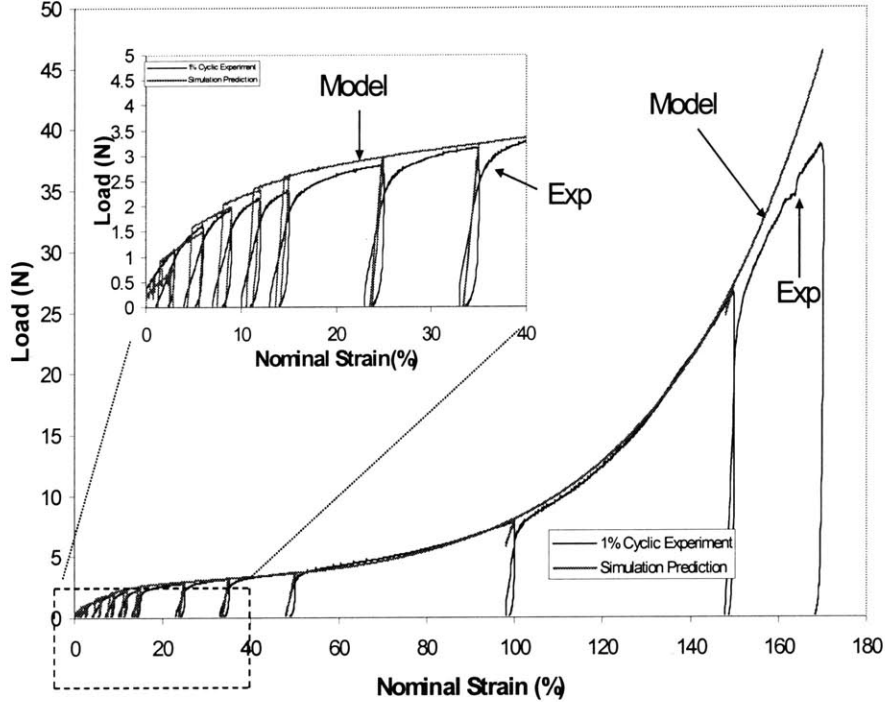


Figure 4-4: Fitted simulation prediction with the experimental data of the uniaxial cyclic loading test at 0.01 / second of the Dyneema Fraglight

0.01 s⁻¹) and to also provide a reasonable prediction of the uniaxial cyclic loading data at 0.05 s⁻¹ (figure 4-6). The unloading behavior of the 0.01 s⁻¹ uniaxial cyclic loading test is also well captured within the small strain region (i.e., less than 50%) where the effect of inter-fiber friction dominates. The transition of the linear portion in the unloading stage to the flow (flat) portion is also captured though not precisely. The model prediction of the monotonic shear response (**Figure 4-7**) agrees with the experimental data initially, and starts diverging where the material is found to buckle out of plane experimentally.

In addition, the simulation results show that the constitutive model captures the loading behavior of nonwoven fabrics very well as shown in **Figure 4-5**. The model is found to capture the relatively stiff initial response, followed by a "yield-like" region corresponding to the slippage of the fiber network, followed by the strain hardening and stiffening at the large strain. The model predicts the uniaxial response at different rates of deformation, and captures the essential

Parameters	Value	Unit
Shear modulus of the linear spring in network A, μ	1.41×10^7	Pa
Bulk modulus of the linear spring in network A, κ	2.34×10^6	Pa
Initial flow rate in network A, $\dot{\gamma}_0$	0.01	1/second
Exponent of the flow rate in network A, m	18.8	-
Initial flow stress in network A, S_0	6.0×10^3	Pa
Coefficient of the nonlinear spring in network B, \tilde{C}	4.8×10^4	Pa
Exponential coefficient of the nonlinear spring in network B, β	5	-
Short-term steady state, S_{ss}	1.0×10^5	Pa
Long-term steady state, S_{damage}	3.0×10^3	Pa
Coefficient of short-term steady state evolution, H_{ss}	3.0×10^5	Pa
Coefficient of long-term steady state evolution, H_{damage}	3.0×10^3	Pa

Table 4.1: Model parameters obtained from fitting the Dyneema Fraglight uniaxial cyclic test

features of unloading, short-term hardening, and long-term damage due to inter-fiber friction observed experimentally. The model results indicate that this constitutive representation of an elastic-viscoplastic matrix deformation acting in parallel with an exponential eight-chain spring captures the basic deformation modes of nonwoven fabrics and their underlying mechanisms up to the large deformation where the fabric damage from fiber slip and fiber disentanglement dominate.

However, the model still has limitations as a result of its underlying assumptions. The first limitation of the model originates in the assumption of initial isotropy. The data in **Figures** 4-4 to 4-6 are generated for loading history in one direction (roll) only. The same set of parameters certainly will not provide a reasonable prediction of the fabric response in the other directions since the experimental results clearly indicate the presence of initial material anisotropy.

Another model limitation is its inability to capture the long term damage as a result of fiber slip and fiber disentanglement as illustrated in **Figures** 4-4 and 4-6. The current constitutive model assumes that long term damage is a result of slip in the bulk fiber matrix, which is represented by long-term softening in the elastic-viscoplastic element of the model. However, the fiber slip is actually happening in the fiber network, and should instead be incorporated by an extra inelastic component of deformation in series with the large strain nonlinear spring element.

The third limitation of the model is its inability to capture the volumetric response of the material. Since the material is anisotropic, the volumetric response is not easily determined

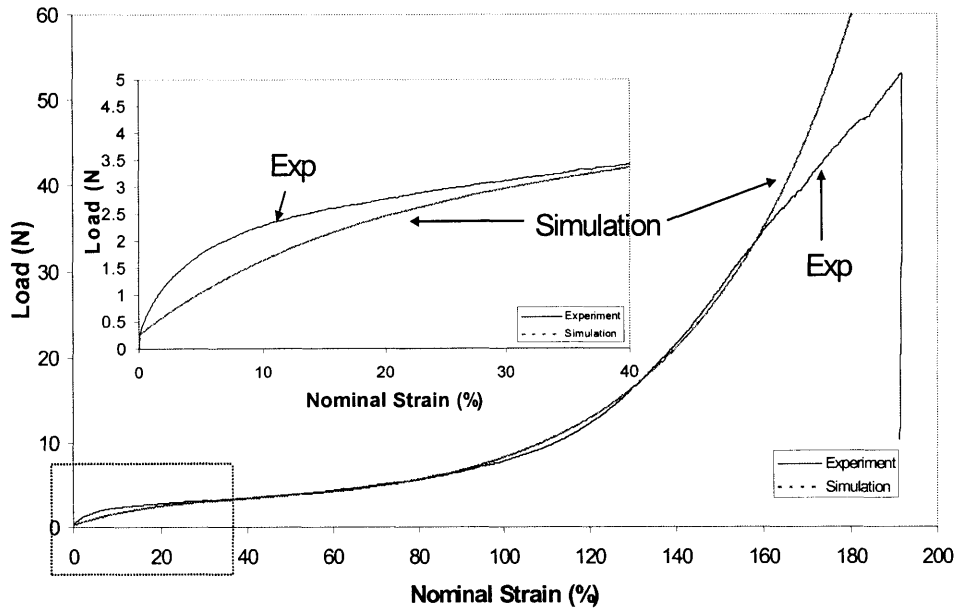


Figure 4-5: Experimental result and simulation prediction of the uniaxial monotonic loading test of the Dyneema Fraglight

experimentally. However, the volumetric response of the material is closely related to the lateral contraction, and hence, a comparison can be made between the lateral contraction observed in the uniaxial experiments and the simulation results. The lateral contraction of the experimental results, obtained by using an image analysis software VIC2D from Correlated Solutions, and the simulation results are plotted against axial elongation as shown in **Figure 4-8**. According to this figure, the experimentally observed lateral contraction decreases at a faster rate than the simulation results. The discrepancy between the simulation predictions and the experimental data arises from the fact that the model is currently assumed isotropic while the actual material is initially anisotropic, and that the long term effect is inaccurately captured by the long-term softening dashpot in the elastic-viscoplastic component rather than in the nonlinear spring component that dominates the response at large strain.

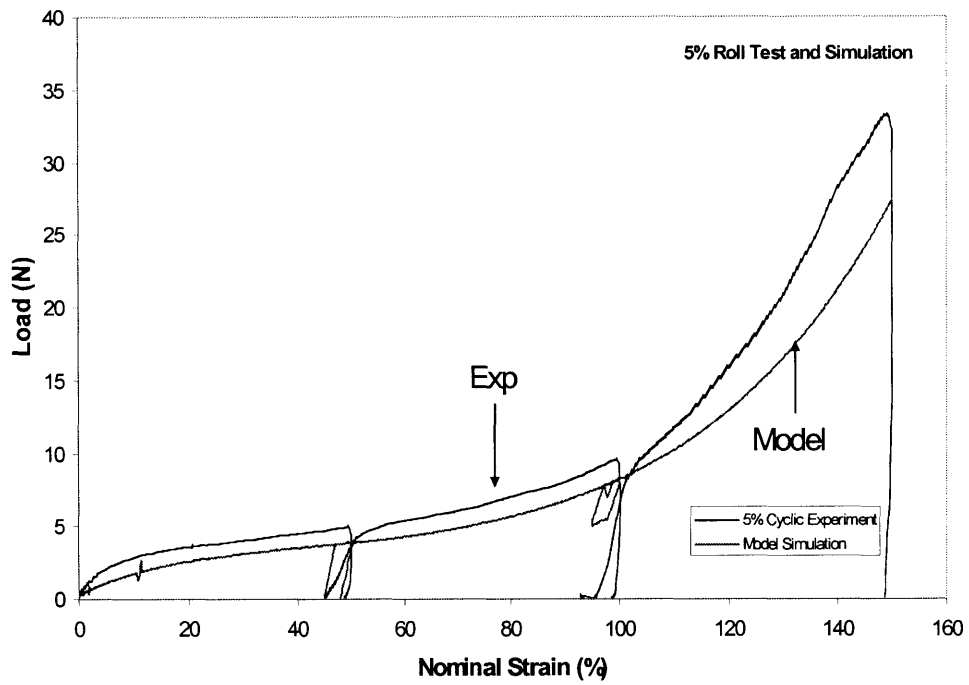


Figure 4-6: Experimental result and simulation prediction of the uniaxial cyclic loading test at 0.05 / sec of the Dyneema Fraglight

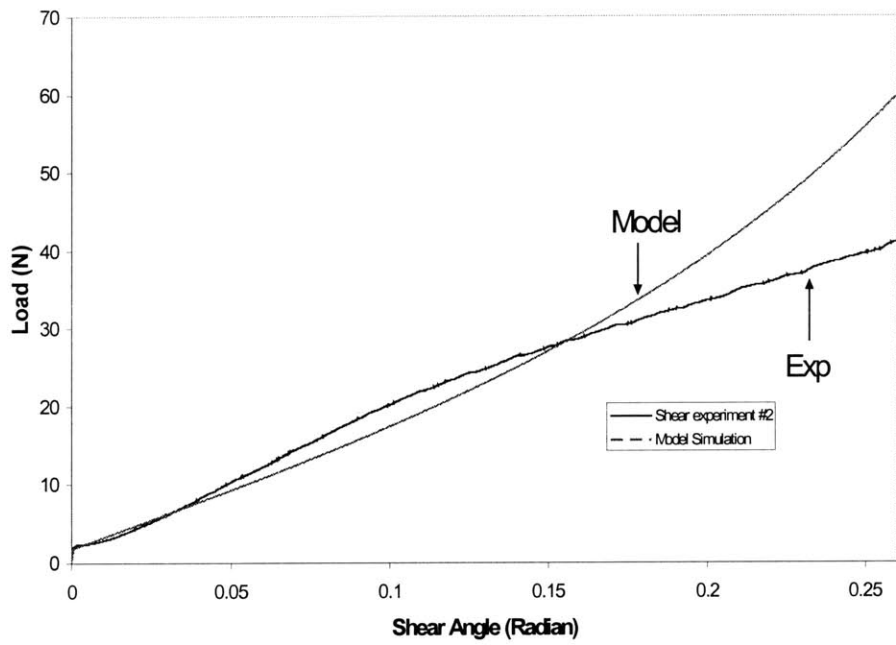


Figure 4-7: Experimental result and simulation prediction of the picture-frame monotonic shear test of the Dyneema Fraglight

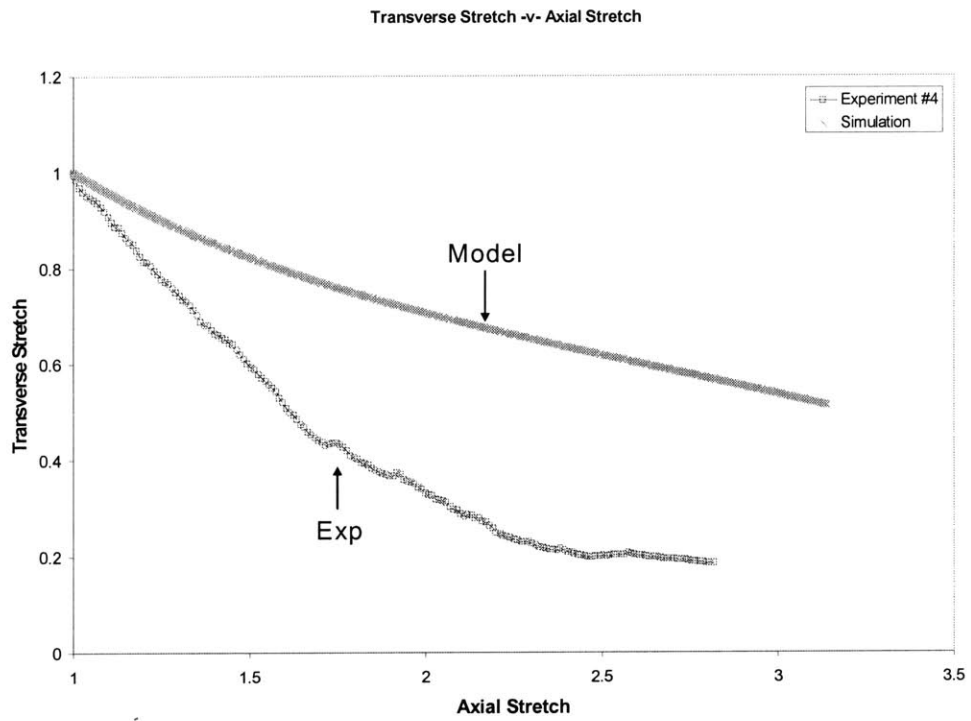


Figure 4-8: Lateral contraction as observed in the experiment and as predicted by the simulation

Chapter 5

Conclusions

5.1 Conclusions

The mechanical responses of high performance ballistic woven and nonwoven fabrics under in-plane quasi-static loading conditions have been investigated. The investigations focused on the responses of fabrics at the mesostructural level as well as at the macroscopic level under uniaxial tensile and in-plane shear modes of deformation. A number of experimental methods have been developed, including techniques to test individual fibers (coupon fiber test), techniques to test fabric specimens with the aid of custom-designed fixtures, and techniques relying on image analysis to capture the deformation response of the fabric. Two continuum models have been developed for each type of fabric based on the deformation and failure mechanisms observed in the experiments. The models are able to capture essential features of the in-plane deformation of the fabrics in a computationally efficient framework.

The experimental investigation of woven fabric was conducted as a companion study with the model development by King [41] and it was aimed at investigating the deformation mechanisms of woven fabric as well as at measuring the necessary parameters for the woven fabric continuum model. A ballistic grade Kevlar[®] fabric style 706 was selected as the representative fabric. The geometric properties of such fabric were characterized by means of microscopy and image analysis. A number of tests were carried out to measure the model constitutive properties: yarn properties were measured from yarn tensile tests and the interactions between the two yarn families were measured from out-of-plane compression tests as well as picture-frame shear

tests. The mechanical response of Kevlar[®] fabric was investigated under uniaxial tensile loads along the yarn family directions and along the bias direction to gain an insight into the fabric deformation mechanisms and to validate the model. The response of Kevlar[®] fiber was also investigated under uniaxial tension as a comparison to the behaviors of yarns and fabric strips. Using the parameters measured from these experiments, a number of model simulations have been created and found to be generally in good agreement with the experimental data both qualitatively and quantitatively, indicating that the model is capable of capturing the dominant mechanisms of woven fabric deformation under in-plane loading conditions

The experimental investigation of nonwoven fabrics was conducted to study the deformation and failure mechanisms of this material. Two types of the ballistic needlepunched fabrics were selected as the representative materials: ProTechtor[®] and Dyneema Fraglight[®]. The structures of both fabrics were analyzed using optical microscopy and image analysis techniques. The fiber arrangements were found to have some degree of anisotropy with fibers clustered around the needlepunch areas. The mechanical properties of individual fibers were also investigated by means of coupon tensile tests. The constituent fibers of both fabrics exhibit a linear stress-strain response; however, the results of Dyneema[®] fiber tests show some discrepancies due to fiber defects and nonuniform size distribution. The mechanical responses of both fabrics are characterized under uniaxial loads along different fabric directions. The experimental results indicate that both fabrics are highly anisotropic. The principal direction with maximum fabric stiffness lies along the cross direction for both fabrics. Strain rate effects were also investigated for the Dyneema Fraglight[®]. For the range of rates investigated, strain rate was found to have a weak influence on the overall fabric behavior. The effects of damage due to fiber disentanglement and the fiber network orientation for the Dyneema Fraglight[®] were examined by performing uniaxial cyclic loading. The same fabric was also tested under in-plane shear loading using the picture-frame shear test. The results indicate a nonlinear shear response with out-of-plane buckling at large shear angles.

A continuum fabric model was developed to capture the in-plane behavior of nonwoven fabrics by homogenizing the response of fiber networks and incorporating the effects of fabric damage and the texture evolution observed in the experiments. The model consists of two constitutive components acting in parallel. The first component is composed of a linearly

elastic isotropic spring corresponding to the initial fiber rotation and an evolving dashpot representing the effects of inter-fiber friction. The second component contains an exponential elastic eight-chain spring designed to capture the nonlinear evolution of fiber stretch and fiber network rotation. The model parameters were determined by fitting the simulation results to the experimental data of the uniaxial cyclic test at 0.01 s^{-1} . Using these parameters, a number of simulations were performed to predict the responses of the uniaxial monotonic test, the uniaxial cyclic test at 0.05 s^{-1} , and the picture frame shear test. The simulation predictions are found to be in good agreements with the experimental results, indicating that the model is capable of capturing the essential features of the macroscopic response due to the microscopic deformation mechanisms. However, there are still some limitations in the model, especially in predicting the volumetric response, the long-term damage due to fiber slip and fiber disentanglement, and the material anisotropy, mainly as a result of the underlying planar, initially isotropic assumptions. Modifications of the model are needed to overcome the current limitations. In any case, the generally good agreement between the model predictions and the experimental data serves to validate the model, and hence, the modeling approach satisfies the intended objectives.

5.2 Recommendations and Future Work

Though a complete set of in-plane behaviors has been reported for both woven and nonwoven fabrics, there are still many material behaviors that need to be investigated, including the high rate response of the constituent fibers and fabrics, the fabric response under biaxial loading, the fabric wrinkle from the in-plane deformation, and the out-of-plane deformation under quasi-static and impact loading conditions. To investigate such behavior, new sets of experiments must be conducted. Examples of such tests are: high strain rate tests of fibers using a split-Hopkinson bar, biaxial tests, and gas gun impact tests of both types of fabrics.

The characterization of the geometric properties of nonwoven fabric could be enhanced by using an image analysis tool. With this capability, the fiber orientation distribution, the fiber density distribution and the fiber size could be determined from a single micrograph of the nonwoven fabric surface. In addition to the fabric topology, the image analysis technique could provide a better understanding of the deformation mechanisms at the microstructural level of

nonwoven fabrics.

In term of modeling, although the simulation predictions are in good agreement with the experimental data for the presenting cases, the proposed nonwoven fabric model still fails to capture some of the important features of the in-plane fabric response, especially the effects of initial material anisotropy and the long-term damage of nonwoven fabrics. Limitations in the ability of the model to predict long-term damage effects can be overcome by introducing inelastic deformations for the nonlinear network (network B), corresponding to the fiber slip occurring in the fiber network. The material anisotropy needs to be incorporated by relaxing the isotropic assumption and adopting an orthotropic material formulation. In addition, the model parameters at the current stage do not represent physical material properties, and therefore, a modification should be made on the model underlying assumptions such that the parameters incorporate the geometric and constitutive properties of the fibers.

The ultimate goal of this study is to develop a model capable of capturing the nonwoven fabric response under a ballistic impact. The current model has been implemented only for quasi-static in-plane implicit analysis. To incorporate ballistic response, the model should be expanded to include a thin, three dimensional structure (shell) and implemented into an explicit code for dynamic analysis.

Appendix A

Uniaxial Tensile Grips for Fabric Sheets

A new gripping mechanism is proposed here to eliminate the difficulties in using conventional jaws grips in the fabric tests. Typical problems of the conventional jaws grips such as uneven gripping forces and sample slips arise mainly due to the non-uniform thickness of woven and nonwoven fabrics. The new fixture design is supposed to eliminate such problems by means of wrapping the fabric around a thin long rod and clamping the wrapped fabric in a set of grooved jaws inserts that matches the dimension of the rod, which improves the contact area between the fixture and the specimen. The jaws inserts are clamped together using a set of screws, which allows varying clamping force to accommodate the nonuniform thickness. The drawings of the uniaxial tensile grips of the described design are shown in **Figure A-1-A-3**.

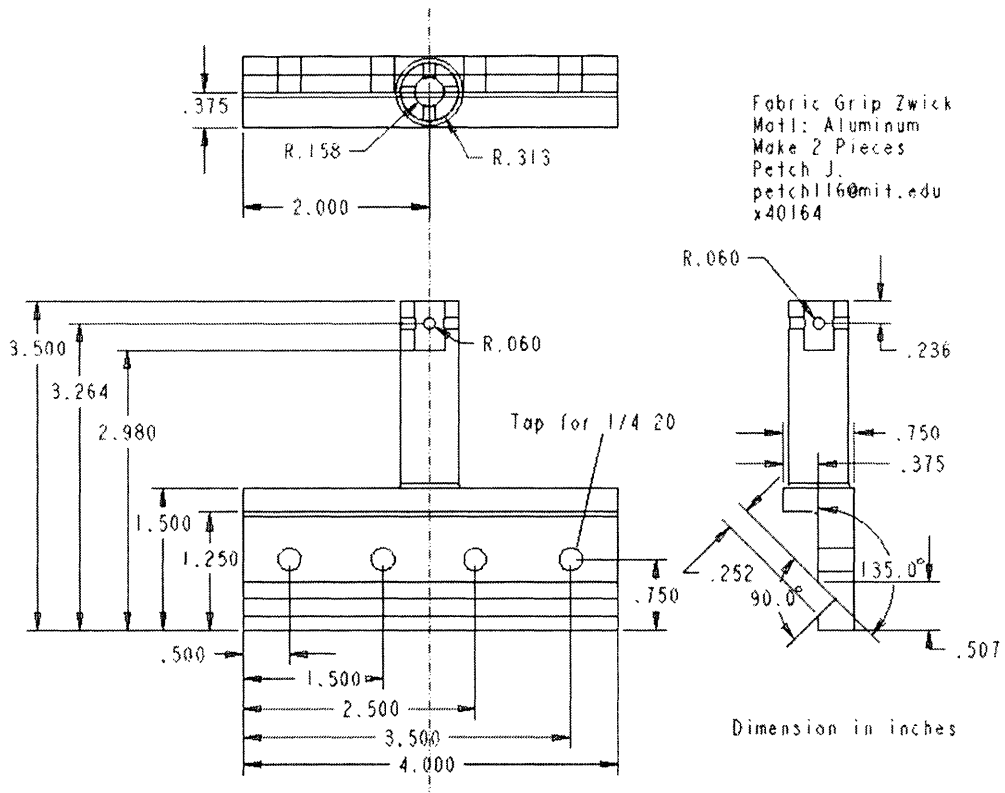


Figure A-1: Drawings of fabric uniaxial tensile grip (A)

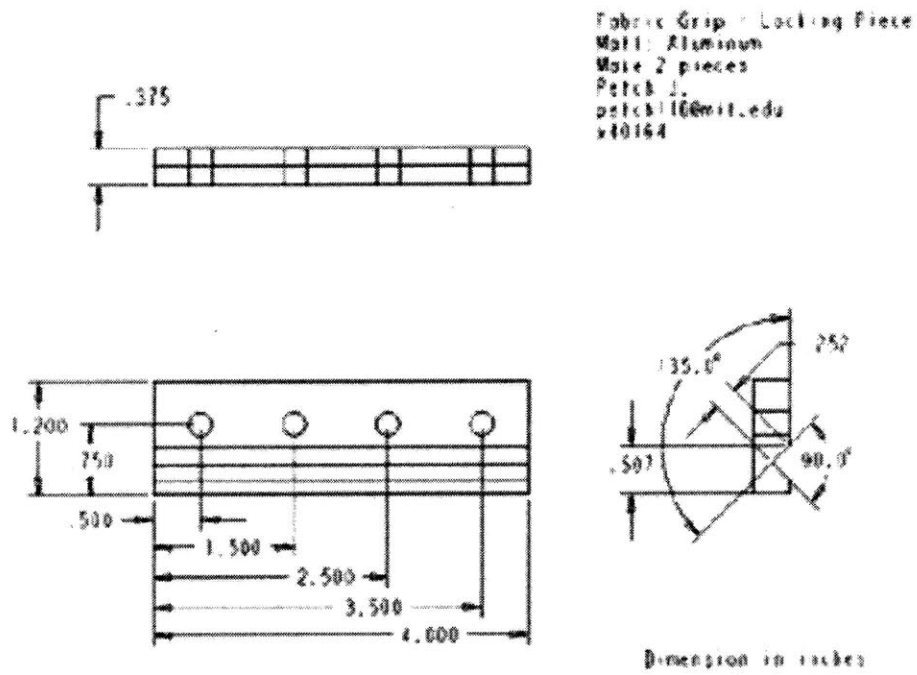


Figure A-2: Drawings of fabric uniaxial tensile grip (B)

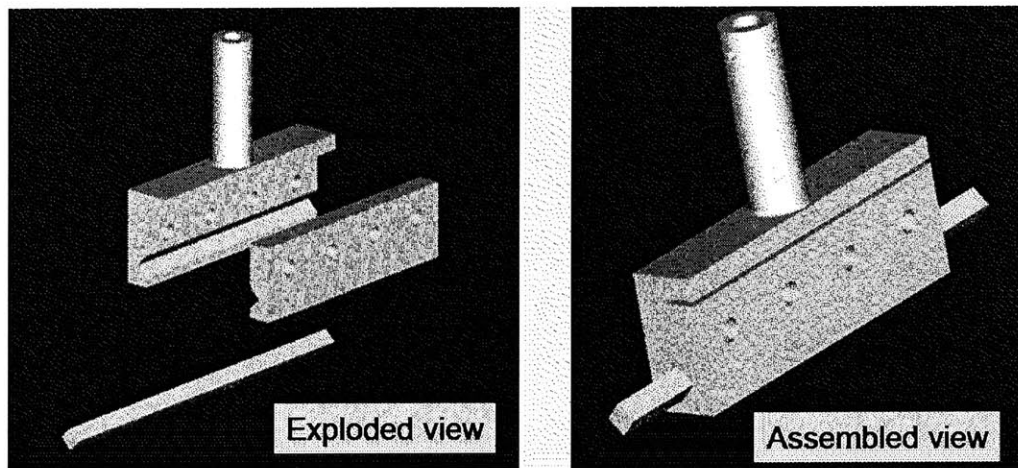


Figure A-3: Drawings of fabric uniaxial tensile grip (C)

Appendix B

Kinematics of Picture-frame Shear Test

The picture-frame shear test has been used to study the in-plane shear response of woven and nonwoven fabrics. The picture-frame shear fixture is essentially a four-bar fixture with hinges corner. The test is performed by fixing one corner of the square fixture, and displacing the diagonal opposite corner. The displacement of one corner imposes a rhomboidal deformation on the specimen initial square shape as shown in **Figure B-1**.

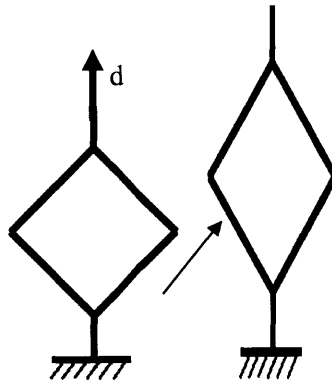


Figure B-1: Deformation imposed by the picture-frame shear test

The level of diagonal displacement can be related to the stretches in the loading and lateral directions, as well as the fabric shear angle according to the following relations:

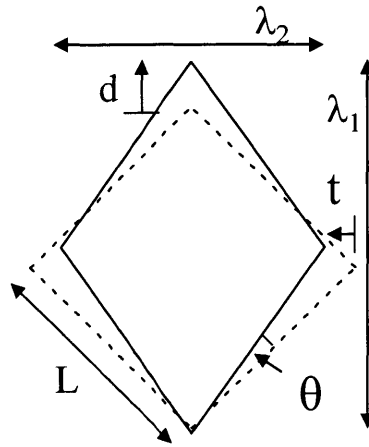


Figure B-2: Shear frame kinematics

$$\lambda_1 = \frac{\sqrt{2}L + d}{\sqrt{2}L} = \sqrt{1 + \sin(2\theta)} \quad (\text{B.1})$$

$$\lambda_2 = \frac{\sqrt{2}L - t}{\sqrt{2}L} = \sqrt{1 - \sin(2\theta)} \quad (\text{B.2})$$

- where
- d = applied displacement
- t = lateral displacement
- L = frame edge length
- θ = shear angle
- λ_1 = stretch in the loading direction
- λ_2 = stretch in the lateral direction

As indicated in the equation B.1, the applied stretch-shear angle relation is non-linear, and

therefore, an applied stretch in the loading direction results in a different level of shear angle compared to the same stretch in the reverse direction (see **Figure B-3**).

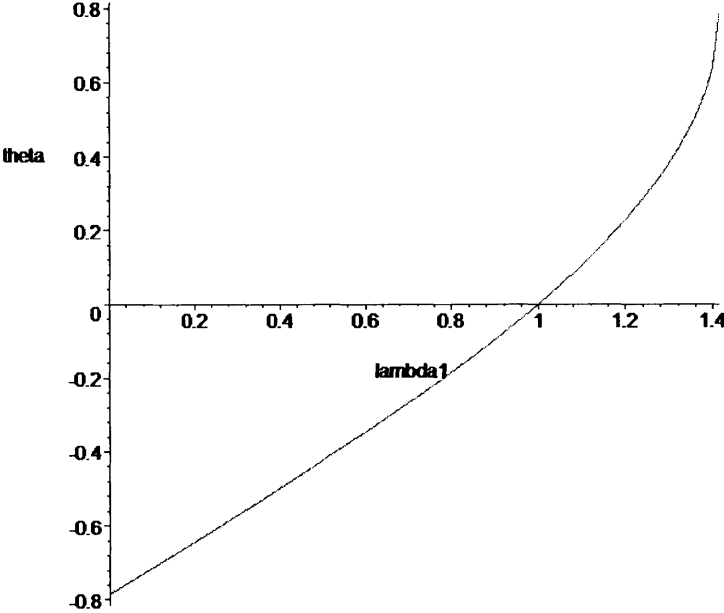


Figure B-3: Plot of the applied stretch (λ_1) and the shear angle (θ)

In addition, the multiplication of stretches in the applied direction and the transverse direction is not equal to unity ($\lambda_1 * \lambda_2 \neq 1$), suggesting that the test configuration is not area-conserving as in the case of pure shear deformation. Instead, the specimen undergoes two modes of deformation: a shear-dominated mode and a lateral-compressive mode. **Figure B-4** illustrates the relationship between the stretches in the applied direction and in the lateral direction, as well as the multiplication of the two stretches indicating the volumetric response of this test.

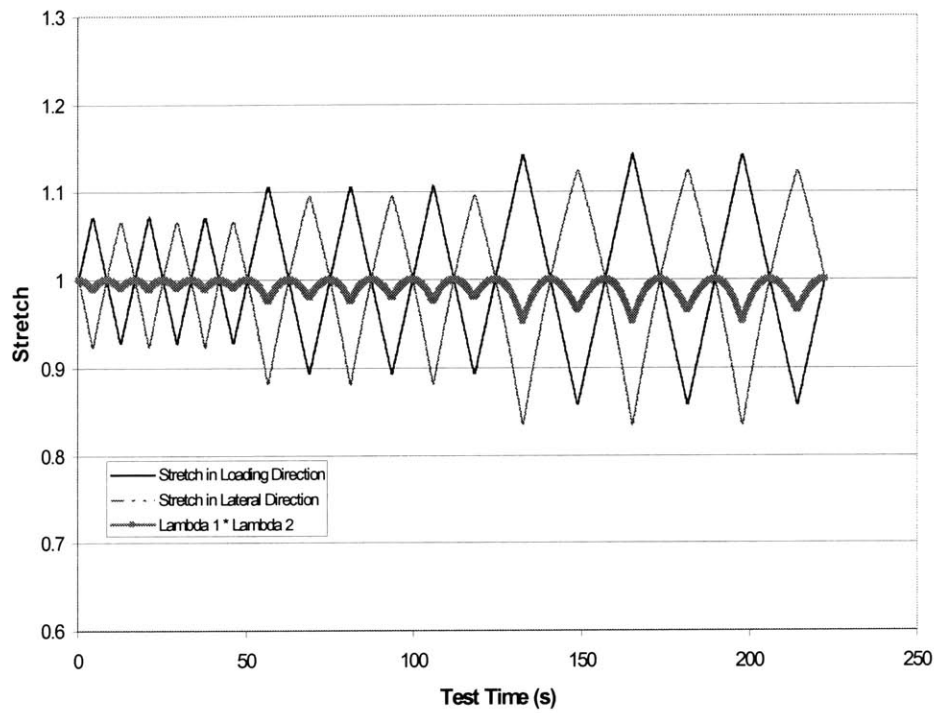


Figure B-4: Plots of the stretch in the loading direction, the stretch in the lateral direction, and the multiplication of the two stretches

Bibliography

- [1] Adanur, S., and Liao, T., "Fiber Arrangement Characteristics and Their Effects on Non-woven Tensile Behavior", *Textile Research Journal*, **69**(11):816-824, 1999.
- [2] Allen, S.R., Roche, E.J., Bennett, B., and Molaison, R., "Tensile Deformation and Failure of Poly(p-phenylene terephthalamide) Fibres", *Polymer*, **33**(9):1849-1854, 1992.
- [3] Anandjiwala, R.D., and Leaf, G.A.V., "Large-Scale Extension and Recovery of Plain Woven Fabrics. Part I Theoretical", *Textile Research Journal*, **61**(11):619-634, 1991.
- [4] Anandjiwala, R.D., and Leaf, G.A.V., "Large-Scale Extension and Recovery of Plain Woven Fabrics. Part II Experimental and Discussion", *Textile Research Journal*, **61**(12):743-755, 1991.
- [5] Arruda, E.M., and Boyce, M.C., "A Three-Dimensional Constitutive Model for the Large Stretch Behavior of Rubber Elastic Materials", *Journal of the Mechanics and Physics of Solids*, **41**(2):389-412, 1993.
- [6] Backer, S., and Petterson, D.R., "Some Principles of Nonwoven Fabrics", *Textile Research Journal*, **30**:704-711, 1960.
- [7] Baker, D.J., "Evaluation of Thin Kevlar-Epoxy Fabric Panels Subjected to Shear Loading", American Institute of Aeronautics and Astronautics, NASA.
- [8] Basset, R.J., Postle, R., and Pan, N., "Experimental Methods for Measuring Fabric Mechanical Properties: A Review and Analysis", *Textile Research Journal*, **69**(11):866-875, 1999.

- [9] Bias-Singh, S., Biggers, S.B., and Goswami, B.C., "Finite Element Modeling of the Nonuniform Deformation of Spun-Bonded Nonwovens", *Textile Research Journal*, **68**(5):327-342, 1998.
- [10] Bias-Singh, S., Anandjiwala, R.D., and Goswami, B.C., "Characterizing Lateral Contraction Behavior of Spunbonded Nonwovens during Uniaxial Tensile Deformation", *Textile Research Journal*, **66**(3):131-140, 1996.
- [11] Boisse, P., Borr, M., Buet, K., and Cherouat, A., "Finite Element Simulations of Textile Composite Forming Including the Biaxial Fabric Behavior", *Composites Part B*, **28B**:453-464, 1997.
- [12] Boisse, P., Buet, K., Gasser, A., and Launay, J., "Meso/macro-mechanical Behavior of Textile Reinforcements for Thin Composites", *Composites Science and Technology*, **61**(3):395-401, 2001.
- [13] Boyce, M.C., Weber, G.C., and Parks, D.M., "On the Kinematics of Finite Strain Plasticity", *Journal of the Mechanics and Physics of Solids*, **37**(5):647-665, 1989.
- [14] Britton, P.N., Sampson, A.J., Elliott, C.F., Graben, H.W., and Gettys, W.E., "Computer Simulation of the Mechanical Properties of Nonwoven Fabrics, Part I: The Method", *Textile Research Journal*, **53**:363-368, 1983.
- [15] Britton, P.N., Sampson, A.J., and Gettys, W.E., "Computer Simulation of the Mechanical Properties of Nonwoven Fabrics, Part II: Bond Breaking", *Textile Research Journal*, **54**:1-5, 1984.
- [16] Britton, P.N., Sampson, A.J., and Gettys, W.E., "Computer Simulation of the Mechanical Properties of Nonwoven Fabrics, Part III: Fabric Failure", *Textile Research Journal*, **54**:425-428, 1984.
- [17] Chhabra, R., "Nonwoven Uniformity - Measurements Using Image Analysis", *International Nonwovens Journal*, 43-50, 2003.

- [18] Chocron, S., Pintor, A., Cendon, D., Rosello, C., Sanchez-Galvez, V., "Characterization of Fraglight Non-Woven Felt and Simulation of FSP's Impact in It", *Final Report to The US Army Research Contract No. N68171-00-M-5983*.
- [19] Chudleigh, P.W., "Image Formation by Fibers and Fiber Assemblies", *Textile Research Journal*, 813-820, 1984.
- [20] Cunniff, P.M., "An Analysis of the System Effects in Woven Fabrics Under Ballistic Impact", *Textile Research Journal*, **62**(9):495-509, 1992.
- [21] Ericson, C.W., and Baxter, J.F., "Spunbonded Nonwoven Fabric Studies, I: Characterization of Filament Arrangement in the Web", *Textile Research Journal*, **43**(7):371-378, 1973.
- [22] Fahey, M.T., "Nonlinear and Anisotropic Behavior of High Performance Fibers", Ph.D. Thesis, Massachusetts Institute of Technology, 1990.
- [23] Grindstaff, T.H., and Hansen, S.M., "Computer Model for Predicting Point-Bonded Nonwoven Fabric Strength, Part I", *Textile Research Journal*, **56**(6):383-388, 1986.
- [24] Gong, R.H., Newton, A., "Image-analysis Techniques, Part I: The Measurement of Pore-size Distribution", *Journal of the Textile Institute*, **83**(2):253-268, 1992.
- [25] Gong, R.H., Newton, A., "Image-analysis Techniques, Part II: The Measurement of Fibre Orientation in Nonwoven Fabrics", *Journal of the Textile Institute*, **87**(2):371-388, 1996.
- [26] Harrison, P., Wiggers, J., Long, A.C., Clifford, M.J., "Continuous fibre reinforced composites - Determination of the in-plane shear stress response to shear strain and shear strain rate, using the picture-frame test", *Internal Test Standard University of Nottingham Polymer Composites Research Group*, 2002.
- [27] Hearle, J.W.S., Grosberg, P., and Backer, S., *Structural Mechanics of Fibers, Yarns, and Fabrics*, Wiley-Interscience, New York, 1969.
- [28] Hearle, J.W.S., and Stevenson, P.J., "Nonwoven Fabric Studies, Part III: The Anisotropy of Nonwoven Fabrics", *Textile Research Journal*, **33**(11):877-888, 1963.

- [29] Hearle, J.W.S., and Stevenson, P.J., "Studies in Nonwoven Fabrics, Part IV: Prediction of Tensile Properties", *Textile Research Journal*, **34**(3):181-191, 1964.
- [30] Hearle, J.W.S., and Newton, A., "Nonwoven Fabric Studies, Part XIV: Derivation of Generalized Mechanics by the Energy Method", *Textile Research Journal*, 778-797, 1967.
- [31] Jirsak, O., Lukas, D., and Charvat, R., "A Two-Dimensional Model of the Mechanical Properties of Textiles", *Journal of the Textile Institute*, **84**(1):1-15, 1993.
- [32] Kang, T.J., and Lee, S.H., "Characterization of Reinforcing Web Structures in Needle Punched Nonwoven Composites", *Journal of Composite Materials*, **33**(22):2116-2132, 1999.
- [33] Kawabata, S., Niwa, M., and Kawai, H., "The Finite Deformation Theory of Plain Weave Fabrics Part I:The Biaxial Deformation Theory", *Journal of the Textile Institute*, **64**(1):21-46, 1973.
- [34] Kawabata, S., Niwa, M., and Kawai, H., "The Finite Deformation Theory of Plain Weave Fabrics Part II:The Uniaxial Deformation Theory", *Journal of the Textile Institute*, **64**(2):47-61, 1973.
- [35] Kawabata, S., Niwa, M., and Kawai, H., "The Finite Deformation Theory of Plain Weave Fabrics Part III: The Shear Deformation Theory", *Journal of the Textile Institute*, **64**(2):62-85, 1973.
- [36] Kawabata, S., Niwa, M., and Yamashita, Y., "Recent Developments in the Evaluation Technology of Fiber and Textiles: Toward the Engineered Design of Textile Performance", *Journal of Applied Polymer Science*, **83**:687-702, 2002.
- [37] Kim, H.S., and Pourheyhimi, B., "Computational Modeling of Mechanical Performance in Thermally Point Bonded Nonwovens", *Journal of Textile and Apparel, Technology and Management*, **1**(4):1-7, 2001.
- [38] Kim, H.S., Pourdeyhimi, B., Abhiraman, A.S., and Desai, P., "Characterizing Structural Changes in Point-Bonded Nonwoven Fabrics During Load-Deformation Experiments", *Textile Research Journal*, **71**(2):157-164, 2001.

- [39] Kim, H.S., Pourdeyhimi, B., Abhiraman, A.S., and Desai, P., "Effect of Bonding Temperature on Load-Deformation Structural Changes in Point-Bonded Nonwoven Fabrics", *Textile Research Journal*, **72**(7): 645-653, 2002.
- [40] Kim, H.S., Pourdeyhimi, B., Desai, P., and Abhiraman, A.S., "Anisotropy in the Mechanical Properties of Thermally Spot-Bonded Nonwovens: Experimental Observations", *Textile Research Journal*, **71**(11): 965-976, 2001.
- [41] King, M.J., "An Energy-Based Constitutive Model for the In-Plane Mechanical Behavior of Woven Fabrics", M.S. Thesis, Massachusetts Institute of Technology, 2003.
- [42] King, M.J., Jearanaisilawong, P., Socrate, S., "A Continuum Constitutive Model for the Mechanical Behavior of Woven Fabrics", In Press, 2004.
- [43] Kothari, V.K., and Tandon, S.K., "Shear Behavior of Woven Fabrics", *Textile Research Journal*, **59**(3):142-150, 1989.
- [44] Kothari, V.K., and Patel, P.C., "Theoretical Model for Predicting Creep Behaviour of Nonwoven Fabrics", *Indian Journal of Fibre & Textile Research*, **26**:273-279, 2001.
- [45] Kothari, V.K., and Das, A., "The Compressional Behaviour of Spunbonded Nonwoven Fabrics", *Journal of the Textile Institute*, **84**(1):16-30, 1993.
- [46] Leaf, G.A.V., and Kandil, K.H., "The Initial Load-Extension Behaviour of Plain-Woven Fabrics", *Journal of the Textile Institute*, **71**(1):1-7, 1980.
- [47] Lebrun, G., Bureau, M.N., and Denault, J., "Evaluation of Bias-Extension and Picture-Frame Test Methods for the Measurement of Intraply Shear Properties of PP/Glass Commingled Fabrics", *Composite Structures*, **61**:341-352, 2003.
- [48] Lee, S.M., and Argon, A.S., "The Mechanics of the Bending of Non-woven Fabrics, Part I: Spunbonded Fabric (CEREX)", *Journal of the Textile Institute*, **74**(1):1-11, 1983.
- [49] Lee, S.M., and Argon, A.S., "The Mechanics of the Bending of Non-woven Fabrics, Part II: Spunbonded Fabric with Spot Bonds (FIBRETEX)", *Journal of the Textile Institute*, **74**(1):12-18, 1983.

- [50] Lee, S.M., and Argon, A.S., "The Mechanics of the Bending of Non-woven Fabrics, Part III: Print-Bonded Fabric (MASSLINN)", *Journal of the Textile Institute*, **74**(1):19-30, 1983.
- [51] Lee, S.M., and Argon, A.S., "The Mechanics of the Bending of Non-woven Fabrics, Part IV: Print-Bonded Fabric with a Pattern of Elliptical Holes (KEYBAK)", *Journal of the Textile Institute*, **74**(1):31-37, 1983.
- [52] Liao, T., Adanur, S., and Drean, J.Y., "Predicting the Mechanical Properties of Nonwoven Geotextiles with the Finite Element Method", *Textile Research Journal*, **67**(10):753-760, 1997.
- [53] Liao, T., and Adanur, S., "Computerized Failure Analysis of Nonwoven Fabrics Based on Fiber Failure Criterion", *Textile Research Journal*, **69**(7):489-496, 1999.
- [54] Lussier, D., "Shear Characterization of Textile Composite Formability", M.S. Thesis, University of Massachusetts, Lowell, 2002.
- [55] McGuinness, G.B., and O Bradaigh, C.M., "Development of Rheological Models for Forming Flows and Picture Frame Shear Testing of Fabric Reinforced Thermoplastic Sheets", *Journal of Non-Newtonian Fluid Mechanics*, **73**:1-28, 1997.
- [56] Mohammed, U., Lekakou, C., Dong, L., and Bader, M.G., "Shear Deformation and Micro-mechanics of Woven Fabrics", *Composites Part A*, **31**:299-308, 2000.
- [57] Ng, S., Tse, P., and Lau, K., "Numerical and Experimental Determination of the In-Plane Elastic Properties of 2/2 Twill Weave Fabric Composites", *Composites Part B*, **29B**:735-744, 1998.
- [58] Pan, N., Haig Z. S., and Ryu, H.S., "An Alternative Approach to the Objective Measurement of Fabrics", *Textile Research Journal*, **63**(1):33-43, 1993.
- [59] Pan, N., and Yoon, M.Y., "Behavior of Yarn Pullout from Woven Fabrics: Theoretical and Experimental", *Textile Research Journal*, **63**(11):629-637, 1993.
- [60] Patel, P.C., and Kothari, V.K., "Relationship between Tensile Properties of Fibres and Nonwoven Fabrics", *Indian Journal of Fibre & Textile Research*, **26**:398-402, 2001.

- [61] Patel, P.C., and Kothari, V.K., "Effect of Specimen Size and Strain Rate on the Tensile Properties of Heat-sealed and Needle-punched Nonwoven Fabrics", *Indian Journal of Fibre & Textile Research*, **26**:409-413, 2001.
- [62] Peng, X.Q., Cao, J., Chen, J., Xue, P. Lussier, D.S., and Liu, L., "Experimental and Numerical Analysis on Normalization of Picture Frame Tests for Composite Materials", *Composites Science and Technology*, **64**:11-21, 2004.
- [63] Petterson, D.R., "On the Mechanics of Nonwoven Fabrics", Ph.D. Thesis, Massachusetts Institute of Technology, 1958.
- [64] Pourdeyhimi, B., Ramanathan, R., and Dent, R., "Measuring Fiber Orientation in Nonwovens, Part I: Simulation", *Textile Research Journal*, **66**(11):713-722, 1996.
- [65] Pourdeyhimi, B., Ramanathan, R., and Dent, R., "Measuring Fiber Orientation in Nonwovens, Part II: Direct Tracking", *Textile Research Journal*, **66**(12):747-753, 1996.
- [66] Pourdeyhimi, B., Dent, R., and Davis, H., "Measuring Fiber Orientation in Nonwovens, Part III: Fourier Transform", *Textile Research Journal*, **67**(2):143-151, 1997.
- [67] Pourdeyhimi, B., and Dent, R., "Measuring Fiber Orientation in Nonwovens, Part IV: Flow Field Analysis", *Textile Research Journal*, **67**(3):181-187, 1997.
- [68] Pourdeyhimi, B., Dent, R., Jerbi, A., Tanaka, S., and Deshpande, A., "Measuring Fiber Orientation in Nonwovens, Part V: Real Webs", *Textile Research Journal*, **69**(3):185-192, 1999.
- [69] Pourdeyhimi, B., and Dent, R., "Measuring Fiber Diameter Distribution in Nonwovens", *Textile Research Journal*, **69**(4):233-236, 1999.
- [70] Rao, Y., and Farris, J., "A Modeling and Experimental Study of the Influence of Twist on the Mechanical Properties of High-Performance Fiber Yarns", *Journal of Applied Polymer Science*, **77**:1938-1949, 2000.
- [71] Realff, M.L., Boyce M.C., and Backer S., "A Micromechanical Model of the Tensile Behavior of Woven Fabric", *Textile Research Journal*, **67**(6):445-459, 1997.

- [72] Realff, M.L., "Mechanical Properties of Fabrics Woven from Yarns Produced by Different Spinning Technologies", Ph.D. Thesis, Massachusetts Institute of Technology, 1992.
- [73] Rebouillat, S., "Tribological Properties of Woven Para-aramid Fabrics and their Constituent Yarns", *Journal of Materials Science*, **33**:3293-3301, 1998.
- [74] Schaff, A.J., and Ogale, A.A., "Tensile Viscoelastic Properties of Spunbonded Nonwoven Polypropylene Backing", *Textile Research Journal*, 61(7):386-392, 1991.
- [75] Seo, M.H., Realff, M.L., Pan, N., Boyce, M.C., Schwartz, P., and Backer, S., "Mechanical Properties of Fabrics Woven From Yarns Produced by Different Spinning Technologies" Yarn Failure in Woven Fabric", *Textile Research Journal*, **63**(3):123-134. 1993.
- [76] Shim, V.P.W., Lim, C.T., and Foo, K.J., "Dynamic Mechanical Properties of Fabric Armour", *International Journal of Impact Engineering*, **25**:1-15, 2001.
- [77] Shockey, D.A., Elrich, D.C., and Simons, J.W., "Improved Barriers to Turbine Engine Fragments: Interim Report I", DOT/FAA AR-99/8,I, 1999.
- [78] Shockey, D.A., Elrich, D.C., and Simons, J.W., "Improved Barriers to Turbine Engine Fragments: Interim Report II", DOT/FAA AR-99/8,II, 1999.
- [79] Shockey, D.A., Elrich, D.C., and Simons, J.W., "Improved Barriers to Turbine Engine Fragments: Interim Report III", DOT/FAA AR-99/8,III, 2001.
- [80] Shockey, D.A., Elrich, D.C., and Simons, J.W., "Improved Barriers to Turbine Engine Fragments: Interim Report IV", DOT/FAA AR-99/8,IV, 2002.
- [81] Shockey, D.A., Elrich, D.C., and Simons, J.W., "Improved Barriers to Turbine Engine Fragments: Final Annual Report", DOT/FAA AR-99/8,V, 2002.
- [82] Termonia, Y., "Fundamental Study of the Deformation Behavior of Nonwoven Heat-Bonded Sheets", *Chemical Engineering Science*, **52**(17):3003-3009, 1997.
- [83] Termonia, Y., "Lattice Model for the Drape and Bending Properties of Nonwoven Fabrics", *Textile Research Journal*, **73**(1):74-78, 2003.

- [84] Wang, J., Page, J.R., and Paton, R., "Experimental Investigation of the Draping Properties of Reinforcement Fabrics", *Composite Science and Technology*, **58**:229-237, 1998.
- [85] Wang, Y., and Xia, Y.M., "Experimental and Theoretical Study on the Strain Rate and Temperature Dependence of Mechanical Behavior of Kevlar[®] Fibre", *Composite Science and Technology*, **30**:1251-1257, 1999.
- [86] Wang, Y., and Xia, Y.M., "The Effects of Strain Rate on the Mechanical Behavior of Kevlar[®] Fibre Bundles: An Experimental and Theoretical Study", *Composites Part A*, **29A**:1411-1415, 1998.
- [87] Warren, W., "The Large Deformation Elastic Response of Woven Kevlar[®] Fabric", *Polymer Composites*, **13**(4):278-284, 1992.
- [88] Xu, B., and Ting, Y.L., "Measuring Structural Characteristics of Fiber Segments in Non-woven Fabrics", *Textile Research Journal*, **65**(1):41-48, 1995.
- [89] Xu, B., Pourdeyhimi, B., and Sobus, J., "Characterizing Fiber Crimp by Image Analysis: Definitions, Algorithms, and Techniques", *Textile Research Journal*, **62**(2)73-80, 1992.
- [90] Xue, P., Peng, X., and Cao, J., "A Non-orthogonal Constitutive Model for Characterizing Woven Composites", *Composites Part A*, **34**:183-193, 2003.